FACULTÉ DES ÉTUDES SUPÉRIEURES ET POSTOCTORALES

uOttawa

L'Université canadienne
Canada's university

FACULTY OF GRADUATE AND POSDOCTORAL STUDIES

Sierra Grace Pope
AUTEUR DE LA THÈSE / AUTHOR OF THESIS

M.Sc. (Geography)
GRADE / DEGREE

Department of Geography
FACULTÉ, ÉCOLE, DÉPARTEMENT / FACULTY, SCHOOL, DEPARTMENT

Changes in Multiyear Landfast Sea Ice in the Northern Canadian Arctic Archipelago
TITRE DE LA THÈSE / TITLE OF THESIS

Luke Copland
DIRECTEUR (DIRECTRICE) DE LA THÈSE / THESIS SUPERVISOR

CO-DIRECTEUR (CO-DIRECTRICE) DE LA THÈSE / THESIS CO-SUPERVISOR

A. Viau

M. Sawada

Gary W. Slater
Le Doyen de la Faculté des études supérieures et postdoctorales / Dean of the Faculty of Graduate and Postdoctoral Studies

Changes in Multiyear Landfast Sea Ice in the Northern Canadian Arctic Archipelago

Sierra Grace Pope

Thesis submitted to the
Faculty of Graduate and Postdoctoral Studies
in partial fulfillment of the requirements
for the MSc Degree in Physical Geography

Department of Geography
Faculty of Arts
University of Ottawa

Supervisor:
Dr. Luke Copland (University of Ottawa)

Thesis Committee:
Dr. Mike Sawada (University of Ottawa)
Dr. Andre Viau (University of Ottawa)

Library and Archives Canada

Published Heritage Branch

395 Wellington Street
Ottawa ON K1A 0N4
Canada

Bibliothèque et Archives Canada

Direction du Patrimoine de l'édition

395, rue Wellington
Ottawa ON K1A 0N4
Canada

Your file Votre référence
ISBN: 978-0-494-73846-7
Our file Notre référence
ISBN: 978-0-494-73846-7

NOTICE:

The author has granted a non-exclusive license allowing Library and Archives Canada to reproduce, publish, archive, preserve, conserve, communicate to the public by telecommunication or on the Internet, loan, distribute and sell theses worldwide, for commercial or non-commercial purposes, in microform, paper, electronic and/or any other formats.

The author retains copyright ownership and moral rights in this thesis. Neither the thesis nor substantial extracts from it may be printed or otherwise reproduced without the author's permission.

AVIS:

L'auteur a accordé une licence non exclusive permettant à la Bibliothèque et Archives Canada de reproduire, publier, archiver, sauvegarder, conserver, transmettre au public par télécommunication ou par l'Internet, prêter, distribuer et vendre des thèses partout dans le monde, à des fins commerciales ou autres, sur support microforme, papier, électronique et/ou autres formats.

L'auteur conserve la propriété du droit d'auteur et des droits moraux qui protège cette thèse. Ni la thèse ni des extraits substantiels de celle-ci ne doivent être imprimés ou autrement reproduits sans son autorisation.

In compliance with the Canadian Privacy Act some supporting forms may have been removed from this thesis.

While these forms may be included in the document page count, their removal does not represent any loss of content from the thesis.

Conformément à la loi canadienne sur la protection de la vie privée, quelques formulaires secondaires ont été enlevés de cette thèse.

Bien que ces formulaires aient inclus dans la pagination, il n'y aura aucun contenu manquant.

Canada

Abstract

For most of the 20th century, multiyear landfast sea ice (MLSI) existed in semi-permanent plugs across Nansen Sound and Sverdrup Channel and formed an incipient ice shelf in Yelverton Bay, Ellesmere Island in the northern CAA. Both plugs broke in 1962 and 1998, and several breakups within the last decade indicate that the plugs are becoming temporary seasonal features. The history of the plugs is reviewed using Canadian Ice Service ice charts, satellite imagery and a literature review. The weather systems associated with plug breakup events are related to a sequence of synoptic patterns, with most breakups occurring when low pressure centers over the Asian side of the Arctic Ocean and a warm pressure ridge develops over the QEI, creating warm temperatures, clear skies, and frequent wind reversals. The 2005 simultaneous breakup of the plugs was accompanied by the removal of 690 km^2 of 55-60 year old MLSI from Yelverton Bay. Ground Penetrating Radar (GPR) and ice cores taken in June 2009 provide the first detailed assessment of the remaining MLSI in Yelverton Inlet, which in turn provides ground-truthing of satellite scenes and air photos used to chart historical changes in the MLSI. The last of the Yelverton Bay MLSI was removed in August 2010. The removal of these MLSI features in recent years aligns with the larger trend of reductions in age and thickness of sea ice in the Canadian Arctic Archipelago.

Acknowledgements

I am infinitely grateful for the support I have received from so many throughout this process. First and foremost, I am grateful to my supervisor, Dr. Luke Copland, who cultivated my interest in glaciology when I was an undergraduate student at University of Ottawa, and who has taught me so much during my graduate work. Field courses and field work under Dr. Copland's supervision have taken me to some of the most beautiful and amazing places on Earth, and I will always be indebted to him for those opportunities.

My fellow Laboratory for Cryospheric Research members were always available for support and discussion throughout the research and writing process, including Norah Foy, Colleen Mortimer, Wesley Van Wychen, Tyler Sylvestre, Amaris Page, Emilie Herdes, Samantha Darling, and Adrienne White.

Many Department of Geography Faculty members were supportive of my work. I am thankful to the members of my thesis committee, Dr. Andre Viau and Dr. Mike Sawada, both for helpful comments at the thesis proposal stage and for their instruction of graduate and undergraduate courses which gave me a crucial foundation for this project. Jim McGrath provided important technical support for my LCR computer. I am also incredibly grateful for the support and encouragement from Sylvie Theriault and Dr. Brian Ray.

Thank you to Derek Mueller, Luke Copland and Colleen Mortimer for assistance in field data collection, and to Bea Alt for sharing her insight and incredible knowledge. Completion of Chapter 2 relied on helpful comments from two anonymous reviewers and Derek Mueller, wind data from Ed Hudson, and RADARSAT-2 imagery from Matt Arkett. Funding contributions from Natural Sciences and Engineering Research Council of Canada, Canada Foundation for Innovation, Ontario Research Fund and the University of Ottawa enabled this research.

Last but certainly not least, I am indebted to my friends and family for their immeasurable love and encouragement. My father told me that my friendships during Graduate School would be the best and strongest of my life, and I believe he is correct. My friends have cheered me on, listened to my ideas, and made my time in Ottawa unforgettable. A special thank you in this regard goes to my best friend Annelise Petlock, who always gives me strength and love when I needed it most. I am very grateful to my grandparents, Bill and June Osborne, to my extended family, and to my brother, Ian Pope, for a lifetime of support. I am thankful to my parents, Karen and Roger Pope, who instilled in me a passion for the environment and a love of learning, and who have always shown confidence in me and in my work. This accomplishment is truly because of them. Finally, I would like to thank Sam Muñoz, who has listened to and encouraged me daily during this degree, and whose support means the world. Thank you so much.

"Polar ice cannot be studied as other branches of science, philosophy, medicine or law are studied. The study of sea ice belongs among the most exhausting disciplines which have to be studied on the spot, *in loco nascendi et vitae*, and which require strong men, absolutely sound in mind and body, courageous, willing and fit to renounce all comfort, thoroughly prepared both in theory for the work and ready to face all the hardships that may come like a bolt from the blue and in the most unfavourable moments. The sea-ice has to be studied far away, in the north or south, in white deserts of ice, where there is nothing, nothing else, no shelter, no help; and where, on those vast plains in which the chasms of the sea keep tearing open and insurmountable obstacles in the shape of mountains of ice keep piling up, the Lord only is with man."

-J. Zukriegel
Cryologia Maris
The Geographical Institute of the Charles IV University
Prague, 1935

Table of Contents

List of Tables

List of Figures

1. Introduction

Recent studies indicate that ice shelves and sea ice in the Canadian Arctic are responding to external changes at an increasing rate (Copland et al., 2007; Maslanik et al., 2007; Stroeve et al., 2007). Changes in glacier, ice shelf, and sea ice extent indicate responses to many processes, including surface air temperature and wind conditions, as well as mass balance and local ice dynamics. These changes can therefore provide valuable information about the impacts of climate change in the High Arctic. Atmospheric warming in the Arctic has been identified by the IPCC (2007) as nearly twice that of the rest of the planet since the late 1960s, and projected air temperature increases in this region over the next century are estimated to be between 3° and 11°C. This warming may be expected to significantly influence the Arctic cryosphere.

1.1 Sea Ice Characteristics and Observations

Surrounding much of the Canadian Arctic Archipelago (CAA) is a complex network of first year and multiyear sea ice. Sea ice covers 7% to 12% of the planet's surface at any one time (Wadhams, 2000), and plays a pivotal role in the global energy exchange. Solar radiation absorbed at the equatorial zones is transported to the poles, and the rate of energy loss through sea ice to the atmosphere is dependent on the extent and characteristics of the ice cover (Serreze and Barry, 2005). The position of sea ice between air and ocean makes it highly responsive to temperature changes and potentially a more rapid and direct indicator of climate warming than glaciers and ice caps.

The initial growth of sea ice in the Arctic Ocean typically occurs in the form of vertical crystal projections (dendritic/congelation growth), with the rejected brine from ice formation collecting in the narrow spaces between crystal dendrites (Wadhams, 2000). This brine rejection process leads to gradients in ocean salinity and temperature, contributing to the global thermohaline circulation and oceanic heat transport patterns (Serreze and Barry, 2005). Though most salt is rejected immediately as the sea water crystallizes into ice, rapid ice growth below and around these brine collections can allow brine to be captured in pockets within the ice, giving young first-year sea ice (FYI) salinities of up to 10 psu (Wadhams, 2000). Brine rejection, in the form of cell migration, expulsion, or gravity drainage, occurs continually within the growing ice structure, and significant salt is lost due to meltwater flushing during the summer. Thus, older first-year ice has a typical salinity of 4-6 psu, and multi-year ice (MYI), which has survived at least one melt season, can become nearly freshwater with salinities of only 1-3 psu (Wadhams, 2000). The advanced growth and movement of MYI by currents and wind also lead to increases in its thickness and ridging with age. Alternatively, in stable landfast conditions, meltponding and a dominant wind direction can lead to the formation of surface ridging on sea ice that remains in place over periods of years to decades, similar to the development of ice shelf rolls (Wadhams, 2000; Jeffries and Sackinger, 1990a).

Sea ice identification methods vary depending on the observation medium, but key identifiers for old ice have been established using the World Meteorological Organization (WMO)'s sea-ice nomenclature and the Manual of Standard Procedures for Observing and Reporting Ice Conditions (MANICE). Visual characteristics to identify MYI versus FYI include increased and interconnected ponding and drainage, increased thickness, a weathered hummock surface, and thick, less uniform snow cover (Johnston and Timco, 2008). Salinity, thickness, and surface feature differences create unique sensor spectral signatures that also allow for remote monitoring of sea ice extent and changes. For example, the Canadian Ice Service pairs satellite imagery with aerial observations, on-ice measurements, and ship-based observations to produce operational maps of sea ice conditions across northern Canada. Synthetic aperture radar (SAR) scenes are of particular use for monitoring sea ice in the CAA since they enable observations during darkness and cloud cover, and are sensitive to differences in ice surface roughness, salinity, and bubbles in sea ice (volume scattering), key identifiers of sea ice age.

1.2 Recent Sea Ice and Ice Shelf Changes in the Arctic

Arctic sea ice summer minimum extent has decreased at an average rate of 7.8% per decade during the period of modern observation, from 1953 to 2006 (Stroeve et al., 2007). Sea ice extent during the 2009 melt season reached the third-lowest level since 1979 when satellite observations began, bringing the negative trend in September extent to -11.2% per decade (NSIDC, 2009). In addition to an overall decrease in sea ice extent, there has also been a decrease in the average age and thickness of the remaining sea ice cover since the 1960s as old, multiyear ice is destroyed and replaced with thinner first and second year ice (Kwok, 2007; Maslanik et al., 2007; Nghiem et al., 2007; Rigor and Wallace, 2004; Wadhams and Davis, 2000). The decrease in proportion of this old perennial ice signifies a decrease in overall thickness of the Arctic sea ice mass, as well as an increased sensitivity to drift motion and summer melting. The total Arctic Ocean MYI volume has been reduced by 40% since 2005, and as a result, seasonal ice is now the dominant sea ice type in the Arctic Ocean (Perovich et al., 2010). Recent reductions in summer Arctic sea ice extent and the associated increase of open water areas in the Arctic Ocean have been linked to changes to large scale atmospheric circulation patterns, via the additional storage and fall release of heat from the ocean to the atmosphere (Overland and Wang, 2010).

Multiyear sea ice in the Canadian Arctic Archipelago that is attached to land is called multiyear landfast sea ice (MLSI). MLSI between channels and in fiords can form semi-permanent plugs, which may exist for decades and accumulate mass via snowfall on their surface and basal freeze-on of sea water. Decreases in these thick, stable MLSI plugs are highlighted in the 1998 breakups of the Nansen Sound and Sverdrup Channel ice plugs along the coasts of Ellesmere Island and Axel Heiberg Islands, respectively, which had been stable throughout most of the historical record (Alt et al., 2006). Similarly, the survival of MLSI in Yelverton Bay on the northern coast of Ellesmere Island since the late 1940s created an incipient ice shelf, until the sudden removal of almost its entire area in August 2005 (Copland et al., 2007).

Coincident with these MLSI changes, there has been a decrease in ice shelf extent in the Canadian High Arctic of more than 90% in the last century (Mueller et al., 2008). Ice shelves are thick, floating masses of ice formed primarily via the flow of grounded ice into the ocean, and are restricted in North America to areas > 82°N on Ellesmere Island. While glacier ice input may have initially promoted the formation of these ice shelves, current accumulation mainly relies on surface snowfall and basal freeze-on of sea water (Mueller et al., 2006). Driftwood deposition dates along the coast of northern Ellesmere indicate that multiyear landfast sea ice formation became prevalent around 5500 years BP, and that the current sea ice and ice shelf breakups are largely unprecedented since that time (England et al., 2008). A continuous "Ellesmere Ice Shelf," as observed by explorers in the early 1900s (Aldrich and Peary), has now broken apart (Jeffries, 2002), producing several well-documented ice islands and leaving behind ice shelves of varying sizes and compositions (Copland et al., 2007; Mueller et al., 2008). In just over a century, the total ice shelf area on northern Ellesmere Island was reduced from ~10,000 km^2 in 1906 (Vincent et al., 2001) to only 1,043 km^2 over 6 ice shelves in 2004. Recently, the losses of the Ayles Ice Shelf in 2005 and Markham Ice Shelf in 2008 have created additional open fjords along the NW Ellesmere coast (Copland et al., 2007; Mueller, 2011).

Multiyear sea ice frequently fills the areas vacated by calved and broken ice shelves along northern Ellesmere Island (Jeffries, 2002), and MLSI has been identified as a buffer to prevent landfast ice loss (Copland et al., 2007; Reeh et al., 2001). This suggests a relationship between the presence of MLSI in the CAA and the health and survival of the remaining ice shelves. However, very little analysis has been completed on the properties and characteristics of this MLSI, or on the historical changes of MLSI in the region. This study aims to examine these changes in detail, focusing on the MLSI remnants in Yelverton Bay and on the MLSI plugs in Nansen Sound and Sverdrup Channel. Field data and remote sensing image analysis will allow for a clearer characterization of the MLSI in order to examine the interactions between the reductions in floating ice, MLSI changes, and recent ice shelf breakup events along Ellesmere Island and the northern CAA.

1.3 Thesis Objectives

The overall goals of this project are to improve understanding of historical changes and characteristics of MLSI, the interactions between the reductions in floating sea ice and MLSI changes within the northern CAA, and the interactions between recent MLSI changes and ice shelf breakup events. This is undertaken via detailed analyses of:

1. Long term changes in the semi-permanent Nansen and Sverdrup MLSI plugs on northern Ellesmere and Axel Heiberg Islands.
2. Changes in the MLSI in Yelverton Bay on northern Ellesmere Island, focusing on its major losses since 2005.

Fieldwork completed in May 2009 provides the first detailed assessment of the remaining MLSI in Yelverton Bay. In turn, this provides ground-truthing of satellite scenes and air photos that aid in understanding the causes and characteristics of the previous MLSI breakup events from the ice plugs and fiords of northern Ellesmere Island.

1.4 Thesis Format

This thesis is presented in article format, with two manuscripts intended for publication. Chapter 2, "Recent Changes in Sea Ice Plugs along the Northern Canadian Arctic Archipelago," was written as a book chapter to be published in:

> Copland, L. and Mueller, D.R., (eds.). 2011. Arctic Ice Shelves and Ice Islands. Springer SBM, Dordrecht.

This work, consisting of a literature review and analysis of ice plug systems and their recent changes in the CAA, was written by Sierra Pope. Bea Alt and Luke Copland helped edit, revise, and analyze data, and are credited with secondary authorship. The chapter was peer-reviewed by two anonymous reviewers, revised, and has been accepted for publication.

Chapter 3, "Reductions in Multiyear Landfast Sea Ice in Yelverton Bay, Ellesmere Island, Nunavut, Canada" is written by Sierra Pope as a manuscript ready for submission to a publication such as "Journal of Glaciology". Luke Copland and Derek Mueller assisted with editing and data collection, and will be credited with secondary authorship. Chapter 4 provides a general conclusion that summarizes the findings presented in Chapters 2 and 3, and all references cited throughout the thesis are listed at the end of the document.

2. Recent Changes in Sea Ice Plugs along the Northern Canadian Arctic Archipelago

2.1 Introduction

There is strong evidence that Arctic sea ice extent is decreasing, with large area losses in 2005, 2007 and 2008 compared to the long-term mean (Stroeve et al., 2007; NSIDC, 2009), together with dramatic recent reductions in average sea ice age and thickness (Maslanik et al., 2007; Nghiem et al., 2007). Additionally, there is evidence of other cryospheric changes in the Arctic such as the melting and acceleration of outlet glaciers of the Greenland Ice Sheet (Rignot and Kanagaratnam 2006), the breakup and mass loss of the Ellesmere Island ice shelves (Vincent et al., 2001; Copland et al., 2007; Mueller et al., 2008; Mueller, 2011), and widespread melting of discontinuous permafrost (ACIA, 2005).

This chapter reviews recent changes in ice plugs, which are semi-permanent sea ice features that form across channels in the Queen Elizabeth Islands (QEI) in the Canadian High Arctic, north of 74.5°N. In the past they remained in place for decades, but they have largely failed to reform since major breakup events in 1998. When they remain in place for many years, these semi-permanent multiyear landfast sea ice (MLSI) features attain significant thicknesses via snow accumulation on their surface and ice accretion on their base. In turn, they often develop a rolling surface texture similar to that of many ice shelves in the Canadian Arctic (Jeffries, 2011). Recent changes to the ice plugs have occurred in tandem with ice shelf losses in the CAA (Canadian Arctic Archipelago); this chapter addresses the history of these MLSI features and the mechanisms surrounding their breakups. This may provide insights into the long-term formation and stability of Arctic ice shelves.

The recent response of Arctic sea ice to changing climate conditions assists in putting ice plug changes in context. Observations from 1953 to 2006 indicate that end of summer minimum Arctic sea ice extent has decreased at an average rate of 7.8% per decade (NSIDC, 2007). The record low sea ice concentrations in four out of the last five summers (2005, 2007, 2008, 2009) show that these losses have accelerated, with September average ice extents declining at 11.2% per decade (NSIDC, 2009) relative to the 1979-2000 average. The increasing melt of first year ice (FYI), formed during the previous winter, is coupled with a decrease in area and thickness of floating multiyear ice (MYI), sea ice which has survived at least one melting season (Maslanik et al., 2007; NSIDC, 2009). An increased percentage of the total Arctic sea ice cover is therefore now first year ice, representing a significantly thinner and weaker barrier between ocean and atmosphere. The breakup and subsequent melting of the thick, multiyear ice plugs and their replacement by thinner, annually-melting first year ice represents a rapid reduction in sea ice thickness and exemplifies the limited recovery of the old ice regime since 1998 within the CAA.

2.1.1 Definition and Significance

Atmospheric circulation patterns in the Canadian High Arctic typically result in thick, multiyear sea ice being pushed against the northwest edge of the QEI (Agnew et al., 2001; Jeffers et al., 2001). This process contributes to the formation of MLSI, described in detail by Jeffries (2011). This multiyear sea ice forms semi-permanent blockages, known as ice plugs, at the head of channels between islands. The presence of these decades-old plugs can act as effective barriers against movement of pack ice from the Arctic Ocean into the interior channels of the QEI (Jeffers et al., 2001; Agnew et al., 2001; Kwok, 2006).

There is some disagreement about the terminology of sea ice blockages in these regions, so here we follow the definitions of Alt and Lindsay (2005). Ice arches or ice bridges are defined as structurally controlled, short-lived summer features that occur between narrow points of land surrounding a channel, sound, or between islands (e.g., Nares Strait; Figure 2.1). Ice barriers are generally poorly defined, but are taken here to consist of large areas of consolidated ice at the border between the Arctic Ocean and the channels and seas of the QEI (e.g., Peary Channel, Figure 2.1). Finally, ice plugs are small areas of consolidated perennial sea ice formed between narrow points of land, and are defined largely by their longevity/presence over decades. In the Canadian High Arctic there are only two ice plugs known to have existed over the past century: the Nansen and Sverdrup (Figure 2.1). These are the focus of this chapter.

The Nansen Sound and Sverdrup Channel Ice Plugs have been observed as perennial ice features since the first exploration of the Canadian High Arctic in the early 20th century. Peary described that the entire northern coastline of Ellesmere Island was fringed by a permanent body of ice in 1907, continuing across Nansen Sound, a blockage now known as the Nansen Ice Plug (Vincent et al., 2001). The ice plugs form due to the in situ growth and agglomeration of sea ice in narrow channels in the coldest, most northerly parts of the QEI, where nearby land pins them in place and summer melting is insufficient to remove them (Jeffers et al., 2001; Serson, 1972). Their formation is also supported by the fact that the Beaufort Gyre typically pushes thick, old sea ice towards the northwest coast of the QEI. This has the effect of providing a near-continual supply of additional ice and protects their northern margins from wave action. Once formed, the sea ice within ice plugs typically remains landfast and builds over time via snow accumulation and basal freeze-on of sea water.

These ice plugs are subject to in situ fracture and melting during the summer, but have retained their old MLSI for much of recorded history in this region. While each of the ice plugs has experienced occasional individual breakups, the particularly warm summer of 1998 saw the breakup of both ice plugs for the first time since 1962 (Table 2.1) (Alt et al., 2006; Jeffers et al., 2001). Since 1998 the MLSI ice plugs have largely failed to reform, and in this chapter we describe the climate and synoptic conditions which contributed to both earlier breakup events and the recent changes.

2.2 Regional Background

Sea ice atlases published by the Polar Continental Shelf Project (PCSP) provide data on ice plug conditions between 1961-1978 (Lindsay, 1975, 1977, 1981). Ice charts produced by the Canadian Ice Service (CIS) provide coverage of the ice plugs from 1960-present, and weekly regional ice charts are available online from 2003-present, detailing recent plug activity (http://ice-glaces.ec.gc.ca/). Early CIS charts used visual reconnaissance from ships and aircraft to determine sea ice concentration and types; this has been supplemented over time with meteorological satellite imagery (visual and thermal bands, ~1-4 km resolution), and most recently by radar satellite imagery (~25-200 m resolution) from sensors such as ENVISAT and RADARSAT-2. Data sources prior to 1960 are sparse and consist largely of visual observations associated with expeditions to the northern QEI (Peary, 1907; Sverdrup, 1904; Stefansson, 1938). A comprehensive survey of sea ice in the QEI was completed by Black (1962), who observed the fracturing of the Nansen and Sverdrup Ice Plugs and a subsequent movement of polar-basin ice into the interior passages of the QEI. Melling (2002) completed an overview of the region's sea ice conditions using CIS digital ice chart archives from 1970 to 1999 and ice thickness measurements. His study indicated that landfast ice at 10/10ths concentration covers the Sverdrup Basin for over half the year, with 9/10ths ice presence during the summer months and a minimum ice extent in early September. The semi-permanent Sverdrup and Nansen Ice Plugs are a noted exception to this summer disintegration, remaining fast in most years of the study (Melling, 2002). The Climate Change Action Fund (CCAF) Summer 1998 Project team (http://www.socc.ca) completed a comprehensive review of cryospheric variability in the Canadian Arctic over the anomalously warm summer of 1998. This included analysis of the 1998 Sverdrup and Nansen Ice Plug breakups, as well as comparisons of regional temperature, wind, and sea ice coverage patterns surrounding these events (Alt et al., 2001; CCAF, 2001; Jeffers, 2001; Jeffers and McCourt, 2001).

Sea ice flux, near Sverdrup Ice Plug, was estimated using AMSR-E and scatterometer image data at 2 ±6 x 10^3 km^2 yr^{-1} from the Arctic Ocean to the northern QEI between 1997-2002 (QEI-North Flux Gate in Kwok, 2006). Agnew et al. (2008) calculated no net ice flux between 2002-2007 for the same region, noting lower annual variability in motion than the westerly regions of the northern QEI. The limited movement through this northern gate, which demonstrates the landfast nature of the sea ice in this region, suggested limited winter ice movement even without the presence of the northern plugs. However, recent behaviour of sea ice in response to extremely warm summers (decreasing ice proportion and increasing ice movement), suggests that the areas of mobile sea ice and the open-water limit will continue to move northward (Jeffers et al., 2001, Agnew et al., 2008). Regional studies of multiyear sea ice activity from 1968 to 2006 by Howell et al. (2008) indicate recent apparent increases in dynamic import of multiyear ice through the QEI. This is consistent with evidence of weakening multiyear ice barriers in the QEI (Alt et al., 2006). Old sea ice import and export in Sverdrup Channel was assessed by Alt et al. (2006) following the 1998 plug breakup, who concluded that significant loss of old ice occurred there via melt and its movement out of the channel. Limited import of old Arctic Basin sea ice into the channel was observed in 1999 and 2005, and significant through-flow of old ice was observed in 2000 (Alt et al., 2006).

The location of the QEI at a critical boundary between the ice-covered Arctic Ocean and open-water Baffin Bay creates difficulty in isolating a distinct system of synoptics to characterize weather behaviour in this region (Alt, 1987). Early mass balance studies in the northern QEI were completed by Koerner (1977, 1979), and indicated low snow accumulation rates in the colder, dry interior of Ellesmere/Axel Heiberg Islands and higher accumulation rates along the Arctic Ocean between Ellesmere Island's northwest coast and Meighen Island (Figure 2.1). The relationships between regional synoptics and mass balance were studied by Alt (1979, 1987), who developed a categorization of summer atmospheric circulation around Meighen Island. These synoptics were revisited by Gardner and Sharp (2007) in an assessment of High Arctic glacier mass balance, and are further discussed in Section 2.4 to provide a context in which the region's MLSI breakups can be better understood.

2.2.1 Nansen Ice Plug

The Nansen Ice Plug occurs at the northern edge of Nansen Sound, between Ellesmere and Axel Heiberg Islands (Figure 2.1). All available evidence points to the fact that it existed as a near-permanent feature for most of the 20th century. For example, while crossing the northern section of Nansen Sound in 1906, Peary noted that the ice in the Sound appeared contiguous with the glacial fringe along Ellesmere's northwest coast (Peary, 1907). Visual observations of new pressure ice and open water north of Axel Heiberg Island from a 1932 expedition suggest minor fracturing in the plug at that time (Krüger Search Expeditions 1934), but that the blockage was still in place. The first formal sea ice surveys of this area also note its presence (Black, 1962), and the plug appears on all ice charts from the beginning of the regional record in 1961 (Alt et al., 2001). The first detailed studies of this plug were completed by Serson in 1970-1971, who estimated an ice thickness of >6 m at the plug's northern edge and 10 m near the southern edge. The rolling ice surface featured hummocks ranging in height from 1-3 m (Serson, 1972). Hummock heights increased across the plug, from the Ellesmere Island side with 60 cm of snow cover to the wind-polished ice on the Axel Heiberg side (Serson, 1972). The plug was observed later by Jeffries et al.

(1992), who concluded that the Nansen ice mass fitted the characteristics of neither an ice shelf nor a large sea ice block, but instead consisted of an 'agglomeration of ice of different ages and thicknesses... subject to rearrangement of its component floes'. This complicated floe matrix indicated that the plug may be unstable and subject to rearrangement or disintegration (Jeffries et al., 1992).

2.2.2 Sverdrup Ice Plug

The Sverdrup Ice Plug occurs at the northern edge of Sverdrup Channel, between Axel Heiberg and Meighen Islands (Figure 2.1). In this region, thick multi-year sea ice that is pushed by the polar ice pack from the northwest in the summer and fall meets a ridged mix of first year, second year and multi-year ice to the south (Melling, 2002). The resulting MLSI plug creates a semi-permanent feature that is clearly identified in early sea ice maps (Black, 1962; Alt et al., 2001). Sverdrup (1904) described the ice in the channel as 'going up and down in waves', indicating the rolling surface typical of MLSI and Arctic ice shelves. The curved northern boundary of this ice plug was observed in 1916 by Stefansson (1938), and appears to be the same in aerial photography from 1950 and 1959 (Serson, 1974). Spot depth measurements were conducted on the ice plug in the early 1970's by Serson (1974), who identified ice up to 6 m thick near its northern margin on the Axel Heiberg side. The ice surface was rolling, paralleling the dominant northwest winds and featured steep-sided hummocks and melt pools extending downwind and undercutting the hummock sides (Serson, 1974). The position of Sverdrup Ice Plug makes it the more vulnerable of the two plug features and thus more frequently broken (Table 2.1). Open water areas to the north and south of the plug, and frequent lead development north of Meighen Island, leave the Sverdrup Plug less protected from wind and ocean currents than the Nansen Plug. In addition, frequent sea ice fracturing occurs adjacent to the Fay Islands (Figure 2.1), located directly to the south of the Sverdrup Plug.

2.3 Chronology of Recent Ice Plug Breakups and Activity

Previous observations of the behaviour of the ice plugs has been undertaken via ground surveys (1900+), aerial reconnaissance (1960s-1980s) and satellite image analysis (1990s+) (Alt et al., 2006; Black, 1962; Jeffers et al., 2001; Jeffries et al., 1992; Serson, 1972, 1974). In this study, we use previously published papers and reports, ice charts from the CIS and

PCSP, and satellite imagery to quantify the presence/absence and area changes of the Nansen and Sverdrup Ice Plugs since the early 1960s (Table 2.1). Over this time the plugs have been semi-permanent features, with only limited fracturing occurring in most years. However, the breakup of one or both of the ice plugs has occurred in 11 years during the recorded period (Table 2.1). Simultaneous breakups of both plugs occurred only twice in the last half of the twentieth century, but have occurred frequently within the first decade of the 2000s. The chronology and detailed characteristics of these events is presented below.

2.3.1 1962 ice plug events

The first recorded breakup of either of the ice plugs occurred in summer 1962, when they both broke up during an extremely warm period characterized by high temperatures at all climate stations in the QEI. This summer featured the highest percentage of open water in channels of the QEI from 1961 until the extreme light ice year of 1981 (Jeffers et al., 2001). The Ward Hunt Ice Shelf also experienced a significant calving event in 1961/1962, forming several ice islands and reducing the size of the 'Ellesmere Ice Shelf' of the early 1900's by 596 km^2 (Hattersley-Smith, 1963). In terms of glaciers in this region, Koerner (1979) states that 1962 was the most negative mass balance year over the period 1960-1977, noting that significant melt was so widespread at high elevations over the ice caps of Devon, Ellesmere, and Axel Heiberg Islands that the 1962 melt layer is used as a reference horizon in ice core stratigraphy.

Black (1962) observed the breakups of both ice plugs in 1962, noting fracturing around Meighen Island beginning in early August during dominantly NW, N and NE winds at 10-14.7 knots (5.1-7.6 m s^{-1}). The ice atlas images for August and September 1962 demonstrate the temporal progression of the Nansen and Sverdrup Plug breakup events (Figure 2.2; Lindsay, 1975). The August 4-5, 1962 image shows solid ice in both Nansen Sound and Sverdrup Channel that had not yet experienced any fracturing that summer (Figure 2.2a). In contrast, the August 26 to September 5, 1962 (the time of maximum open water for the season) composite ice chart, shows a broken Nansen Plug with a large, refrozen plug fragment present at the channel's northern edge and a weakened, pre-breakup Sverdrup Plug (Lindsay, 1975). There are no ice charts of the plug area after September 5, 1962, but late September ice charts from the region directly south of Meighen Island show 8/10 old ice and

1/10 young ice, suggesting that the Sverdrup Plug area had fractured. Moreover, direct observation by Black (1962) confirms that the Sverdrup Ice Plug experienced complete breakup in the 1962 melt season.

2.3.2 1963-1997 Ice Plug Events

In 1963, both the Nansen and Sverdrup Ice Plugs appear to have been re-established based on spring map and air photo observations. Between 1963 and 1997, occasional individual breakups and fractures of the plugs were observed. The Nansen Plug remained stable until 1971; on August 11 of that year an area of open water was observed in Nansen Sound, and by September 6, 1971, the plug had completely broken up (Lindsay, 1977). First-year ice in Nansen Sound on ice charts from spring 1972 provides evidence of the previous year's breakup (Lindsay, 1977). Despite open water to the south of the Sverdrup Ice Plug and along Meighen Island, the Sverdrup Plug remained intact in 1971 (Lindsay, 1977). The Sverdrup Plug experienced a breakup in 1975, observed on a September 21, 1975 flight, while the Nansen Plug remained solid throughout 1975. A flight directly over Meighen Island for the September 30 - October 9, 1977 sea ice atlas chart observed a solid (10/10) Nansen Plug and a late season Sverdrup Plug fracture and breakup in 1977 (Lindsay, 1981). Regional ice charts indicate that in the following year the weak first-year ice in Sverdrup Channel broke, but the Nansen Plug remained fast.

In 1981 there was extensive open water in the QEI, as evidenced in the sea ice coverage data provided by the CIS (Figure 2.3a). However, there was no identified breakup of the Nansen or Sverdrup Plugs in this year despite the warm summer temperatures and high percentage of open water. Generalized ice chart coverage in August and early September of 1981 suggests that there may have been limited fracturing in the plug areas, but the September 8 regional chart indicates 10/10 ice in clearly outlined plug areas. Daily temperature and wind data indicates that temperatures dropped below freezing in the last week of August and winds shifted from S/SW to SE during the second half of the month. This change in temperature and wind direction could have limited any possible early plug fracturing from becoming full break-ups during 1981.

2.3.3 1998 Ice Plug Events

In 1998 the melt season began early, characterized by a high pressure ridge, creating warm southerly flow, increased solar radiation due to clear skies, and above-normal spring temperatures. This continued with high summer air temperatures, high melt percentages of first and multi-year sea ice, and a long melt season (Figure 2.4a; Jeffers et al., 2001). Based on an analysis of CIS Regional Ice Analysis Charts and RADARSAT ScanSAR Wide (SCW) imagery, Jeffers et al. (2001) found that the sea ice was significantly weakened during this summer, with a notable maximum of open water and the latest maximum open water date (Sept. 28) in the 38-year period since 1961. Areas of light ice conditions in the QEI (less than 1/10 sea ice) were more prevalent in 1998 than in the years preceding it (Figure 2.3b), and the larger areas of open water and greater dispersal of sea ice exacerbated the ice decay.

Between August 17 and 24, 1998, the Sverdrup Plug fractured and a large piece of the Nansen Plug broke off as a single ice mass. The large areas of open water to the south of the plugs facilitated the southward movement and melt of some of the plug fragments (Jeffers et al., 2001); however, some large fragments survived to return to the plug area as the wind direction shifted. New ice growth in the fractured plug region began between August 31 and September 7, 1998, with a RADARSAT-1 image from September 21 (Figure 2.5) indicating a portion of landfast ice which had remained intact along the margin of Nansen Sound, and the formation of new nilas and grey ice south of this location. Jeffers and McCourt (2001) attribute this new ice formation to decreasing maximum temperatures measured at Eureka (Figure 2.4a), and to the light and variable winds near the channel.

A contributing factor that made 1998 an unusual year was the fact that between September 21 and 27, 1998, a low-pressure system brought warmer than average temperatures and strong southerly winds to the area. A surface low pressure system then moved northeast through the region behind an upper warm trough and brought gale force winds to Sverdrup Channel and winds >20 knots (10.29 m s^{-1}) to Nansen Sound (Alt et al., 2006). These factors completed the final breakup of the Nansen Ice Plug and completely dislodged the Sverdrup

Ice Plug, melting and fracturing the new ice which had formed in the previous month (CCAF, 2001).

The impact of these strong winds is indicated in RADARSAT-1 images from September 21 and 28, 1998, which show the damage sustained to the regional MLSI (Figure 2.5). In the September 28 image, pieces of the broken Nansen Plug are visible north and east from its original position, and the area to the south of Nansen Sound does not feature the newly formed nilas ice from earlier in the month. Sverdrup Channel is clear of ice, with open water as far north as Meighen Island. The remnants of the Sverdrup Plug are not identifiable; Jeffers and McCourt (2001) suggest that they may have melted completely or drifted and were incorporated into the Arctic Ocean ice pack, while Alt et al. (2006) suggest they returned to the plug area when the winds shifted to northwesterly behind the storm track.

2.3.4 1999-2005 Ice Plug Events

The response of the Nansen and Sverdrup Ice Plugs to the extreme summer of 1998 continued well into the following year. Alt et al. (2006) present an overview of the movement of ice in Sverdrup and Peary Channels between the 1998 extreme breakup events and 2005 (Table 2.1). The reformed ice in southern Nansen Sound broke again in the summer of 1999, but an absence of strong winds allowed it to stabilize as an in situ blockage. Wilson et al. (2004) note that reformation of the Nansen Plug appeared to consist of a different type of ice than had been previously found there, forming from in situ landfast ice, as opposed to the Arctic Ocean MYI floes combined with FYI that dominated before. The Sverdrup Plug fractured in both summer 1999 and 2000, which allowed ice to move from Sverdrup Channel north to the Arctic Ocean. The freeze-up in Sverdrup Channel occurred over 3 weeks earlier in 2000 than in 1999, due to a weather system that enhanced the flow of cold air from the north.

Summer 2001 was characterized by a relatively cold summer season (Figure 2.6a) with heavy old-ice presence and early freeze-up, featuring the first summer without a Sverdrup Plug breakup since 1997 (Alt et al., 2006). The Sverdrup Plug remained stable in 2002, but in 2003 an early melt season and complete FYI loss lead to its fracturing, although the ice remained in place. The plug also fractured in situ in 2004, following a short melt season and very limited ice loss, and in late August 2005 it broke up once again. The Nansen Plug also broke up in August 2005, after maintaining relative stability since its 1998 breakup. The simultaneous breakup of the Nansen and Sverdrup Plugs in 2005 was not matched by the light sea ice conditions of the previous breakup events (Alt et al., 2006), although many other ice losses also occurred along northern Ellesmere that summer. For example, almost the entire 87.1 km^2 Ayles Ice Shelf was lost during a strong offshore wind event on August 13, 2005, together with the removal of 330 km^2 of young MLSI and 690 km^2 of 58+ year old MLSI from Yelverton Bay (Copland et al., 2007).

The frequent fracturing of the Sverdrup Plug and the 2005 simultaneous breakup event suggest that a solid recovery of the plugs did not occur after the extreme summer of 1998. Alt et al. (2006) and Wilson et al. (2004) used CIS digital ice charts from 1997 to 2003 to track ice movement and gains/losses of MYI from Sverdrup and Peary Channels, and found that the removal of the ice blockages has allowed for increased movement southward of old ice through the QEI.

2.3.5 2006-2008 Ice Plug events

CIS weekly ice charts and MODIS satellite imagery were used to determine the activity of the ice plugs between 2006 and 2008 (Table 2.1). Summer 2006 featured less ice loss and earlier regional freeze-up than in summer 2005. The Sverdrup Plug, now consisting of first year and refrozen pack ice, remained solid, and the Nansen Plug fractured in situ in late August 2006. Ice charts from August 28, 2006, indicated 9+/10 ice in the Nansen Plug area, with areas of 1/10 - 2/10 ice alongside both plugs.

The Sverdrup Plug fractured in early August 2007 and broke away completely between August 20 and 27, 2007, allowing for the movement of pack ice and a piece of the Ayles Ice Island into the southern part of Sverdrup Channel (Van Wychen and Copland, 2011). The Nansen Plug also broke up in mid-August 2007.

CIS ice charts from 2008 indicated reductions in sea ice concentration along the northwestern coast of Ellesmere Island and throughout the study region compared to the two previous years, and show fracture and breakup of both ice plugs between July 31 and August

4, 2008. MODIS images show the process of breakup and export of this ice (Figure 2.7). The breakup of the plugs occurred during a period of very strong wind and wind reversals; marine wind prognosis charts indicate strong southeasterly winds at up to 35 knots (18 m s^{-1}) moving directly parallel with both Sverdrup Channel and Nansen Sound on August 2, 2008 (M. Schaffer, pers. comm., 2009). The Sverdrup Plug area remained filled with fractured ice through the second week of August 2008, when northerly winds dominated the region, but by August 17, 2008, both plugs had completely cleared.

2.4 Discussion

Over the past 50 years (prior to 2008), our analysis indicates that both the Sverdrup and Nansen Ice Plugs broke up in 1962, 1998, 2005, 2007 and 2008 (Table 2.1). Individual breakup or fracture events are less representative of a systematic or regional signal than the instances where the MLSI plug features were removed from both regions of study simultaneously; therefore, our classification and discussion of weather events is focused on these dual breakup events. Dual breakups have occurred during five of the six warmest summers on record at Eureka, and correspond with five of the six highest incidences of melting degree days (MDDs) (Figure 2.6b). Many of the breakups also occurred during strong regional wind events with a southerly component, making it clear that the plug breakups are strongly related to regional weather patterns.

2.4.1 Weather systems affecting the CAA

The Nansen and Sverdrup Ice Plugs respond to weather systems which have been described in detail by Alt (1979, 1987) and Gardner and Sharp (2007). Alt (1979, 1987) developed a classification system of three distinct synoptic systems for the Canadian High Arctic based on the summer position and characteristics of the 500 mb circumpolar vortex, a midtropospheric cyclonic system with counterclockwise winds moving around a cold polar air mass (Table 2.2). Further discussion and examples of each synoptic type can be found in Alt (1979). Following this classification system, Gardner and Sharp (2007) described the relationship between arctic circumpolar vortex variability and glacier mass balance in the Canadian High Arctic. As regional weather patterns associated with these synoptics have distinct influences on the behaviour and survival of sea ice in this region, the synoptic types are useful in explaining the breakup of the ice plugs.

Synoptic Type I of Alt (1979, 1987), Polar Arctic Circulation, describes conditions dominated by a high pressure system in the Arctic Ocean to the west of Meighen Island and a low pressure system over Baffin Bay. Low stratus or fog is carried from the Arctic Ocean pack ice to the northern QEI via northerly flow during this circulation type, resulting in limited precipitation as generally trace amounts of drizzle, freezing drizzle or snow. The winds are then controlled by the Baffin Bay low, with the related upper cold low leading to frequent storm tracks from the north continental coast of mainland Canada to Baffin Bay (Alt, 1979). Type I scenarios are used by Alt (1979, 1987) to explain periods of low MDDs on Meighen Ice Cap, when there is a 'suppression of ablation'. Type I features the lowest occurrence of MDDs of the three scenarios. When combined with frequent northerly and northwesterly wind flow, limited wind reversals, and frequent fog blocking solar radiation, this reduces the potential for Type I systems to cause multiyear sea ice melt and breakup.

Synoptic Type II, termed Cyclonic System Circulation, occurs when there is a notable 500 mb cold low over the Beaufort Sea region. The frontal systems between the radiatively heated Siberian and Alaskan landmasses and the colder polar ocean pick up moisture over the peripheral ice-free ocean areas and move around the upper cold low (Alt, 1979). This results in a tracking surface low and developed frontal zones along the upper edges of the CAA, low temperatures and significantly high precipitation. The differences in precipitation type produce a secondary classification into Type IIs (tracking cyclone with snow) and Type IIr (tracking cyclone with rain). Type II systems feature strong winds and potential wind direction reversals, but do not feature the high temperatures and solar radiation which would facilitate ice weakening and MLSI breakup.

Synoptic Type III, termed Island Circulation, occurs when a low at the 500 mb level is positioned on the Asian side of the Arctic Ocean and a ridge develops at all levels over the eastern CAA and Greenland. A warm ridge in eastern North America can dominate air flow, causing the western Arctic to experience higher temperatures, lighter winds and increased solar radiation reaching the ground and ice surface. Gardner and Sharp's (2007) classification system, using the circumpolar vortex position and strength, present a corresponding synoptic condition to Alt's Type III, which they refer to as Type I-B. This situation features a vortex centered in the Eastern Hemisphere that is either weak or strong with no trough reaching into the Canadian High Arctic, and is associated with warm air temperatures and extreme negative glacier mass balances in the region (Gardner and Sharp 2007). Circulation Type III frequently develops only partially, but even this is enough to produce clear, warm weather and southerly wind flow over Meighen Ice Cap. Alt's (1979) data for this synoptic type features significantly more MDDs over the measured period than the other two synoptic conditions. Additionally, Type III is identified as bringing storms northward and creating southerly and easterly winds, tracking from the land surfaces rather than the Arctic Ocean. Intrusion of well-developed mid-latitude frontal systems are also observed in Type III cases, leading to strong winds in the QEI and rapid wind direction reversals. Preconditioning of the ice by high MDDs and disturbance by strong, changeable winds strongly impact the ability of local freeze-up to maintain or rebuild ice.

2.4.2 Synoptic controls on ice plug breakup events

These synoptic situations indicate that the position of low pressure systems (and the Polar Vortex) is of vital importance to local climate, influencing both temperature and wind patterns and snow and ice changes in this region. The high summer temperatures associated with Type III synoptic patterns increase the likelihood of ice plug breakup, as demonstrated by the occurrence of warm temperatures at Eureka during years of known ice plug losses (Figure 2.6a). The dynamic system of lows in the CAA means that there is potential for significant wind direction reversals. These wind shifts enhance both ice melt, via warm southerly flows, and ice removal in the northern QEI, with northerlies transporting the melted and separated ice southward away from its origin.

Summer 1962 is identified via several climatic parameters as a clear example of a dominantly Type III synoptic condition. Alt (1987) notes that a ridge extending from Hudson Bay to the QEI in early June 1962 led to near-melting temperatures in the region. This was followed by well above normal seasonal temperatures at most stations in mid-July, corresponding to significant anticyclonic circulation, and well above normal temperatures at the remaining stations in late July, during the passage of the warm frontal system (Alt, 1987). Similarly, the high summer temperatures and winds in summers 1998 and 2008 provided ideal conditions for the final fracture and removal of the Nansen and Sverdrup Ice

Plugs. Gardner and Sharp (2007) describe a weak, Eastern Hemisphere centered 500 mb Arctic circumpolar vortex in July 1998 (categorized as their Type 1-B condition), which created warm July surface air temperatures and a very negative regional mass balance that summer. Conditions just before the simultaneous plug breakup in 2008, illustrated in an NCEP/NCAR reanalysis for July 28, 2008, exemplify a Type III synoptic condition (Figure 2.8), which contributed to the strong southeasterly winds associated with the 2008 breakup events.

2.4.3 Comparisons between Nansen and Sverdrup Ice Plug breakup events

As discussed above, well above normal summer temperatures and sea ice melt occurred during all of the years in which both the Nansen and Sverdrup Ice Plugs broke. However, there is a distinction of scale between the two earlier and three latest breakups. The older 1962 and 1998 breakup events occurred as anomalous removals of decades-old MLSI plugs within a context of infrequent break-up events and long periods of stability. In contrast, the more recent events consist of the almost annual fracture and breakup of FYI and young MYI (Table 2.1). This facilitates a classification of the simultaneous breakups into two distinct groups: early (1962 and 1998) and recent (2005, 2007, 2008).

In the early period, Alt et al. (2001) indicate a similarity between the July mean 500 mb pattern in 1962, noted by both Alt (1987) and Gardner and Sharp (2007) as a significant negative mass balance and open water situation, and the 500 mb pattern for spring 1998. Jeffers (2001) notes that the temperature patterns preceding the 1962 and 1998 breakup events were very similar, although melt in the region of the plugs was much higher following the 1998 breakups than the 1962 events. In 1962, the Sverdrup Ice Plug broke, but the ice did not clear into the Arctic Ocean in the same way that it did in 1998. In summer 1962, the climatology featured strong southerly flow and a freeze-up beginning 3-4 weeks earlier than in 1998. This explains the moderate post-breakup melting in 1962, whereas in 1998 the open water season lasted until late September and late summer storms delayed the fall freeze-up (Alt et al., 2001). Daily mean temperatures at Eureka showed a steady decrease in late August and September 1962, whereas they remained close to 0°C through the end of September 1998 (Figure 2.4b). The extension of warm temperatures into fall 1998 is the most significant difference between the 1962 and 1998 situations, and these increased temperatures impacted the timing of freeze-up around the ice plugs.

In the recent period, ice plug breakup events have occurred in young MYI (2005 and 2007) or in FYI (2008). There is a strong connection between sea ice age and thickness, which in turn determines its ability to withstand melt and wind forcing (Maslanik et al., 2007). This is evident in the timing of the three latest breakups: the 2005 and 2007 breakups occurred in mid/late August, whereas the 2008 breakups of FYI occurred at the beginning of August. Daily mean temperatures from Eureka show very little difference between years which featured complete plug breakups (2005, 2007, 2008) and years with no breakups or with single plug fractures (2004, 2006). A more important variable associated with these recent simultaneous breakup events is the presence of a lead of low sea ice concentration along the northern edges of the plugs, occurring as the pack ice is pushed away from the land. CIS ice charts indicate that prior to the 2005 breakups, a lead with 5/10 sea ice concentration developed along the coast across all of Nansen Sound and extended into Sverdrup Channel. In 2007, sea ice at 1/10 concentration bordered the northern coast in the two weeks preceding the plug breakups. Similarly, in 2008, 2/10 concentration sea ice was present along the plugs' northern borders one week prior to their breakups. This area of low-concentration ice (lead) was not present in 2004 or 2006; these years feature sea ice at 9+/10 concentration flush against the fast coastal ice. This suggests that the concentration of sea ice present between the Arctic Ocean and the plugs' northern edges is an important factor in the survival or breakup of ice in these waterways. A relationship between low sea ice concentrations and landfast ice breakup events has been identified in several recent studies; Copland et al. (2007) relate the 2005 Ayles Ice Shelf breakup in part to reductions in the MLSI buffer along the ice shelf front, and Reeh et al. (2001) observe the calving of a floating glacier in NE Greenland following the loss of its MLSI fringe. Similarly, the presence of a lead at the MLSI plug edge can reduce the stability of the landfast ice features; Mahoney et al. (2007) suggests that this is caused by wave action or solar radiation absorption by the adjacent open water.

2.5 Conclusions

From the review presented here, it is clear that the creation of ice plugs is gradual and takes many years, requiring summer climate conditions of cool temperatures and frequent northwesterly winds. The plugs have historically resisted breakup due to their thick ice and because of the presence of anchoring land on either side. The breakup events, on the other hand, have occurred rapidly during warm summers characterized by an early melt season and long warm periods sufficient to produce significant surface melting and a weakened plug structure. These conditions are typically associated with Alt's (1979, 1987) Type III synoptic system when a warm ridge dominates eastern North America, bringing southerly winds, warm temperatures, and high wind speeds with reversals in direction. For the complete breakup of both MLSI plugs to occur, as happened in 1962 and 1998, there must also be weakening of the surrounding sea ice. For example, Jeffers (2001) discusses the importance of high proportions of open water to the south of the ice plugs, which weakens the protective matrix around them, adding tension to the system and facilitating greater fracture and movement of the ice plug pieces.

An important second phase of the breakup process is the requirement for strong storm systems to move through the region, which fracture the pre-weakened ice plug. This was particularly evident in the case of the 1998 plug losses, when a low pressure system and high winds in mid to late August created a forcing strong enough to cause a distinct fracture in the Sverdrup Plug and complete breakage of the Nansen Plug. Continued warm weather into fall 1998 facilitated open water conditions northward into Sverdrup Channel and the removal of the last piece of the Nansen Plug. Higher summer temperatures in recent decades have created a backdrop of less ice and more snow-free land and open water; this results in storms that draw in moisture, track along the land edges, and behave more distinctly like southerly storms. For example, Gardner and Sharp (2007) note that their Type I-B synoptic condition, associated with Alt's Type III classification (1979) and exemplified by the 1962 and 1998 weather systems, created a temperature system in the high arctic which was 'almost thermally homogeneous with continental North America'.

Following the 1998 breakups, the patterns of late fall sea ice buildup appear to have changed. Since 1998 there has not been a classifiable 'extreme heavy ice year' in the northern QEI. This is in contrast to the 1962 breakups and the extreme light ice year of 1981, after which there were heavy ice years recorded within 5 years, which aided in the recovery of the plugs and local MLSI. The plug breakup events of 1962 and 1998, occurring in conditions of thick MLSI, represent responses to anomalous years of high average MDDs, high proportions of open water, and extreme southerly wind events and wind reversals. The recent lack of old ice recovery in the northern QEI means that the plug breakups and fractures since 1998 have occurred in conditions of young MLSI or first year ice. Significant inter-annual variability in ice conditions within the 1960-2008 measurement period and the 2005, 2007 and 2008 breakups indicate a changing sea ice regime around the plugs. The two-part plug breakup process can now be placed within the context of the younger, thinner Arctic ice regime, suggesting limited plug recovery in the future.

One of the major potential impacts of recent ice plug losses is the increased ability of old sea ice to move from the Arctic Ocean in to the CAA. For example, Black (1962) observed that the 1962 Sverdrup Plug clearing allowed for a significant movement of MYI from the Arctic Ocean into the QEI between late 1962 and fall 1963. Simultaneously there was a northward movement of the open-water limit, which was largely attributed to the extreme summer air temperatures contributing to sea-surface temperature increases (Jeffers et al., 2001). More recently, Howell et al. (2009) found an increase in dynamic import of MYI from the Arctic Ocean into the QEI.

The removal of the Nansen Sound and Sverdrup Channel Ice Plugs represents only part of the destabilization of previously landfast sea ice in the northern CAA. The breakups of these ice plugs have occurred in tandem with the removal of significant areas of ice shelf and MLSI from embayments along northern Ellesmere Island. The loss of landfast sea ice in this region represents an increase of open water and the removal of an important buffer against further old ice export and ice shelf breakup.

Table 2.1: Recorded breakup and fracture events of the Sverdrup and Nansen Ice Plugs, 1961-2008[a].

	Sverdrup	Nansen
1961	▨	⧄
1962	■	■
1963	▨	⧄
1964	□	□
1965	□	□
1966	□	□
1967	▨	▨
1968	▨	□
1969	▨	□
1970	□	□
1971	□	■
1972	□	□
1973	□	□
1974	□	□
1975	■	□
1976	□	□
1977	■	□
1978	■	□
1979	□	□
1980	▦	▦
1981	▦	▦
1982	□	□
1983	□	▨
1984	□	□
1985	□	□
1986	▨	□
1987	□	▨
1988	▦	▦
1989	▦	▦
1990	□	□
1991	▦	□
1992	□	□
1993	□	□
1994	▦	▦
1995	▦	□
1996	□	□
1997	□	□
1998	■	■
1999	■	□
2000	■	□
2001	□	□
2002	□	□
2003	▓	□
2004	▓	□
2005	■	■
2006	□	▓
2007	■	■
2008	■	■

■ break-up
▓ fracture
▦ possible fracture
▨ likely no breakup
□ no breakup
⧄ no data

[a] Years without complete melt season coverage of the plug areas are analyzed for possible breakups via ice codes and concentrations at the end of the summer or the behaviour of the plug ice the following spring. Instances where in situ fractures cannot be ruled out due to lack of coverage or generalized ice codes are listed as 'possible fracture' and instances with no evidence of breakup but incomplete coverage are listed as 'likely no breakup.'

Table 2.2: Synoptic type classifications (after Alt, 1987).

Synoptic Classification	**Name**	**Characteristics**	**Placements**
Type I	Polar Arctic Circulation	Baffin low, polar ocean high	Vortex in North American sector
Type IIs	Cyclonic System Circulation with Snow	Tracking cyclone with snow	Vortex moving across QEI from central Polar Ocean
Type IIr	Cyclonic System Circulation with Rain	Tracking cyclone with rain	Vortex in Beaufort Sea sector
Type III	Island Circulation	Anticyclone	Ridge in QEI; vortex in Eurasian sector

Figure 2.1: (a) Location map of northern QEI islands and waterways. (b) Location of major ice blockages on MODIS TERRA image, August 13, 2005 (courtesy of MODIS Rapid Response Project, NASA/GSFC and University of Maryland - http://rapidfire.sci.gsfc.nasa.gov)

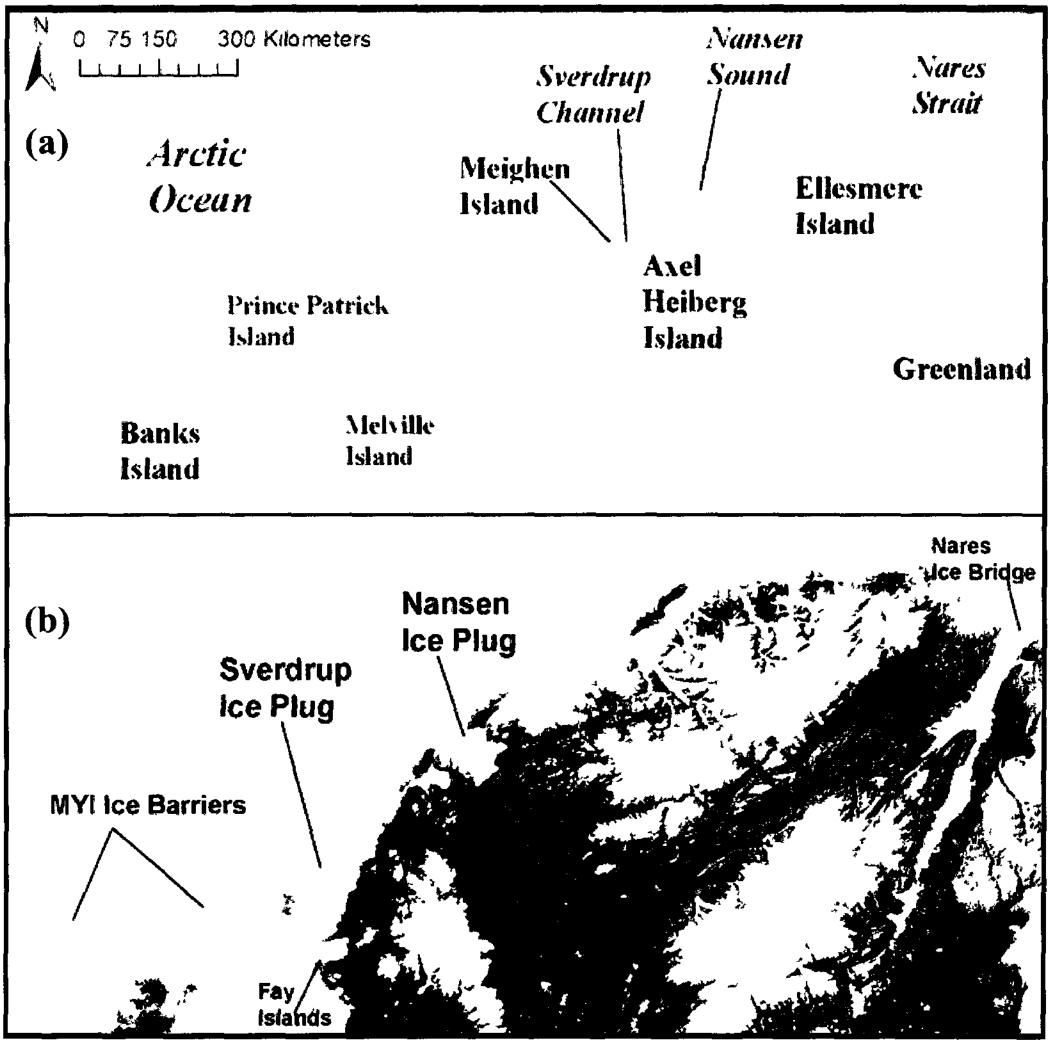

Figure 2.2: PCSP Ice Atlas images of the Nansen and Sverdrup Ice Plugs in summer 1962 (Lindsay, 1975). Ice plug locations are circled. (a) August 4-5, 1962; (b) August 26-September 5, 1962.

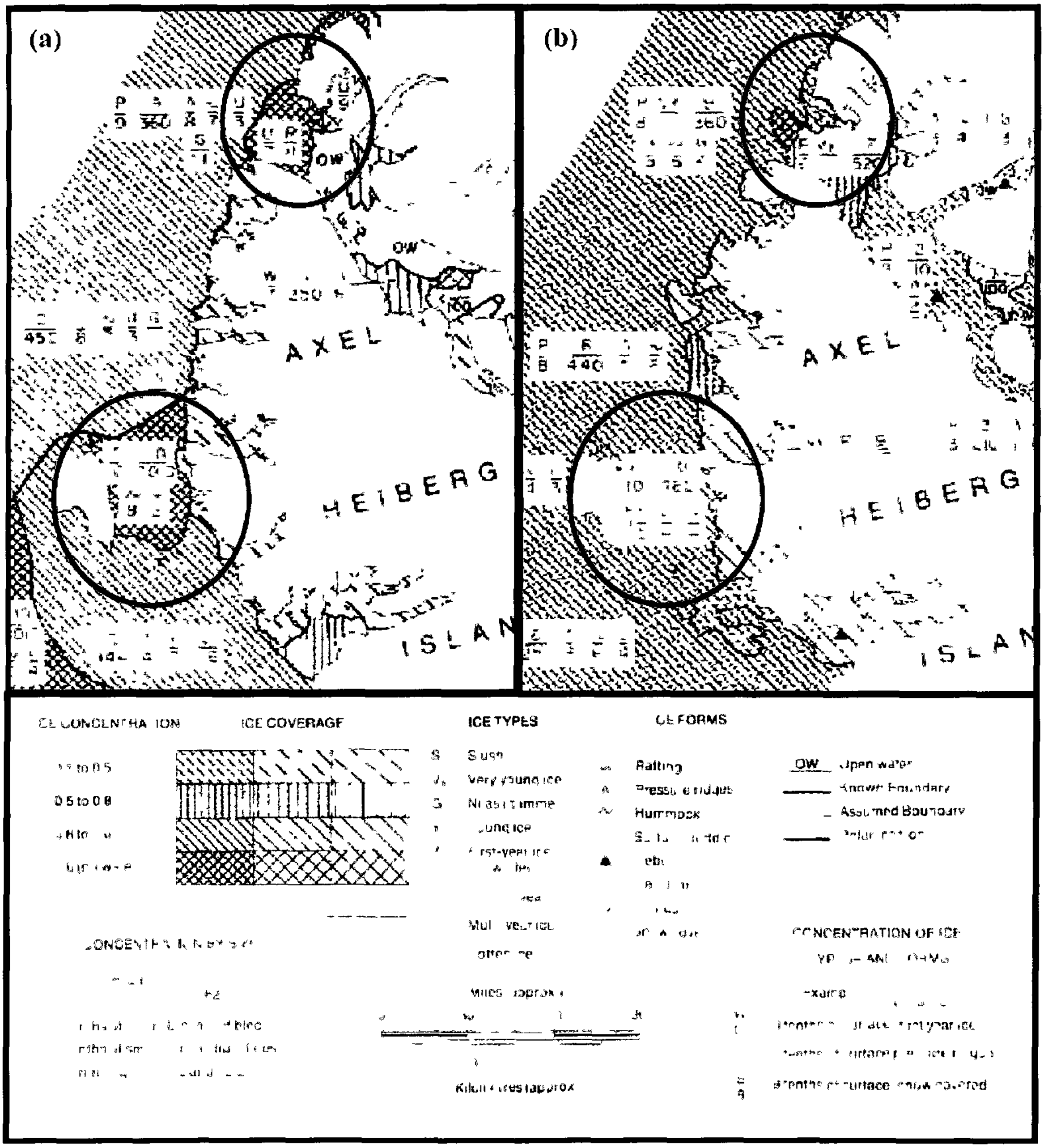

Figure 2.3: Regional ice coverage indices. (a) Total ice coverage graph for Sept. 10, 1971-2000, for the Canadian Arctic Archipelago (CIS, 2002); (b) Median concentration of sea ice around ice plugs for Sept. 24 for 1971-2000 period (CIS, 2002); (c) Concentration of sea ice around ice plugs on Sept. 28, 1998 (Modified from Environment Canada, 1998).

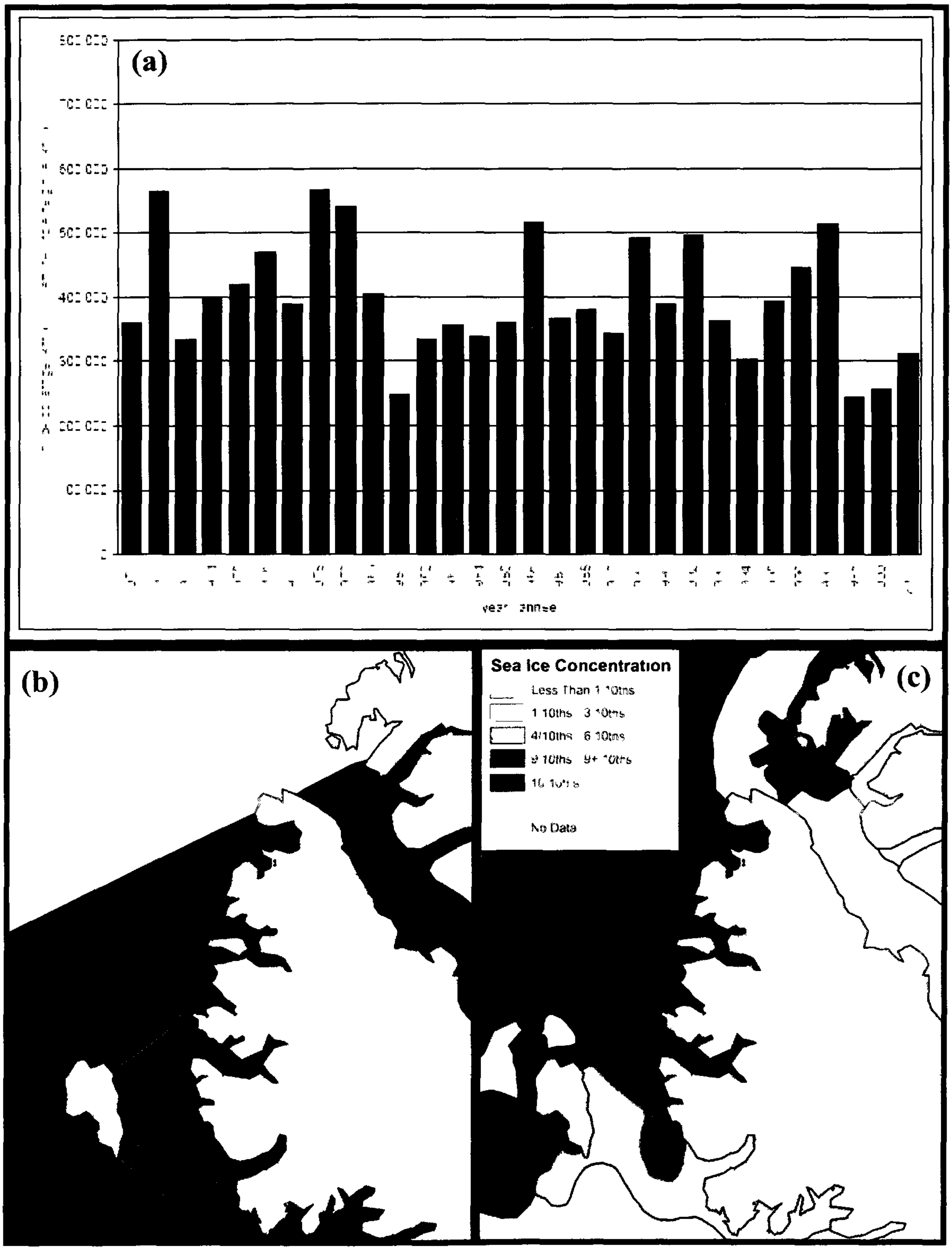

Figure 2.4: Summer conditions at Eureka weather station: (a) Summer 1998 daily maximum and minimum air temperatures. (b) Daily June-October air temperatures for 1962, 1998 and long-term mean (Environment Canada, 2009).

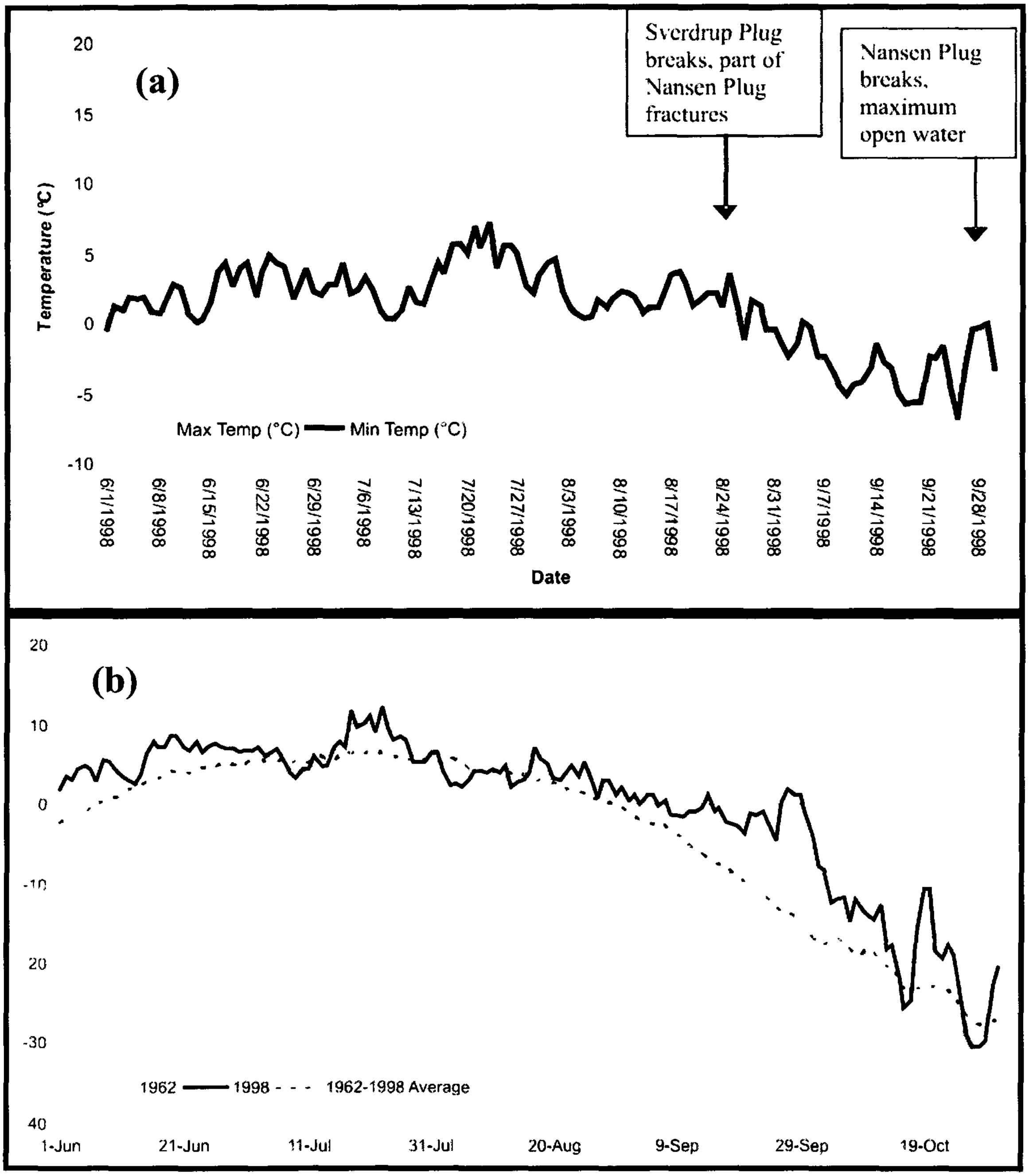

Figure 2.5: RADARSAT-1 images of 1998 plug breakups. (a) September 21, 1998; (b) September 28, 1998. RADARSAT images copyright Canadian Space Agency.

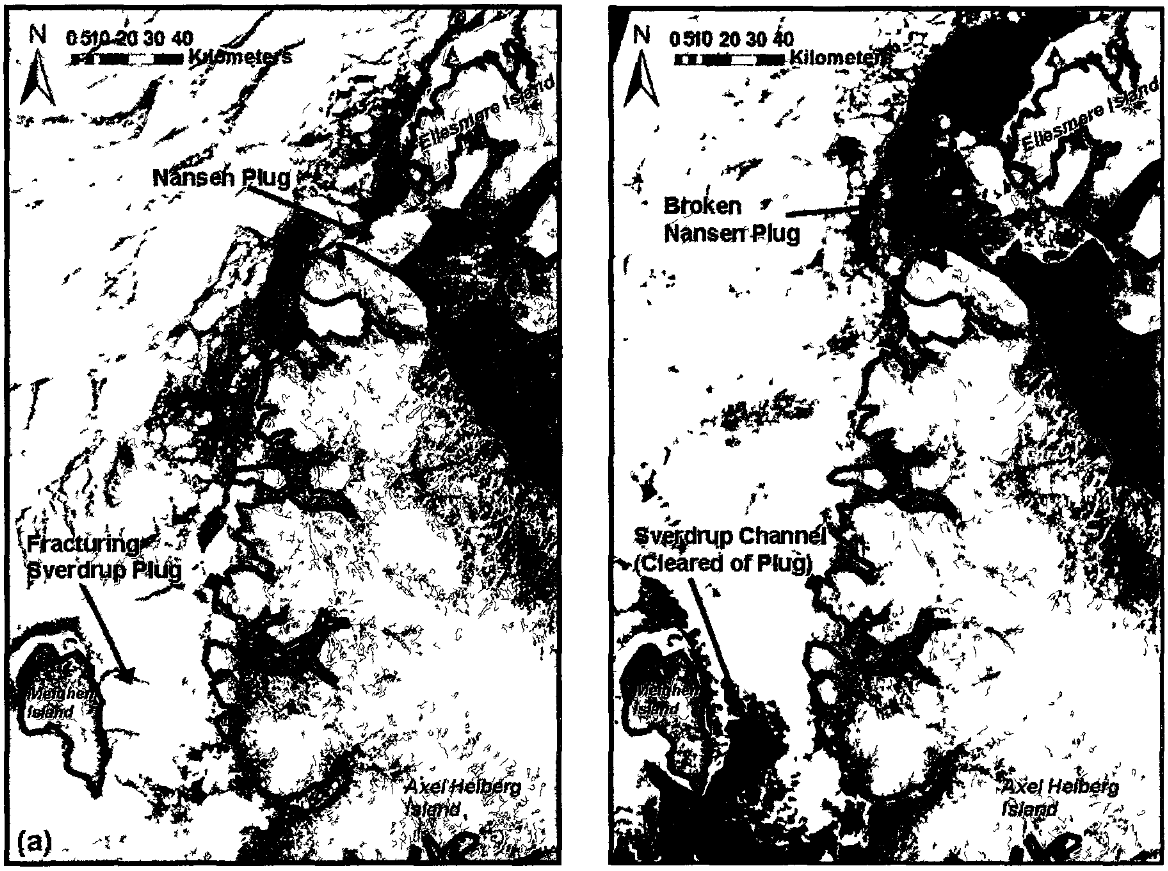

Figure 2.6: (a) Eureka summer temperatures, 1948-2008; (b) Melting Degree Day (MDD) and Freezing Degree Day (FDD), 1948-2008. Vertical lines indicate years when both Nansen and Sverdrup Ice Plugs broke up (Environment Canada, 2009).

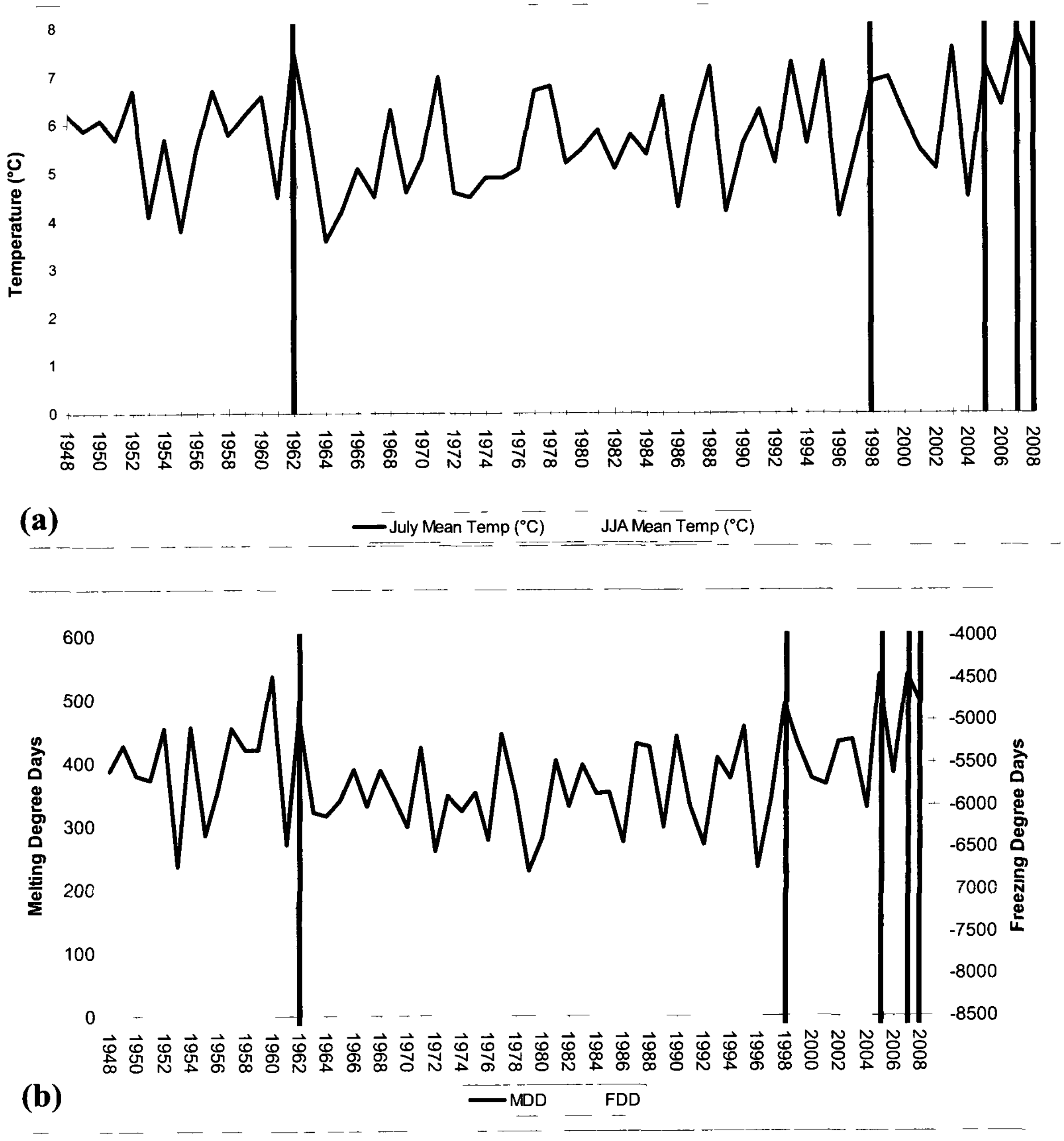

Figure 2.7: MODIS imagery of the 2008 ice plug breakups: (a) July 31, 2008: plugs appear stable; (b) August 6, 2008: both plugs fractured, ice movement northwards into Arctic Ocean; (c) August 29, 2008: Nansen Sound and Sverdrup Channel are largely ice-free, southerly pack ice movement ice into Eureka Sound and through Sverdrup Channel is evident.

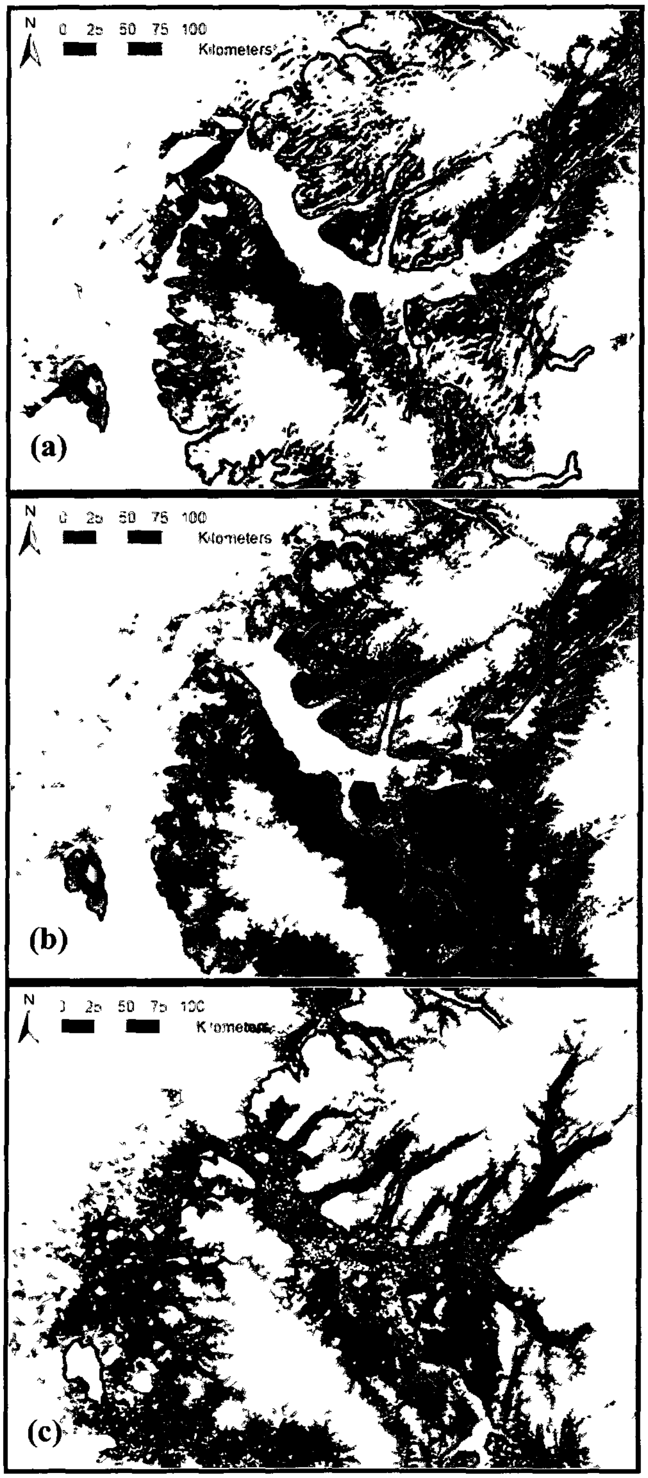

Figure 2.8: Example of Type III Synoptic conditions: NCEP/NCAR reanalysis of 500 mb geopotential height from July 28, 2008, just before the vortex begins to move into the Beaufort sector of the Arctic Ocean and fractures appear in Nansen and Sverdrup Ice Plugs. Note the position of the low on the Asian side of the Arctic Ocean, and the development of a ridge in the Eastern QEI.

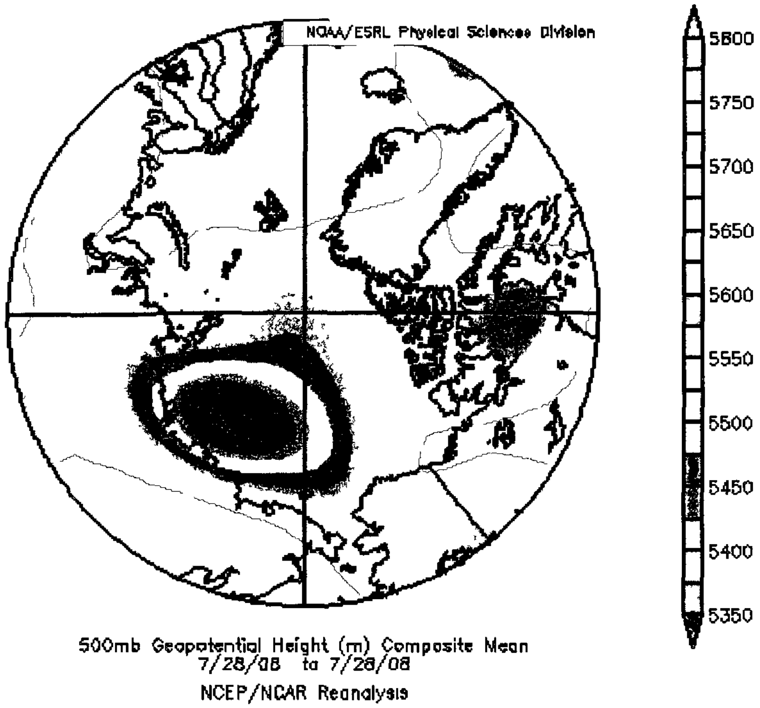

3. Reductions in Multiyear Landfast Sea Ice in Yelverton Bay, Ellesmere Island, Nunavut, Canada

3.1 Introduction

Sea ice in the Arctic Ocean has undergone dramatic recent changes. The rate of decrease in Arctic sea ice extent at the end of the melt season from 1953-2006 was -7.8% per decade, and this rate is even higher (-9.1% per decade) over the period of satellite measurement (1979-2006) (Stroeve et al., 2007). Sea ice area decreases have been most pronounced during the month of September (Serreze et al., 2007), in which the lowest ever recorded minimum ice extents were produced in 2007, 2008 and 2009 (NSIDC, 2009). In addition to the negative trends in Arctic sea ice area and summer minimum extent, several recent studies have determined reductions in age and thickness of multiyear ice in the Arctic Ocean (Rothrock et al., 1999; Maslanik et al., 2007), particularly in the eastern Arctic Ocean (Rigor and Wallace, 2004; Nghiem et al., 2006). Kwok and Rothrock (2009) reported a decrease in mean sea ice thickness over the Arctic Ocean from 3.64 m in 1980 to 1.89 m in 2008. As thick, perennial sea ice is more likely to survive the summer melt season, a smaller proportion of perennial ice will negatively impact future sea ice extents in the Arctic Ocean (Maslanik et al., 2007; Nghiem et al., 2007).

The presence and behavior of this multiyear sea ice (MYI) has been studied in detail in the Canadian Arctic Archipelago (CAA), a series of islands north of mainland Canada. Trends of sea ice decrease in the CAA largely mirror those of the Arctic Ocean, with the regional average September MYI area decreasing at a rate of -6.4% per decade from 1979-2008 (Howell et al., 2009). Much of the CAA features sea ice which remains predominantly landfast for 6-8 months of the year (Melling, 2002), and the movement of sea ice between the Arctic Ocean and the CAA is impacted by the presence of landfast ice blockages (Alt et al., 2006; Howell et al., 2009; Kwok, 2006).

The protective nature of the many channels in the CAA, and the tendency of the Beaufort Gyre to force thick multiyear ice against the NW edge of the CAA, has led to the formation of several semi-permanent multiyear landfast sea ice (MLSI) features there. MLSI has historically formed plugs in Sverdrup Channel and Nansen Sound in the Northern CAA

(Jeffers et al., 2001) and has developed in and around the ice shelves found on the northwest coast of Ellesmere Island (Jeffries, 1987). The relationship between MLSI and the stability of the Arctic ice shelves has been explored, identifying that a stable MLSI fringe can be important for the stability of land-based ice features (Copland et al., 2007; Reeh et al., 2001). The dramatic losses of these ice shelves in the last decade (Copland et al., 2007; Mueller et al., 2008) have been accompanied by the loss of significant areas of MLSI in the region. A dominant factor in the loss of these features is regional atmospheric warming at nearly twice the global average rate (IPCC, 2007). For example, the very warm summer of 2005 was accompanied by record low sea ice concentrations (Serreze et al., 2007), the loss of most of the Ayles Ice Shelf (87.1 km^2) from the NW coast of Ellesmere Island, and the breakup of 690 km^2 of 60+ year old MLSI in nearby Yelverton Bay (82°26' N, 83°30' W) (Copland et al., 2007). Prior to this study, detailed analysis of the history and characteristics of MLSI changes in this region has never been conducted.

This study combines fieldwork and remote sensing image analysis to quantify the characteristics and changes in MLSI for the last 60 years in Yelverton Bay and Yelverton Inlet, on the NW coast of Ellesmere Island. In 2009, Yelverton Bay featured a range of ice types, including first and second year sea ice, rolling-surface multiyear sea ice, and calved glacier ice; this study presents the first dedicated, in situ assessment and sampling of these. The role of ground-penetrating radar (GPR) in determining snow depth, sea ice thickness and sea ice internal structure is also explored, and the directional dependence of GPR return strength is assessed. These results provide improved understanding of the ability of synthetic aperture radar (SAR) satellite imagery for remote determination of ice types, and enable improved mapping of sea ice changes in the region since the early 1950s using air photos and RADARSAT, MODIS (Moderate Resolution Imaging Spectroradiometer), and ASTER (Advanced Spaceborne Thermal Emission and Reflection Radiometer) satellite scenes.

3.2 Study Site and Previous Measurements

Yelverton Bay lies between the Serson and Milne Ice Shelves and extends across the Petersen Ice Shelf on the NW coast of Ellesmere Island, in the Canadian Arctic Archipelago (Fig. 3.1). Environment Canada Climate Normals (1971-2000) for Eureka Station (79°58.8' N, 85°55.8 W), ~330 km south of Yelverton Bay, indicate an average annual temperature of

-20° C and average annual precipitation of 75 mm. Alert Station (82°31.2'N, 62°16.8' W), ~375 km east of Yelverton Bay, records -18°C and 153 mm average annual temperature and precipitation over the same time period. There are no long-term records available from the ice shelves, but recent short-term records for 2009-10 indicate a mean annual temperature of -16.8° C at nearby Milne Ice Shelf (https://datagarrison.com/users/300034012631040/300034012631040/ plots.php).

The NW coast of Ellesmere Island was documented in the early 1900's as a landscape of thick, rolling ice shelves (Koenig et al., 1952) covering an estimated ~10,000 km^2 (Vincent et al., 2001), formed from grounded land ice and stable growth of multiyear landfast sea ice. Within the last decade, increasing areas of these remaining ice shelves have broken apart, with the total losses of the Ayles Ice Shelf in 2005 (Copland et al., 2007) and the Markham Ice Shelf in 2008 (Mueller et al., 2008) creating new ice shelf-free fjords. Previous work in the region has focused on the characteristics of these ice shelves (Hattersley-Smith, 1963; Jeffries, 1987; Jeffries, 1992; Jeffries, 2002; Jeffries and Sackinger, 1990a; Mueller et al., 2008) and recent changes to these features (Copland et al., 2007; Jeffries, 1986; Mueller et al., 2003).

The pre-1900s "Ellesmere Ice Shelf" covered Yelverton Bay with ice featuring characteristic "rollers" as described in situ by Aldrich and Peary (Koenig et al., 1952), making Yelverton Bay the source of significant ice island and MLSI floe production (Jeffries, 1987). Ice Island T-3 was the first to be identified as originating from Yelverton Bay (Jeffries, 1987), with its ridged topography and surficial rock material indicative of an ice shelf source (Hattersley-Smith, 1957a, 1957b). Morainal material and plant remains found on Ice Island T-3 suggest that it originated from ice shelf ice deep within Yelverton Bay (Crary, 1960), and dendrocronological dating indicates that it calved between 1935 and 1947 (Polunin, 1955). Following the removal of these ice islands from Yelverton Bay, sea ice formed and remained in place due to the protected embayment. Over a period of decades, this MLSI reached substantial thicknesses and formed an incipient ice shelf with rolling surface features. In situ observations of the MLSI in central Yelverton Bay and Yelverton Inlet have never been conducted prior to the 2009 field season.

3.3 Methods

In this study, ice thicknesses in Yelverton Inlet (Fig. 3.1) are derived from GPR measurements and shallow ice cores collected on 2 June 2009. Ice types are determined on a RADARSAT-2 image from the same year, and used to reconstruct regional MLSI changes since the early 1950s using RADARSAT imagery, ASTER scenes and air photo mosaics (Table 3.1).

3.3.1 Field Measurements

3.3.1.1 Ground Penetrating Radar Measurements

Field measurements were conducted in Yelverton Bay and Yelverton Inlet. A Pulse EKKO Pro 250 MHz Ground Penetrating Radar (GPR) system, custom-fitted into a sled (Fig. 3.2a) and towed behind a snowmobile at ~20 km hr^{-1}, was used to collect ice thickness data in a reflection-type survey with a GPR antenna separation of 0.4 m and sample interval of 0.4 ns. A total sampling depth of 300 ns was chosen (deeper than necessary to ensure that the entire ice thickness was measured), and an instant return on the DVL screen allowed for periodic confirmation that the GPR signal was penetrating through the entire ice column. Corresponding GPS measurements (accuracy ~ ±5 m in all spatial coordinates) were taken along the GPR transects at every trace to determine position and elevation and to allow for mapping of the results.

To enhance the visibility of basal and Internal Reflector Horizons (IRHs), post-processing of the GPR data was undertaken using EKKO_View software. The raw lines of GPR data (300 ns depth) were chopped to a viewing window of 100 ns, as the sea ice returns only extended to ~60 ns at the thickest areas and the lower 200 ns showed only noise. The GPR lines were also chopped by position, to exclude any data collected while the sled was not in motion. A Dewow filter was applied to the data to reduce low frequency noise near the start of each trace, and trace differencing (a high-pass spatial filter) was completed to enhance rapidly changing profile features and suppress constant features in the GPR data. The Spherical Exponential Calibrated Compensation (SEC2) gain was used to compensate for spherical spreading losses and dissipation of the radar signal. Finally, in the IcePicker R4 program, the amplitude contrast was increased in the viewing window from 1 to between 30 and 45; this did not change the data, but increased the visibility of changes within traces.

Significant differences in the dielectric constants of snow, ice and saltwater, evident in the post-processed GPR traces, were used to isolate the snow-ice interface, the ice-water interface, and internal ice layering. Two-way return time from the snow surface to the snow base (i.e., ice surface) was determined for each trace, and then subtracted from the two-way travel time between the snow surface and the ice base for each trace. These times were then converted into snow and ice thickness values using the equation:

$$T = (((t + s / 0.3)\, V_I / 2)^2 - s^2 / 4)^{½} \qquad \text{(Equation 1)}$$

Where T is thickness (m), t is two way travel time (ns), V_I is electromagnetic wave velocity (m ns^{-1}), dependent on the material being surveyed, and s is antenna separation (0.4 m in this study).

After the peak amplitude for each trace was identified to determine the depth of the ice base, the strength of the ice base peak was quantified and compared against the strength of other traces' base peaks. It is assumed that the GPR signal was transmitted at a constant power, and therefore variations in the power of the reflection at the base are indicative of changes within or at the base of the ice. The sum of all power returned at the ice base for an individual trace, known as basal reflection power (BRP), has previously been used in GPR studies on glaciers and ice shelves to assess variations in basal conditions (e.g., Narod et al., 1988; Gades et al., 2000; Copland and Sharp, 2001). Similarly, mapped variations in GPR reflection strength have been tested as a means to determine the presence of oil spills beneath sea ice (Bradford et al., 2008; Bradford et al., 2010; Goodman et al., 1985). To determine if any such variations in basal reflection existed in the 2009 GPR profiles of Yelverton Inlet, BRP was calculated for all traces recorded in the Inlet from:

$$\int_{t_1}^{t_2} (s(t))^2\, dt \qquad \text{(Equation 2)}$$

where s is the amplitude and t is time. For the BRP in this study, t_1 is defined as 5 ns before the base peak and t_2 is 15 ns after the base peak; this allows for summation of all of the power returned at the ice base for each individual trace (Fig. 3.3). Raw amplitude data for each sample point (every 0.4 ns) along the GPR traces were extracted from the IcePicker R4 program and squared to remove negative values and determine returned signal power. The summation of BRP for each trace was then normalized to mV^2 ns^{-1} and mapped. This process allowed for an assessment of spatial patterns of BRP along Yelverton Inlet and variations in BRP over different sea ice types.

3.3.1.2 Ice Core Measurements

Shallow ice cores were drilled through the entire sea ice thickness (~1-3 m) with a Kovacs Mark II ice coring system (core diameter 8.8 cm, barrel 1.15 m long) and processed in a sled (Fig. 3.2b). This allowed for immediate temperature measurement via probe thermometers inserted into holes drilled at 10 cm intervals into the core, and visual observation of internal characteristics of the ice. The latter included presence, size, and patterns of bubbles in the ice, ice 'colour,' and ice cloudiness. Ice thickness at the core sites was measured using a Kovacs Ice Thickness Gauge, lowered into the empty boreholes. Ice cores were cut into 10 cm sections, which were photographed and then melted for conductivity measurement (within 24 hours of coring) using a temperature-corrected YSI probe. Temperature and salinity profiles and the visible characteristics of the cores were compared with descriptions of sea ice types and FYI / MYI profiles in established reference texts (Wadhams, 2000; Johnston and Timco, 2008). This allowed for age classification of the sampled Yelverton Inlet sea ice. Snow pits at each of the ice core locations were completed to measure snow depth, stratigraphy and changes in crystal structure through the snowpack, and density at each of the snow layers.

3.3.2 Image Analysis

3.3.2.1 Aerial Photography

A search was completed at the National Air Photo Library (NAPL), Ottawa, for air photos taken over Yelverton Bay and Yelverton Inlet. Air photos were scanned at 600 dpi from NAPL prints. The images were loaded into Corel Photo-Paint, cropped to exclude framing and writing on the images, and converted to grayscale. Trimetrogon (T-Series) air photographs taken by the Royal Canadian Air Force (RCAF) from August 1950 provide oblique, but not nadir, coverage of Yelverton Bay (Table 3.1). Varying look angles in the oblique T-Series air photographs made orthomosaicing impossible, but the images provide coverage of Yelverton Bay and Inlet (Fig. 3.4), and were used for qualitative assessment of MLSI presence, as well as comparison with features in 1959 images. Stereo aerial photos taken by the RCAF between July and August 1959 provide almost complete coverage of Yelverton Bay, Yelverton Inlet, and nearby Kulutingwak Fjord, and were georeferenced using a 15 m resolution ASTER image (Fig. 3.1) from July 2009. Each photograph was georeferenced in ArcGIS using a minimum of 20 ground control points, chosen from varying areas on the photograph to create as uniform and complete coverage of the image as possible, and preferentially over permanent land features. A first order polynomial interpolation was used to georeference 94% of photos; a third order polynomial was used for photos requiring a higher degree of warp to accommodate mountainous terrain. All air photos were georeferenced with a root mean squared error (RMSE) of <15 m and mosaicked together in ENVI. Complete georeferencing information for the mosaic is in Table 3.2.

RCAF air photos from 1974 and 1984 (not shown) were also collected (Table 3.1). These years provide very limited coverage of the Yelverton Bay Area due to sparse and largely coastal flightlines, and limited snow-free ground cover made accurate georectification impossible. The images were catalogued to provide qualitative estimates of MLSI presence in Yelverton Bay, but were not relied upon for analysis.

After the 1959 images were georectified, ice area polygon differencing was used to determine changing extent of MLSI, ice shelves, and glacier termini between the June/July 1959 air photo mosaic and a 15 m resolution July 2009 ASTER image mosaic.

3.3.2.2 Satellite Imagery

Satellite imagery acquired between 1993 and 2010 showing ice extents in Yelverton Bay was catalogued (see Table 3.1 for acquisition dates and image details). SAR imagery, including ERS-1 images from 1993 and 1994, RADARSAT imagery between 2000 and 2008, and RADARSAT-2 imagery from 2009-2010, allowed for the determination and manual digitization of MLSI, FYI, and ice shelf ice extent based on texture and tone differences in the imagery. The classification of sea ice via SAR signature (brightness and texture) has been used in numerous previous studies (Askne and Dierking, 2008) and operationally by the Canadian Ice Service (CIS); guidelines for classification are outlined by Johnston and Timco (2008). Winter SAR scenes were used whenever possible, when the ice/snow surface was cold and dry. Summer warming of the snowpack increases the amount of water and limits the ability of SAR imagery to penetrate to the ice surface or subsurface, with the resultant SAR signature at these times dictated by scattering and absorption of the snowpack, rather than characteristics of the sea ice below (Johnston and Timco, 2008). The intensity of backscatter in the SAR imagery is dependent on the proportion of direct versus diffuse reflection, and indicates distinct surface and internal characteristics which differ between ages and types of sea and glacier ice (Askne and Dierking, 2008; Johnston and Timco, 2008). The lower salinity of MYI than FYI allows for RADARSAT C-band energy to penetrate deeper into the ice, allowing the bubbles and unconformities within the ice to create a strong return on the image and a brighter signature than FYI (Johnston and Timco, 2008). Similarly, MYI or MLSI presents a weaker signal return than ice shelf ice in SAR imagery (Jeffries and Sackinger, 1990a). SAR imagery analysis of the Milne Ice Shelf (Jeffries, 1992) demonstrated these differences, with MLSI reentrant ice appearing darker than an ice island it was attached to. SAR imagery can also identify a distinctive ribbed texture on both ice shelf ice and MLSI (Jeffries, 1992; Jeffries and Sackinger, 1990a; Jeffries and Sackinger, 1990b), with ice shelf ridges appearing larger in height (1-4 m) than MLSI ridges (0.5-1 m) (Jeffries and Sackinger, 1990b).

The distinctive surface texture of MLSI makes it identifiable in visible imagery as well. For a quantitative comparison of MLSI area changes with the 1959 air photo mosaic, eight clear-sky, georectified ASTER L1B images from July 2009 were selected and downloaded from NASA's Earth Observing System Data Gateway. The 15 m resolution ASTER scenes were co-registered (Bands 3N, 2, and 1 loaded as R,G, B respectively) then mosaicked together in ENVI. Polygon differencing was then used to quantify the reduction in MLSI area between 1959 and 2009. Areas of interest within the region were highlighted to catalogue changing ice shelf, MLSI, and glacier extent, including the Wootton Peninsula Ice Shelf and Kulutingwak Fjord (Fig. 3.1).

RADARSAT-2 images acquired March 5 and 15, 2009 were also used for comparison. Despite the different acquisition dates, the March 2009 RADARSAT-2 and July 2009 ASTER images are comparable for analysis since sea ice within Yelverton Bay did not experience any movement between these periods. However, snow melt created backscatter on a June 2009 RADARSAT-2 image, rendering it useless for analysis of ice types beneath the snowpack. The brightness and texture differences of the sea ice in the March 5 2009 RADARSAT-2 image were used to delineate the extents of MLSI and FYI in Yelverton Bay and Inlet using classification recommendations from Johnston and Timco (2008), visual comparison with the 2009 ASTER mosaic, and ice depth and type indications from the 2009 in situ GPR and ice core measurements. Brightness values (between 1 and 255) were extracted from the 2009 RADARSAT-2 scene in each of the determined ice types to confirm accuracy of the divisions. Finally, 250 m resolution MODIS imagery from NASA's Rapid Response Near-Real Time Aeronet Subset was collected over the 2008 melt season and again in 2010. These images were assessed to chart the removal of Yelverton Bay MLSI.

3.4 Results and Discussion

3.4.1 GPR and Ice Cores

3.4.1.1 Snow depth determination

The strong reflection in the GPR traces at the snow-ice interface allowed for determination of snow depths across the study area using a learned wavelet to pick the pulse reflection point in the Ice Picker R4 program. Using a radio-wave of velocity 0.2 m ns^{-1}, as established by previous GPR snowpack studies (Annan, 2002), snow depths were determined over all GPR traces in Yelverton Bay (Fig. 3.5). Average snow depth was 0.453 meters, with a standard deviation of 0.082 m. Calculated snow depths along the GPR lines were verified by comparing in situ snow pit depth measurements to the average values derived from GPR data collected within a 10 m radius of each pit. Snow depths at Core Sites 1, 2, and 3 were 37 cm, 47 cm, and 39 cm respectively, all well within 1 standard deviation of the average GPR-derived snow depth values of 35.3 cm, 44.1 cm, and 42.2 cm. This suggests that a radar velocity of 0.2 m ns^{-1} is appropriate for the local snowpack. At Core 4, snow depth was measured at 71 cm, whereas nearby GPR-derived depths averaged 44.5 cm. A highly variable snowpack and surface rolls were observed around this site, so it is suspected that these local factors accounted for the particularly high sampled snow depth.

Overall, GPR-derived snow depth measurements indicate that thicker snow is found at the head of Yelverton Inlet and into Yelverton Bay, with depths decreasing into the Inlet (inset graph, Fig. 3.5). This trend of greater snow accumulation near the coast appears to be common along northern Ellesmere Island, although it has been poorly quantified before. This pattern is dictated by the largely coastal moisture sources in the region. The growth of MLSI and ice shelf ice relies in part on the accumulation of snow at the ice surface. Lower snow accumulation inland suggests that losses at the front of landfast ice features, including calvings and breakups of ice shelves, are not being balanced by new ice formation and glacier flow from inland. This could be a factor in the recent negative trends in ice shelf mass balance reported at Ward Hunt Ice Shelf (Braun et al., 2004) and Ayles Ice Shelf (Copland et al., 2007).

3.4.1.2 Ice thickness determination

Identification of signal peaks at the ice-water interface was complicated by signal attenuation (a common complication in sea ice GPR measurements), caused by density contrasts between the ice crystals and salty brine inclusions (Kovacs and Morey, 1978; Woodward and Burke, 2007). Each of the 40,911 GPR traces from Yelverton Inlet was manually assessed to determine if a signal peak was identifiable at the ice base, and only 25,388 traces showed clear ice base peaks. To determine the correct radar velocity for calculating ice thicknesses, a range of radar velocities were modeled using Equation 1, and the resulting ice thicknesses were compared to the ice core depth measurements. GPR-derived ice thickness values (calculated with radar velocities ranging from 0.145 m ns^{-1} to 0.167 m ns^{-1}) were averaged within 100 m buffers around each ice core site. A radar velocity of 0.15 m ns^{-1} was found to produce ice thickness values which most closely matched the in situ thickness measurements. Ice core thicknesses were within 1 standard deviation of the averaged GPR-derived thicknesses (using 0.15 m ns^{-1} as V in Equation 1) within 100 m around each core site.

This radar velocity is significantly lower than established velocities for snow (0.2 m ns^{-1}) and glacier ice (0.167 m ns^{-1}) (Annan, 2002; Woodward and Burke, 2007). Given the higher proportion of salt crystals and other attenuating structures in sea ice as opposed to freshwater glacier ice, and the significantly higher density of sea ice than snow, a slower velocity for sea ice than either medium is reasonable. Similar velocities have been used in past sea ice studies: radar velocities of 0.156 and 0.157 mns^{-1} were used on MYI measurements by Kovacs and Morey (1978) with a 625 MHz GPR system during a study near Narwhal Island, off the northern coast of Alaska. A study of floating FYI in Mikkelsen Bay, Alaska used radar velocities between 0.154 – 0.167 m ns^{-1} to determine ice thickness with a 200 MHz GPR system (Nyland, 2004). More recently, a controlled experiment attempting oil spill detection over sea ice with a 1000 MHz airborne GPR system used sea ice of known thickness (70 cm) to model a radar velocity of 0.14 m ns^{-1} (Bradford et al., 2010).

The GPR-derived sea ice thicknesses in Yelverton Inlet (Fig. 3.6a) averaged 2.06 m with a standard deviation of 0.46 m, ranging from 1.19 m at the inland points to 3.71 m near the mouth of the inlet. These thickness variations correspond with RADARSAT image signature differences and aided in the determination of ice types, as outlined in Section 4.2.

3.4.1.3 Ice core results

Shallow ice cores (Fig. 3.6b) indicate variations in depth, salinity, and temperature of sea ice in Yelverton Inlet. Cores 1 and 2, taken at the back of the Inlet, indicate ice depths of 157 cm and 141 cm respectively (Fig. 3.6b). Salinities exhibited little variation in Cores 1 and 2, increasing with depth from <1 psu to ~2 psu. Temperature measurements ranged from -2.7 °C at the ice surface to -1.1°C at the ice base. The salinities and uniformity of the profiles suggests that this sea ice formed over one winter, as a second or multiyear profile would indicate more than one ice type with a definite salinity demarcation (Johnston and Timco, 2008). The cores were cloudy in appearance, with small, linear bubbles present throughout, which may have been indicators of brine inclusions (Wadhams, 2000). Cores 3 and 4 (Fig. 3.6b) appeared distinctly different from the previous cores: 246 cm and 254 cm thick respectively, with low salinities (<1 psu) from the surface to ~170 cm depth, increasing sharply to >5 psu from ~170 cm to the base. Temperatures at the surface of the cores were between -6 and -4 °C, increasing at the ~170 cm point to just under -2 °C at the base. The temperature and salinity profile patterns of Cores 3 and 4 – steady low values from the surface to approximately halfway down the core, then sharp salinity increases and temperature decreases – are a match to the profiles for multiyear sea ice outlined in the sea ice identification guide by Johnston and Timco (2008) and in Wadhams (2000). The distinction between the upper and lower sections of Cores 3 and 4 are also evident in recorded visual observations. The cores featured frequent small bubble inclusions in a matrix of relatively clear ice from 0 cm to between 175 - 186 cm, then appeared cloudy to the base of the core. This is consistent with the theoretical growth of multiyear sea ice, with brine expulsion creating a nearly fresh layer of ice near the surface and concentrating the brackish saltwater inclusions near the base of the core (Wadhams, 2000).

3.4.1.4 Comparison of ice core properties with GPR traces

The differences in depth and ice type found in the ice cores were also visible as differences between GPR traces collected in different parts of Yelverton Inlet (Fig. 3.7). Traces from Line 2, at the rear of the Inlet (Fig. 3.7a), show a single smooth reflector at the ice base, visible as a peak or red band in the GPR record. In comparison, GPR traces near the mouth of Yelverton Inlet show an internal reflector horizon (IRH; Fig. 3.7b), corresponding with the interface between fresh and saline ice found in Cores 3 and 4 (Fig. 3.6b). The Core 3 profile (Fig. 3.8) indicates that the IRH occurs when the ice reaches a salinity of ~2 psu, with a corresponding increase in ice temperature, decrease in air bubble inclusions, and increase in ice cloudiness. The 500 m section of GPR from the front of Yelverton Inlet (Fig. 3.7b) shows the ice base reflection as a weak and variable signal.

3.4.1.5 Basal reflection power (BRP)

To quantify the differences in ice base reflection identified in the previous section, variations in BRP were calculated along all traces where ice base could be determined (Fig. 3.9). The front and center of Yelverton Inlet demonstrate a uniformly weak basal signal, which may be due in part to the attenuation of the GPR signal by the strong IRH at the interface between fresh and saline ice. The BRP in the rear of Yelverton Inlet indicates a pattern of directional dependence (Fig. 3.9a). GPR lines collected perpendicular to one another over the same area show distinctly different strengths, with lower BRP when the instrument measured along NW-SE transects, and higher BPR along SW-NE transects (Fig. 3.9b, d, e). This pattern is also evident further south in Yelverton Inlet; a single GPR line collected over one ice type increases significantly in BRP when it makes a right turn, NW-SE to SW-NE (Fig. 3.9c, f).

Directional dependence of radar strength in sea ice, or 'radar anisotropy,' has been identified in several previous studies (Kovacs and Morey, 1978; Nyland, 2004; Pringle et al., 2009) as a response to the orientation of the c-axis of sea ice crystals. Ice crystals near the surface of sea ice tend to have a vertical c-axis orientation, and with depth sea ice crystals typically increase in width, their c-axes becoming horizontal (Wadhams, 2000). A preferred azimuthal direction of these horizontal c-axis crystals at the base of the ice has been identified as a regional pattern, with a common azimuthal orientation existing over large areas of sea ice in the polar pack (Schwarzacher, 1959), and in the Canadian Archipelago (Campbell and Orange, 1974). Studies indicate that the preferred c-axis azimuth is a product of the movement of currents at the sea ice-water interface and subsequent alignment of the ice lamellae perpendicular to the current direction (Campbell and Orange, 1974; Kovacs and Morey, 1978). In Nyland (2004), the parallel alignment of the radar antenna field with the ice crystal c-axis produced strong GPR returns, and perpendicular orientation lead to weak returns. The spatial patterns of BRP in Yelverton Inlet are comparable to the reflection strength differences described in these studies, but crystallographic analysis of the Yelverton Inlet ice cores was not conducted. Future analyses could conduct larger-scale ice base crystal orientation observations to confirm that radar anisotropy is occurring here.

3.4.2 Image Analysis

The 2009 ice thickness and ice core measurements were compared with the brightness and texture of the 2009 RADARSAT-2 image, visual interpretation of the 2009 ASTER image, and the field observations. This enabled the determination of three sea ice types in Yelverton Inlet, as delineated in Fig. 3.10. These areas are outlined and the RADARSAT-2 image brightness for each pixel was extracted, using an image value stretch between 1-255, to quantify differences in brightness values observed over the ice (Fig 3.10, inset graph). The ice at the head of the inlet features the brightest SAR return of the three ice areas, likely due in part to it featuring low salinities within the first meter below the surface (see Cores 3, 4 in Fig. 3.6b), allowing for increased radar penetration and volume scattering within the ice (Johnston and Timco, 2008). GPR-derived ice thicknesses over this region average 2.58 m (Fig. 3.6a), and depths at Cores 3 and 4 are similarly thick (Fig. 3.6b). The temperature and salinity profiles of Cores 3 and 4, both located in this ice type, were determined in Section 3.4.1.3 to be representative of multiyear ice. In situ visual observation of this ice identified distinctive surface rolls, shown in Fig. 3.11a. The only type of sea ice known to exhibit this type of rolling surface is MLSI (Jeffries and Sackinger, 1990b), as FYI and young MYI have not been in place long enough to obtain linear melt ponds and the subsequent ribbed surface texture (Jeffries, 1987; Johnston and Timco, 2008). These observations together suggest that the ice at the head of Yelverton Inlet be classified as MLSI.

The remaining two core sites (1 and 2) are located in the ice type found at the rear of Yelverton Inlet. The measured depths at Cores 1 and 2 corroborate GPR measurements indicating an average ice thickness of 1.66 m in this area (Fig. 3.6), the thinnest ice found in the study. This ice has a darker SAR signature than the other areas, with the exception of several bright spots, which were identified in the field as icebergs (Figs. 3.10, 3.11b). Salinities >1 psu within the first meter of ice (See Cores 1 and 2, Section 4.1.3) limit the penetration of SAR into the ice, resulting in a signature largely dictated by surface scattering (Johnston and Timco, 2008; Shokr and Sinha, 1995). The local ice surface in this protected channel was observed in situ to be fairly smooth, with the exception of the frozen-in icebergs (Fig. 3.11b). The ice had very low variations in GPR-derived ice thicknesses (standard deviation of 0.05 m) and no visible hummocks or ridging. The reflection of much of the SAR energy away from the sensor, as a function of this relatively smooth surface, explains the dark SAR signature (Johnston and Timco, 2008). These observations suggest that the ice at the rear of Yelverton Inlet is FYI.

The ice in central Yelverton Inlet features a darker signature than the MLSI at the front of the Inlet, but a lighter tone and more variable texture than the FYI at the rear (Fig. 3.10, inset graph). Surface ridging characteristic of old MLSI was not observed over this area. Regional GPR-derived ice thickness measurements average 1.81 m with a standard deviation of 0.23 m, indicating greater variability than was measured in the FYI. There are no ice core measurements from this ice area, which limits the confidence associated with assigning it an ice type. As the ice thicknesses and SAR brightness values place this region between the MLSI and the FYI, it is classified as Young MLSI. Dowdeswell and Jeffries (2011) describe a similar ice type occurring elsewhere in the Canadian High Arctic and Greenland: young

MYI which remains stable due to the protection of a fjord but typically breaks or melts out every few years, referred to by the Inuit in Greenland as 'sikussak.'

3.4.2.1 General MLSI Changes in Yelverton Bay

The determination of MLSI and two other ice types in the 2009 imagery, using comparisons between 2009 imagery and field measurements, allows for the classification of MLSI over the region for other years with available imagery. Oblique T-Series air photos from 1950 show a relatively uniform ice surface, extending ~30 km into Yelverton Bay (Figs. 3.4, 3.12). Air photos from 1959 indicate the presence of 932.6 km^2 of persistent MLSI, identifiable by its ridged surface and linear meltponds, in Yelverton Bay and Yelverton Inlet (Fig. 3.13a). The identification of several stable ice features on all imagery between 1950 and 2005 confirmed that the body of MLSI in Yelverton Bay was generally stable over the entire period, with the exception of decimeter-scale shifting within the ice mass. The stable ice features used include a large ice island (3.82 km x 1.4 km) in the center of Yelverton Bay (Fig. 3.12), an ice island (1.26 km x 377 m) 4.5 km west of the Petersen Ice Shelf, and a large crack running from Wootton Peninsula NE into the MLSI, near the outer edge of the old MLSI.

The only observed variations in the Yelverton Bay MLSI between 1959 and 2005 occurred along its outermost edge, where it was exposed to the shifting Arctic Ocean ice pack. Changes to this outermost MLSI extent were identified on ERS-1 and RADARSAT imagery between 1993 and 2005 (Table 3.1), the uniform medium/dark grey SAR signature and even texture of this ice clearly differentiating it from the bright, pancaked mobile pack ice (Fig. 3.14). An ERS-1 image (19 May 1993) confirmed that the MLSI extent in Yelverton Bay was largely unchanged since 1959, with the exception of 10-100 m changes along the MLSI front and the loss of 15.2 km^2 of MLSI at the far NE corner (Fig. 3.14). A February 2, 2000 RADARSAT scene shows that the Yelverton Bay MLSI extent had increased, with ~115 km^2 of additional ice between the Milne Ice Shelf and the northern corner of Yelverton Bay attached to the outer edge of the MLSI (Fig. 3.14). This MLSI fringe was also observed by Copland et al. (2007) and includes the 'Milne Reentrant,' reported by Jeffries and Sackinger (1990a). By August 4, 2004, the landfast ice extent has increased again, extending 3-5 km further out along the entire MLSI front, from the Milne Ice Shelf to beyond Wootton

Peninsula (Fig. 3.14). A RADARSAT image 7 months later (March 18 2005) showed most of that extension intact, with the exception of ~42 km^2 of loss near Wootton Peninsula (Fig. 3.14).

All of this younger MLSI reentrant was removed in early August 2005, directly preceding a massive loss of the old Yelverton Bay MLSI later that month. RADARSAT imagery from August 2005 (Fig. 3.15) demonstrates the dramatic sequence of breakup events. The August 5 image (Fig. 3.15a) shows Yelverton Bay before any fracturing or breakup has occurred, with old and reentrant MLSI intact and bordered by Arctic pack ice. By August 8 (Fig. 3.15b), ~330 km^2 of younger reentrant MLSI from outer Yelverton Bay has broken away from the old MLSI and is seen floating in open water. The August 18 image (Fig. 3.15c) shows that 690 km^2 of old MLSI has broken away in several large blocks from Yelverton Inlet, with the innermost break occurring at the location of a pre-existing fracture (Fig. 3.15b). Figure 3.15c also shows the formation of a new fracture deep in Yelverton Inlet.

By September 24, 2005, the large MLSI fragments had refrozen into the FYI matrix in Yelverton Bay (Fig. 3.15d), where they remained for the following 3 summers. A RADARSAT image from February 14, 2008 (Fig. 3.16a) confirms that the MLSI remnants were still frozen in Yelverton Bay; limited GPR ice thickness measurements conducted on one of these pieces in May 2008 by Derek Mueller (Carleton University), determined ice thicknesses of up to 7 m. MODIS images between July 30 and August 31 2008 show the MLSI fragments breaking into smaller pieces and drifting out of Yelverton Bay, along with the landfast ice at the mouth of Kulutingwak Fjord (Fig. 3.16b-d). The August 16 2008 MODIS scene also shows open water at the rear of Yelverton Inlet (Fig. 3.16d); this supports the determination in Section 4.2 that the ice present there the following year was FYI.

By the end of the 2008 melt season, all MLSI in Yelverton Bay had been replaced by open water and pack ice, with only a small plug of MLSI intact at the mouth of Yelverton Inlet (Fig. 3.16d). The extent of this MLSI plug was quantified in the 2009 ASTER mosaic, and polygon differencing between the 1959 and 2009 mosaics indicate a total loss of 90.07% of the MLSI area in Yelverton Bay over the 50 year period (Fig. 3.13b). The major 2005 MLSI loss occurred in tandem with a calving of 20% of the Petersen Ice Shelf and the rapid breakup of the Ayles Ice Shelf on August 13, 2005 (Copland et al., 2007); these events were attributed in part to high positive degree days (PDDs) encouraging summer melting, low sea ice concentrations, and the absence of an MLSI fringe at the ice shelf front.

A MODIS image from August 22, 2010 indicates that the MLSI which had remained in Yelverton Inlet through summer 2009 has now broken away (Fig. 3.17). Yelverton Bay and Inlet are now free of multiyear landfast sea ice, a situation unprecedented in the historical record.

3.4.2.2 Wootton Peninsula Ice Shelf Changes

The 2005 breakup event in Yelverton Bay was not limited to MLSI. 1950 and 1959 air photos and SAR (1993-2005) imagery (Table 3.1) also indicate the existence of a small, unnamed ice shelf in the protected cove to the east of Wootton Peninsula on the western edge of Yelverton Bay (Fig. 3.18). Identified as ice shelf ice (but unnamed) by Jeffries (1987), the 'Wootton Peninsula Ice Shelf' features a rolling surface texture, linear melt ponds (Fig. 3.18a), and a strong return and ribbed texture in SAR imagery (Fig. 3.18b). These characteristics as well as the stability of the feature over time enable its classification as an ice shelf. Polygon differencing between the 1959 air photo mosaic and the July 2009 ASTER image (Fig. 3.18c) indicate a total loss of 16.44 km^2 of this ice shelf (65.6% of its area). This reduction occurred in two phases: the August 18, 2005 RADARSAT image (Fig. 3.15c) shows ~8 km^2 of this ice shelf being removed during the Yelverton Bay MLSI reduction, and MODIS imagery shows the loss of the remaining ice shelf ice between August 6 and 16, 2008 (cloud cover obscures exact timing and measurement of the break). The maintenance of this ice shelf while being bordered by stable MLSI, and the subsequent loss following the 2005 MLSI removal, highlights the importance of MLSI buffering for the survival of ice shelf ice (Copland et al., 2007, Reeh et al., 2001).

3.4.2.3 Kulutingwak Fjord Ice Type Changes

Changes in glacier extents and reductions in multiyear sea ice in Yelverton Bay and surrounding area have led to significant changes in the ice types that are present in the waterways. An example of these changes occurs in northern Kulutingwak Fjord, south of

Yelverton Bay and west of Yelverton Inlet. The 1959 air photo mosaic (Fig. 3.19a) indicated that Kulutingwak Fjord contained a high proportion of glacier ice which extended across the head of the fjord, in the form of glacier termini and floating ice islands surrounded by young sea ice. In a March 15 2009 RADARSAT-2 image (Fig. 3.19b), the glacier extents have been reduced significantly; this loss appears to have been coincident with the 2008 melt and removal of the MLSI fragments, visible in the MODIS imagery from that time (Fig. 3.16). The 2009 RADARSAT-2 also shows several large blocks of ice (totaling 27.3 km^2) in the Fjord with a bright SAR signature identical to that of the ice at the front of Yelverton Inlet, which was determined in Section 3.4.2 to be MLSI. These MYI blocks are surrounded by ice with a dark SAR signature and texture suggesting it to be FYI (similar to that of the ice at the rear of Yelverton Inlet); this is confirmed by the presence of open water in the Fjord the previous year (Fig. 3.16c). The March 3 2010 RADARSAT-2 (Fig. 3.19c) shows that much of the MYI melted or drifted out of the Fjord in the previous summer, with only 2.3 km^2 of multiyear ice blocks remaining in a matrix of FYI. The glaciers do not extend into the Fjord in the 2010 scene.

3.5 Conclusions

GPR measurements and ice core observations of MLSI, MYI and FYI in Yelverton Inlet allowed for the determination of ice properties in relation to SAR image backscatter. This in turn enabled the identification of these ice types in a 2009 RADARSAT image and the examination of changes to the MLSI in other imagery between 1950 and 2010. Large-scale reductions of multiyear landfast sea ice in Yelverton Bay and Yelverton Inlet have occurred over the last 60 years, in tandem with glacial retreat and ice shelf losses along most of the northwest coast of Ellesmere Island. These reductions were dominated by the single loss of 690 km^2 of MLSI in August 2005. Following the 2005 breakup event, sea ice in Yelverton Bay has consisted of displaced MLSI remnants, which were removed in 2008, and first year sea ice. The last remaining MLSI in the area existed in Yelverton Inlet until summer 2010. This ice was observed in situ in 2009 to be an average of 2.58 m in thickness, with a distinct layering of fresh ice over saline ice which was consistently identifiable as an internal reflector in GPR records.

GPR was found to be an effective tool to determine MLSI thickness, with the qualification that adequate in situ thickness measurements are required for calibration of radar velocity. GPR records from Yelverton Bay MLSI suggested a directional dependence of GPR signal strength, which could be attributed to radar anisotropy of the sea ice. This suggests that for future studies, GPR measurements should be completed in lines perpendicular to each other over the same region, to ensure adequate signal strength and effective thickness determination.

Table 3.1. Chronological list of imagery used in the study.

Sensor & Image Type	Date	Time (z)	Resolution (m)
Aerial photography Roll T405R, #223 – 225 Roll T405L, #33 – 35, 222 – 235	August 1950	N/A	N/A
Aerial photography (see Table 3.2 for photo numbers)	June-August 1959	N/A	3
Aerial photography: Roll A23943, #40 – 54	11-July-74	N/A	0.85
Aerial photography: Roll A26535, #170 – 189	23-July-84	N/A	0.8
ERS1 Standard Beam	19-May-93	00:27	30
ERS1 Standard Beam	25-Oct-94	12:25	30
RADARSAT ScanSAR Wide B	2-Feb-00	21:11	75
RADARSAT Standard Beam 1	4-Aug-04	19:50	28
RADARSAT Standard Beam 1	18-Mar-05	19:58	28
RADARSAT Standard Beam 1	5-Jun-05	19:54	28
RADARSAT Standard Beam 1	16-Jul-05	19:58	28
RADARSAT ScanSAR Wide B	5-Aug-05	20:15	100
RADARSAT ScanSAR Wide B	8-Aug-05	20:28	100
RADARSAT ScanSAR Wide B	18-Aug-05	20:36	100
RADARSAT ScanSAR Wide B	24-Sep-05	20:58	100
RADARSAT Standard Beam 1	20-Apr-06	19:50	28
RADARSAT ScanSAR Wide B	27-Apr-06	19:45	100
RADARSAT Fine Beam 1	14-Feb-08	21:33	10
RADARSAT Fine Beam 1	14-Feb-08	21:34	10
MODIS TERRA	30-Jul-08	19:45	250
MODIS TERRA	31-Jul-08	18:50	250
MODIS AQUA	2-Aug-08	14:05	250
MODIS TERRA	3-Aug-08	19:20	250
MODIS TERRA	5-Aug-08	22:25	250
MODIS TERRA	6-Aug-08	18:10	250
MODIS TERRA	7-Aug-08	22:10	250
MODIS TERRA	12-Aug-08	20:50	250
MODIS TERRA	14-Aug-08	20:40	250
MODIS TERRA	16-Aug-08	22:05	250
MODIS TERRA	19-Aug-08	17:40	250
MODIS TERRA	25-Aug-08	20:20	250
MODIS TERRA	31-Aug-08	19:45	250
MODIS TERRA	9-Oct-08	19:40	250
RADARSAT-2 Wide Beam	5-Mar-09	20:17	40
RADARSAT-2 Wide Beam	15-Mar-09	20:26	40
ASTER Level 1B	10-Jul-09	10:55	15
ASTER Level 1B	13-Jul-09	23:26	15
ASTER Level 1B	14-Jul-09	20:53	15
ASTER Level 1B	14-Jul-09	20:53	15
ASTER Level 1B	16-Jul-09	20:41	15
ASTER Level 1B	16-Jul-09	20:41	15
ASTER Level 1B	22-Jul-09	20:04	15
ASTER Level 1B	22-Jul-09	20:04	15
RADARSAT-2 Wide Beam	3-Mar-10	13:50	40
MODIS TERRA	22-Aug-10	22:05	250

Table 3.2. Image information for air photos georeferenced into 1959 mosaic shown in Fig. 3.12.

Image ID	**Date**	**Transformation**	**GCPs**	**RMS Error (m)**
A16606-1	6/7/1959	1st Order	23	10.477
A16606-2	6/7/1959	1st Order	24	11.063
A16606-3	6/7/1959	1st Order	20	12.823
A16606-4	6/7/1959	1st Order	22	14.732
A16606-5	6/7/1959	1st Order	21	14.844
A16688-25	7/29/1959	1st Order	23	12.690
A16706-20	7/29/1959	1st Order	22	14.275
A16724-52	8/13/1959	1st Order	21	14.703
A16724-55	8/13/1959	1st Order	24	11.780
A16724-57	8/13/1959	1st Order	23	13.939
A16724-59	8/13/1959	1st Order	28	13.715
A16724-63	8/13/1959	1st Order	25	14.922
A16724-63	8/13/1959	1st Order	25	14.922
A16724-65	8/13/1959	1st Order	25	13.486
A16724-67	8/13/1959	1st Order	20	14.032
A16724-69	8/13/1959	1st Order	20	10.630
A16728-23	7/28/1959	1st Order	27	13.357
A16734-1	8/17/1959	1st Order	25	14.146
A16734-3	8/17/1959	1st Order	37	12.593
A16734-4	8/17/1959	1st Order	21	13.721
A16734-6	8/17/1959	1st Order	20	13.748
A16734-7	8/17/1959	1st Order	23	13.227
A16785-192	8/17/1959	1st Order	21	14.871
A16785-194	8/17/1959	1st Order	22	13.445
A16785-196	8/17/1959	1st Order	23	12.916
A16785-198	8/17/1959	1st Order	20	14.755
A16785-200	8/17/1959	1st Order	20	13.844
A16785-201	8/17/1959	1st Order	23	14.570
A16785-203	8/17/1959	1st Order	22	8.656
A16785-205	8/17/1959	1st Order	24	6.951
A16785-206	8/17/1959	1st Order	23	13.827
A16785-52	8/17/1959	3rd Order	20	14.797
A16785-55	8/17/1959	1st Order	20	14.227
A16785-56	8/17/1959	1st Order	21	13.033
A16785-62	8/17/1959	3rd Order	29	12.698
A16785-91	8/17/1959	1st Order	23	6.579
A16785-93	8/17/1959	1st Order	21	14.508

Figure 3.1: ASTER mosaic (July 2009, see Table 3.1 for acquisition dates) showing location of Yelverton Bay and surrounding features. Stars indicate locations of side-looking air-photos shown in Figure 3.4.

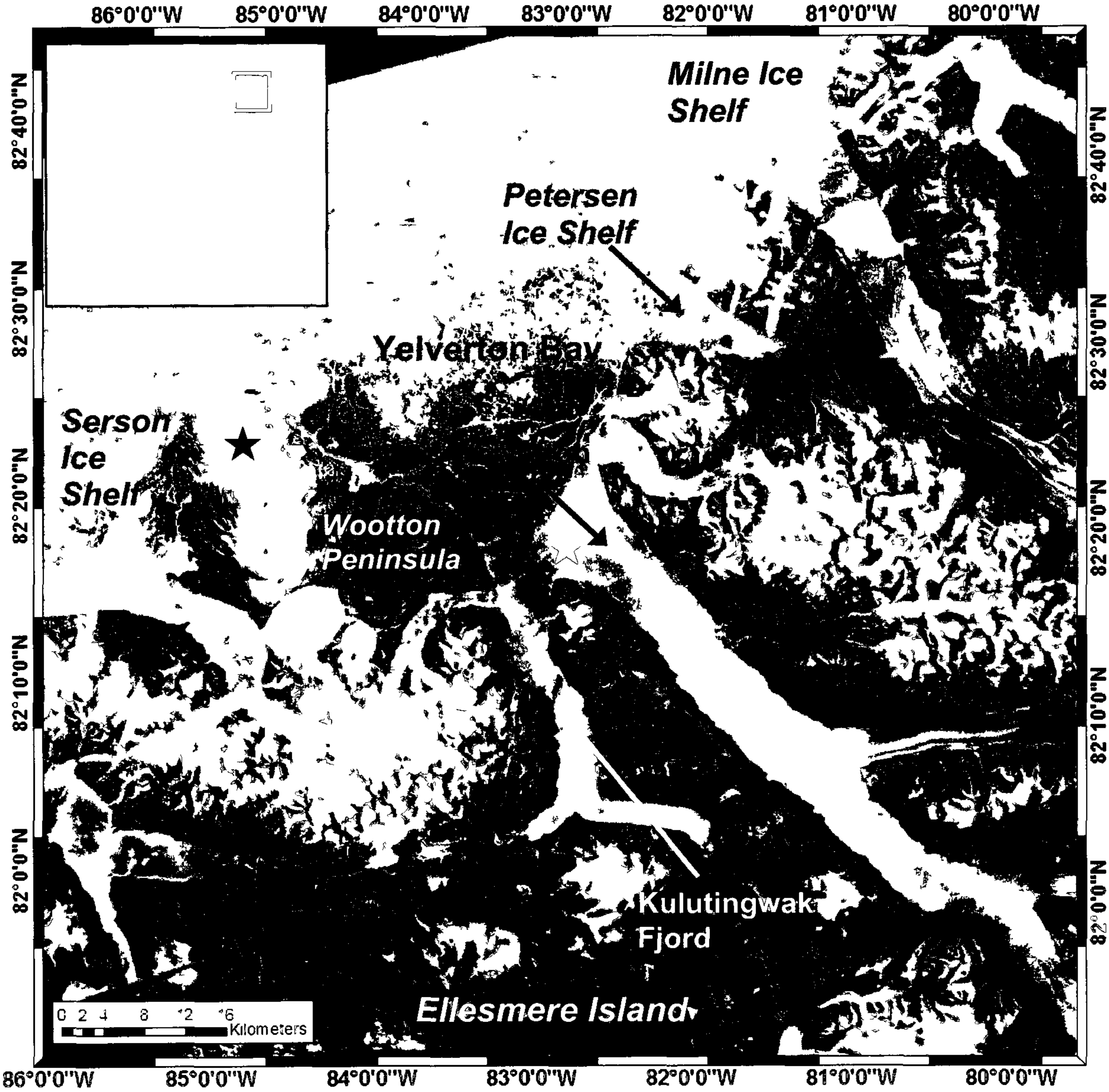

Figure 3.2: Fieldwork preparation and measurements in Yelverton Bay and Yelverton Inlet, June 2, 2009. a) 250 MHz Pulse EKKO Pro GPR system being custom fitted into a plastic sled. b) Temperature measurement and visual observation of an extracted ice core. Photos: Luke Copland.

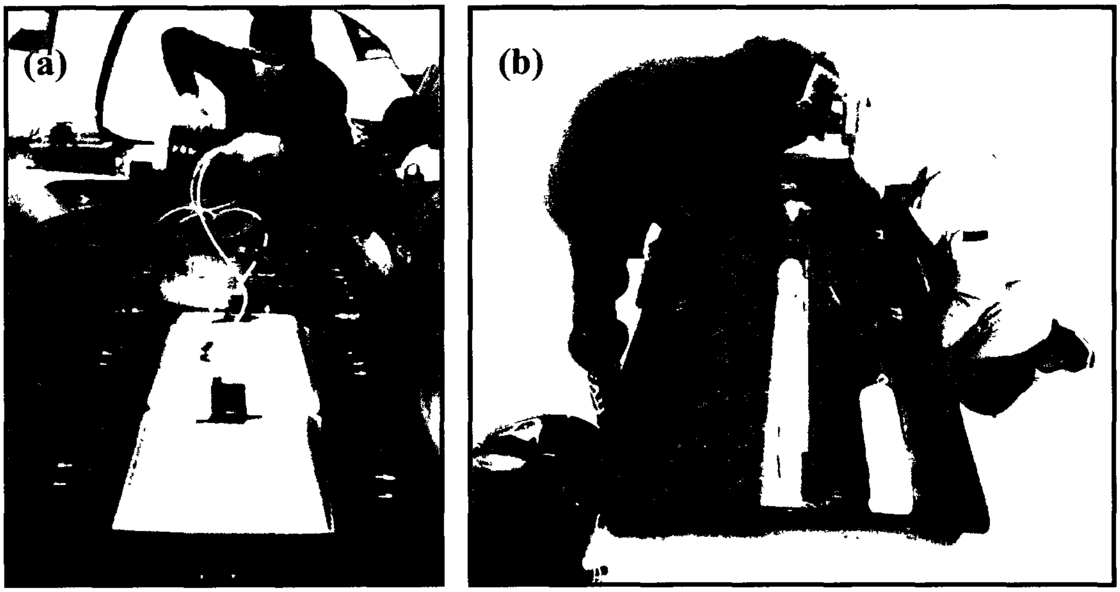

Figure 3.3: Single GPR trace from Yelverton Inlet showing surface and ice base peaks and the chosen BRP calculation window.

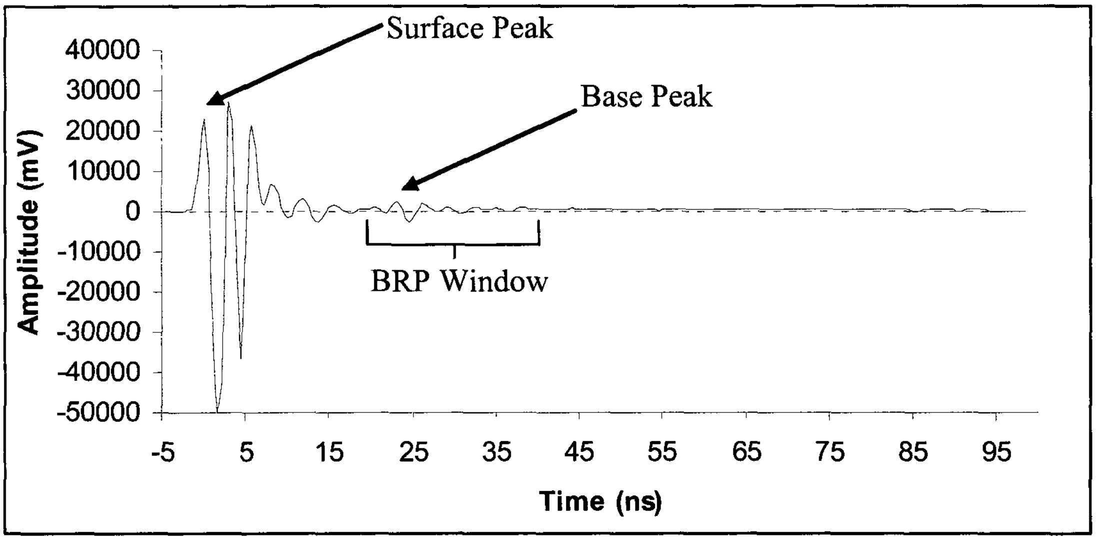

Figure 3.4: Oblique Trimetrogon Series air photos from RCAF flights, August, 1950. a) Photo # T405L-34, from a flight over Wootton Peninsula (black star on Figure 3.1).
b) Photo #T405R-224, View of Yelverton Inlet, taken from the head of the Inlet (white star on Figure 3.1). Photos scanned with permission from the National Air Photographic Library, Ottawa, Ontario.

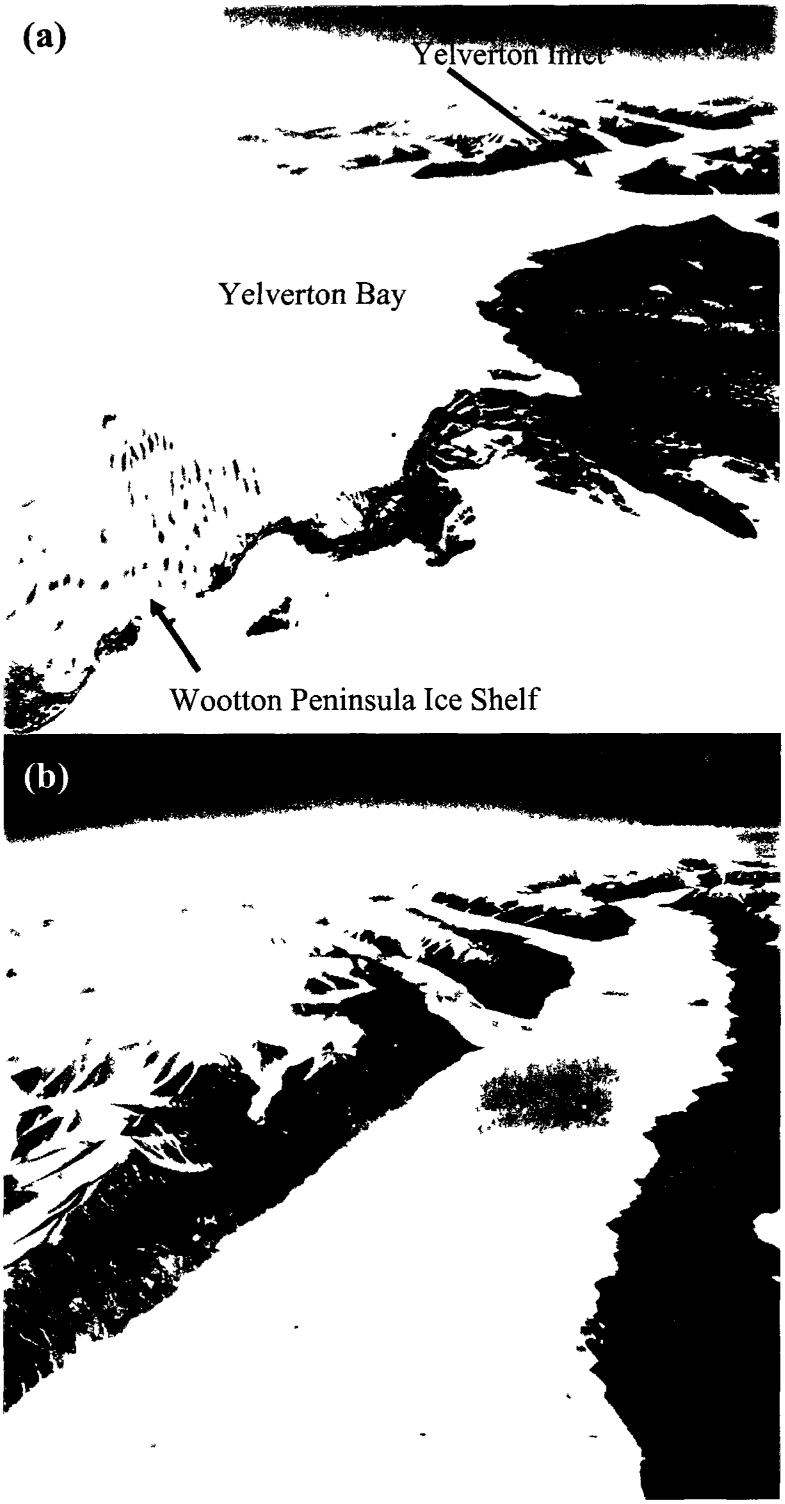

Figure 3.5: GPR-derived snow depths in Yelverton Inlet and Yelverton Bay from 500 MHz surveys on June 2, 2009. Snow depth profile from Point A to B (inset graph) shows decreasing depth from the front to the back of Yelverton Inlet. Background image: ASTER from 16 July 2009 at 20:41:21z.

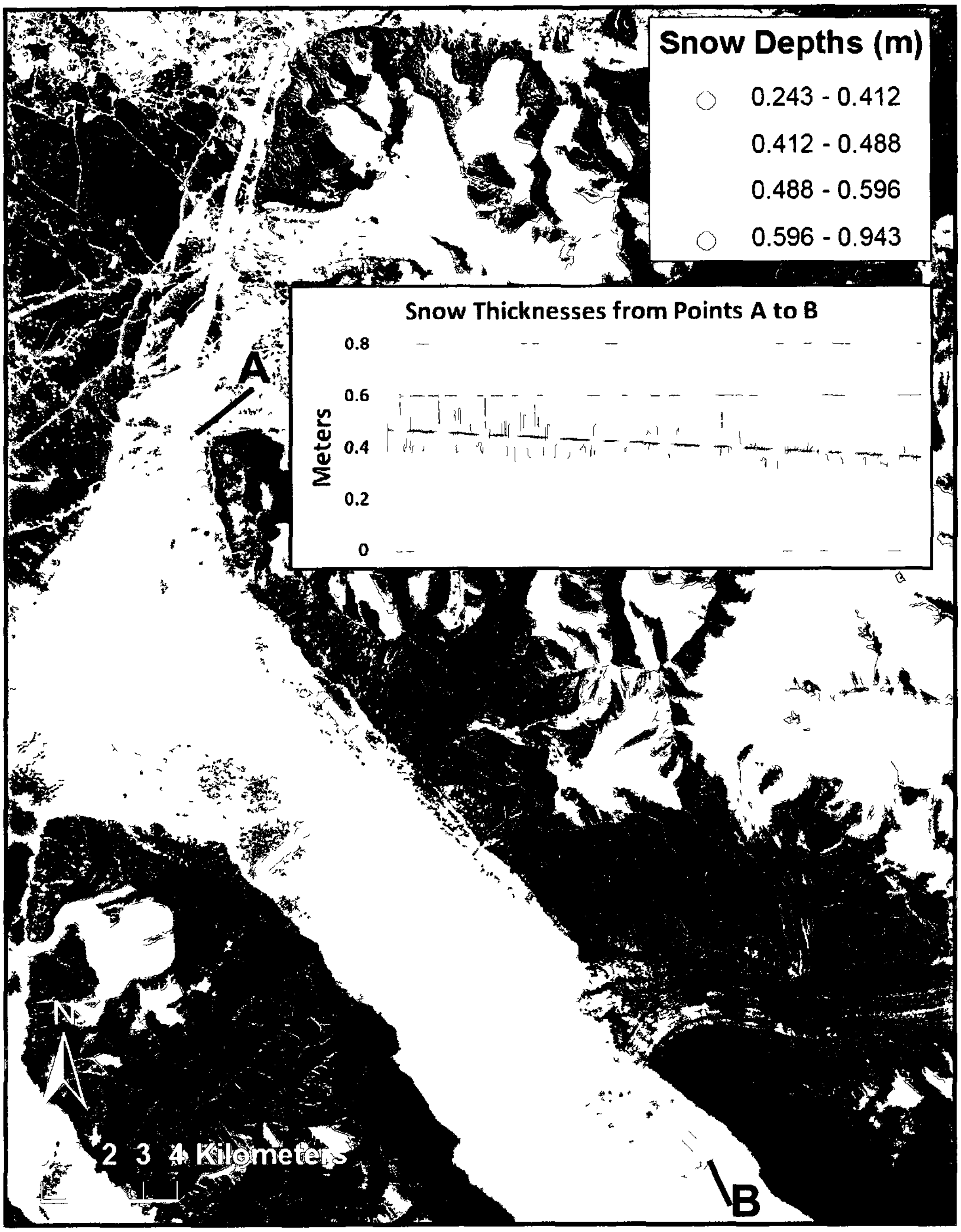

Figure 3.6: Ice properties in Yelverton Inlet. a) Ice core locations and ice thicknesses derived from GPR surveys on June 2, 2009. b) Depth, temperature, and salinity measurements from ice cores 1-4. Background image: ASTER from 16 July 2009 at 20:41:21z. White and black squares identify sections of GPR pictured in Figure 3.7.

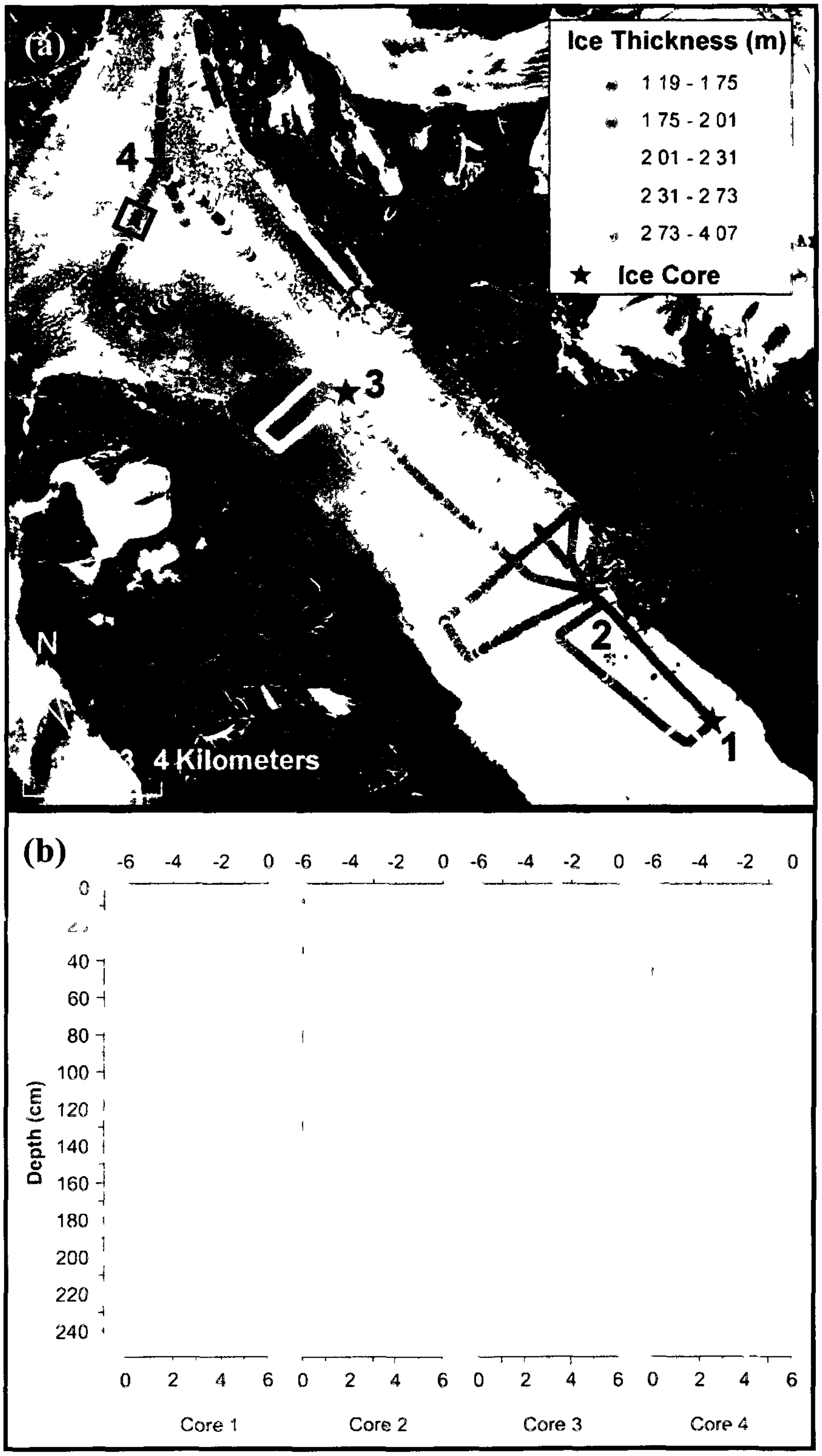

Figure 3.7: 500 m sections from two GPR lines in Yelverton Inlet. a) Traces over FYI at rear of Yelverton Inlet (location identified by the white square in Figure 3.6). b) Traces over MLSI at the head of Yelverton Inlet (location identified by the black square in Figure 3.6). Differences in reflection strength and location are evident between the two ice types, and an internal reflector horizon is visible within the MLSI traces.

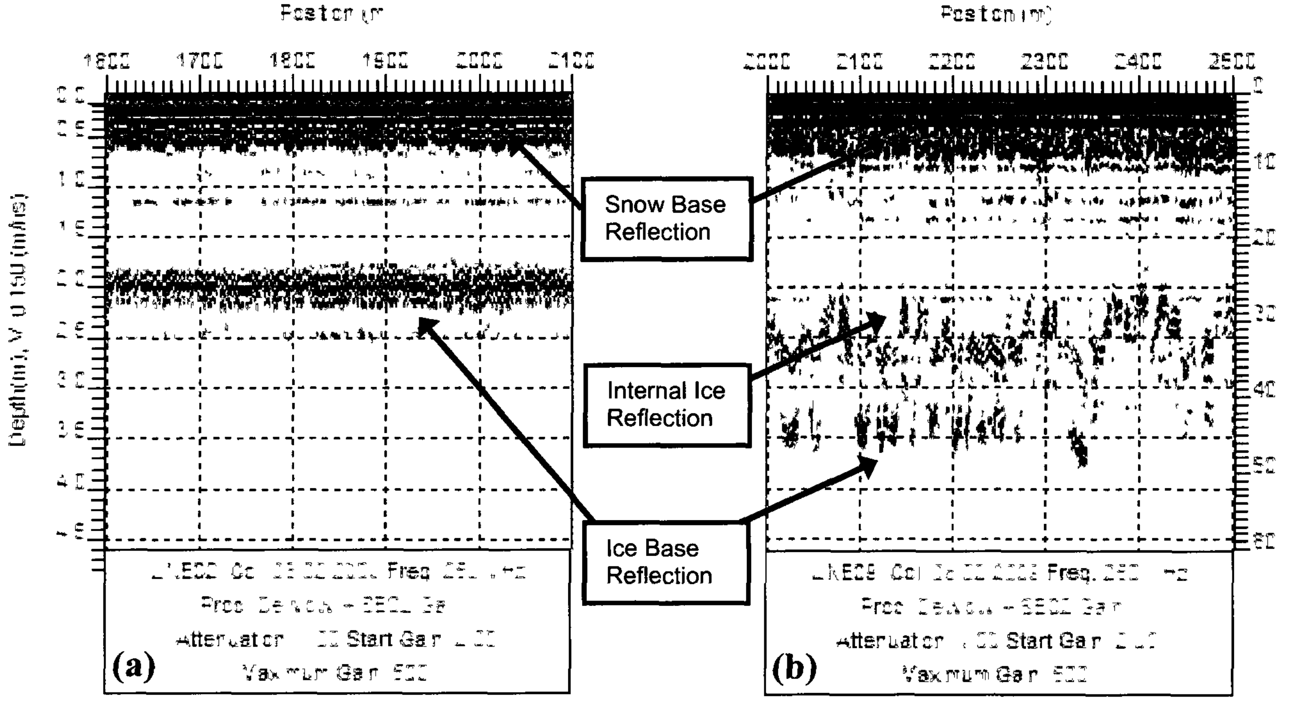

Figure 3.8: Vertical ice stratigraphy at Core 3 in Yelverton Inlet. (a) GPR record: wiggle trace (left) and colour trace (right). (b) YSI salinity measurements of melted ice core segments. (c) Temperature of ice core. (d) Ice core profile and core segment photos.

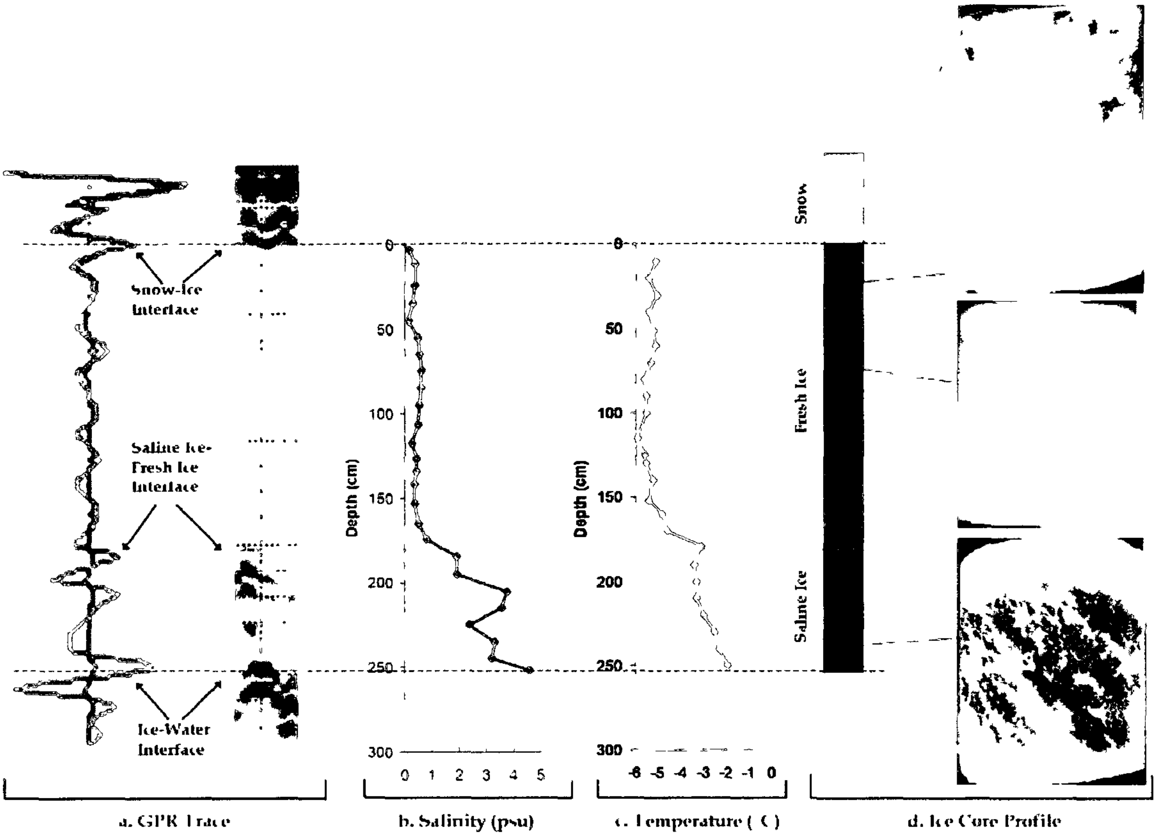

Figure 3.9: Spatial variations in BRP (standardized to mV^2 ns^{-1}) across Yelverton Inlet superimposed over: (a) an ASTER image from July 16 2009 at 20:41:21z.), (b) a RADARSAT-2 image (March 5, 2009) zoomed in to GPR Lines 01 and 04, (c) a RADARSAT-2 image (March 5, 2009) zoomed in to GPR Line 03, (d) Line 01 from A-A', (e) Line 04 from B-B', (f) Line 03 from C to C'. GPR traces in (d) to (f) use a SEC2 Gain.

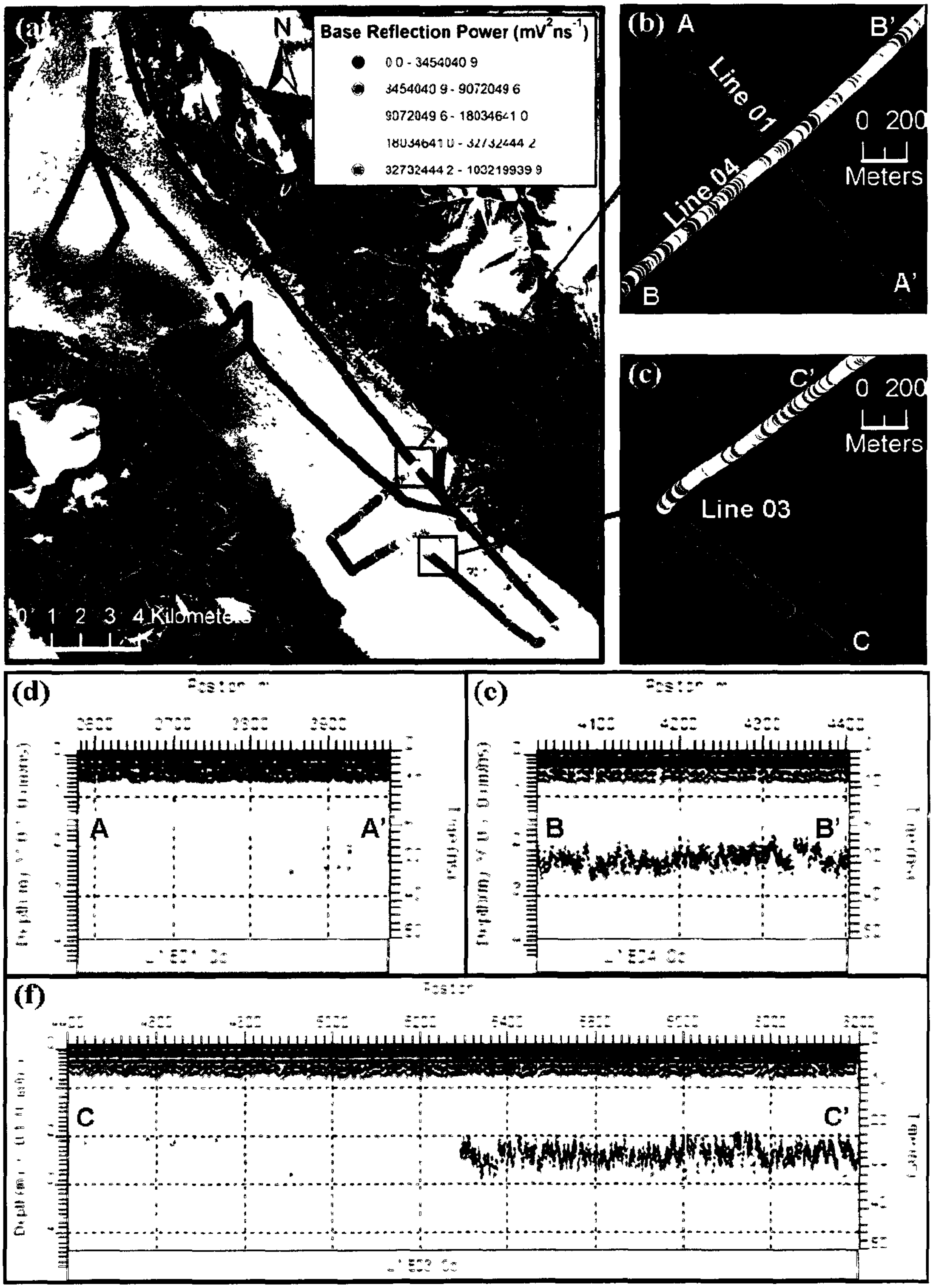

Figure 3.10: RADARSAT-2 image (Widebeam mode, March 5, 2009 20:17z) showing ice type areas, determined from ice thicknesses, ice core properties, and comparison between 2009 ASTER and RADARSAT images. Pixel brightness values (inset graph) for each ice area identify differences between the ice types.

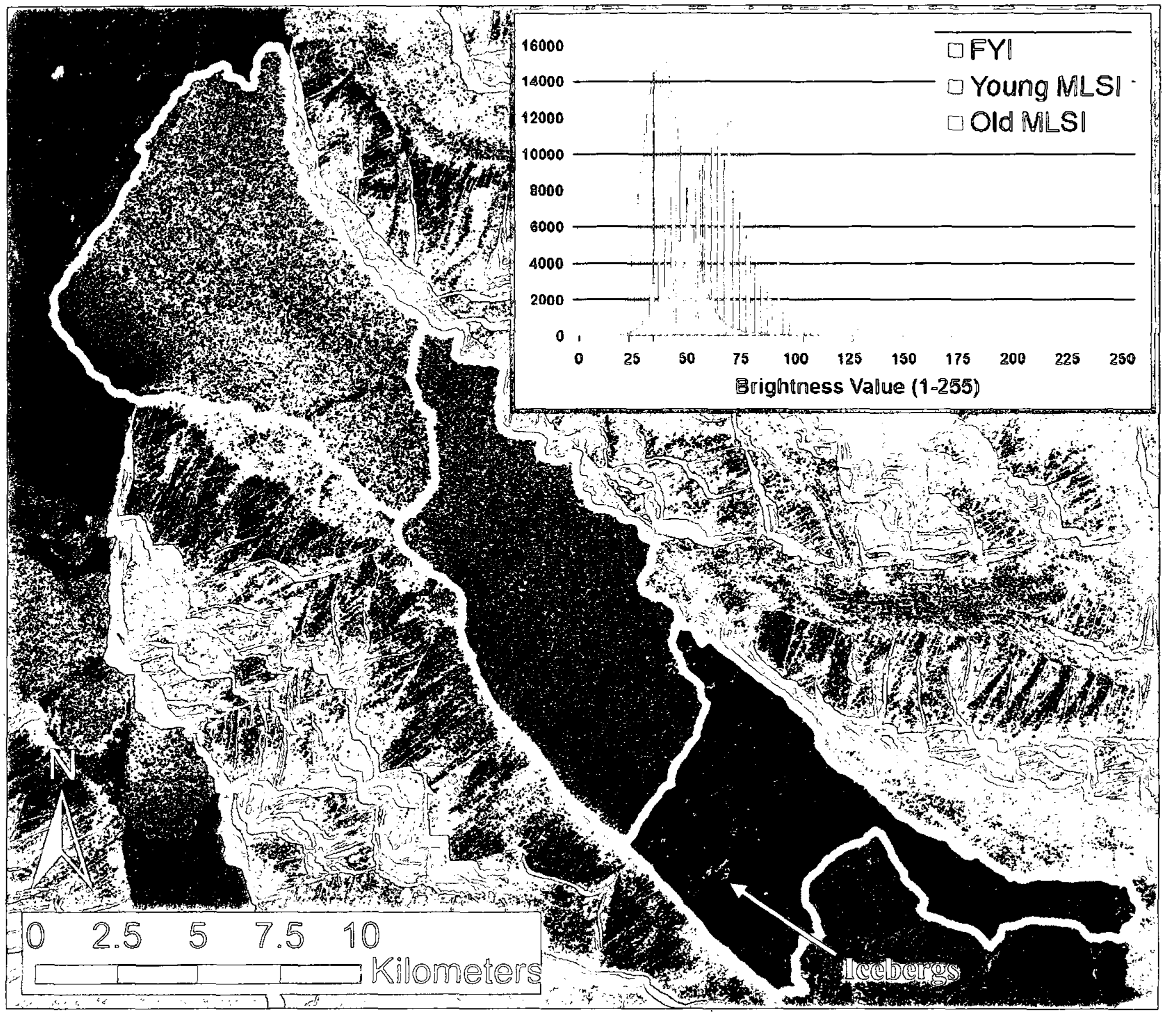

Figure 3.11: Photographs from June 2, 2009 in Yelverton Inlet. a) Ice surface at the front of Yelverton Inlet featuring characteristic 'rolling' texture. b) View of the rear of Yelverton Inlet, showing flat sea ice surface and frozen-in iceberg.

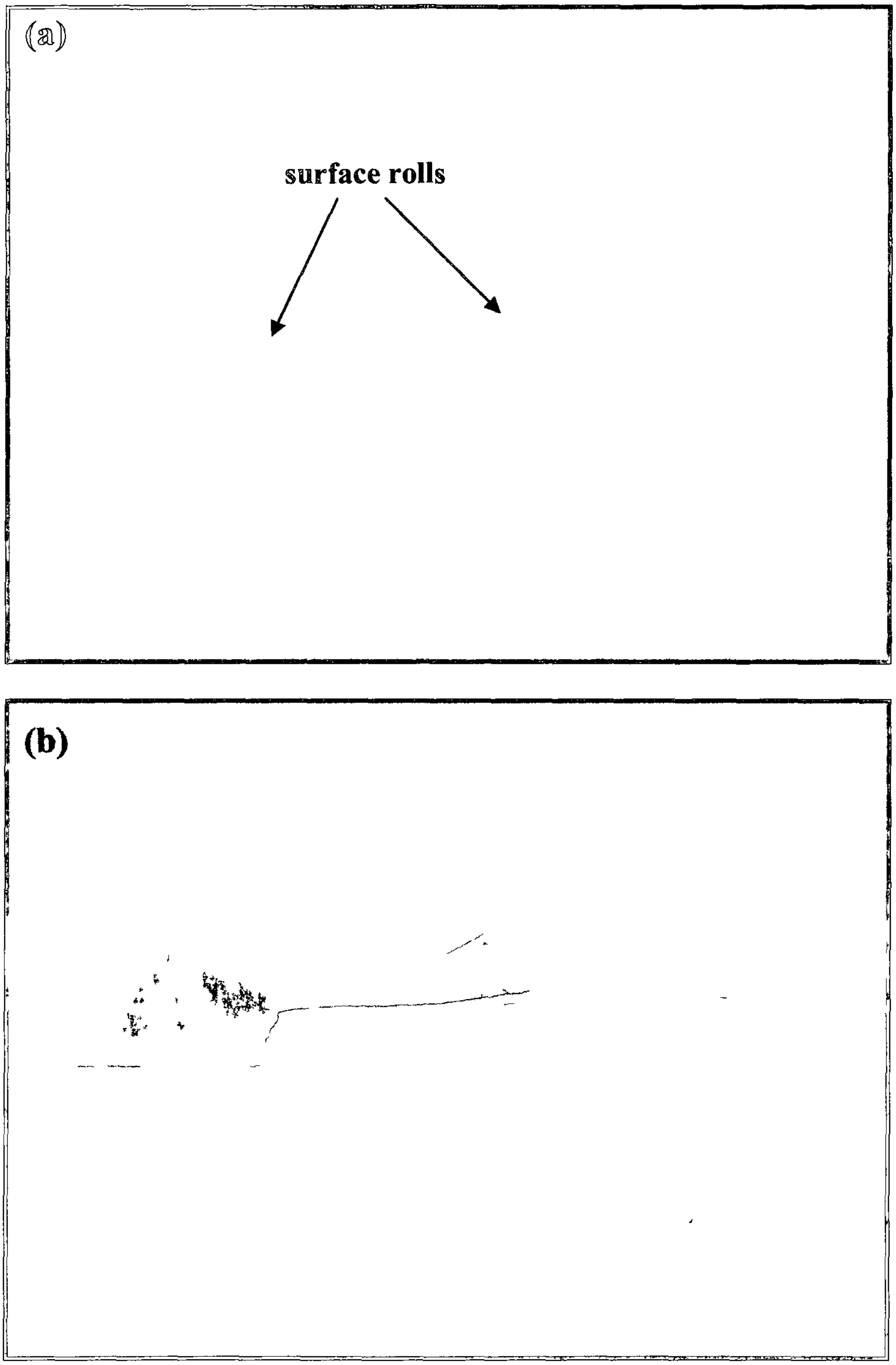

Figure 3.12: Images of an ice island in Yelverton Bay, stationary between 1950 and 2005. a) Area map of Yelverton Bay, with star showing location of photo shown in part (b) and square showing coverage of parts (c) and (d). b) Oblique air photo #T405L-229, August 1950. Ice island outlined in red. c) Nadir air photo mosaic, 1959 (see Table 3.2 for dates). d) RADARSAT-1 image, July 16, 2005 19:58z.

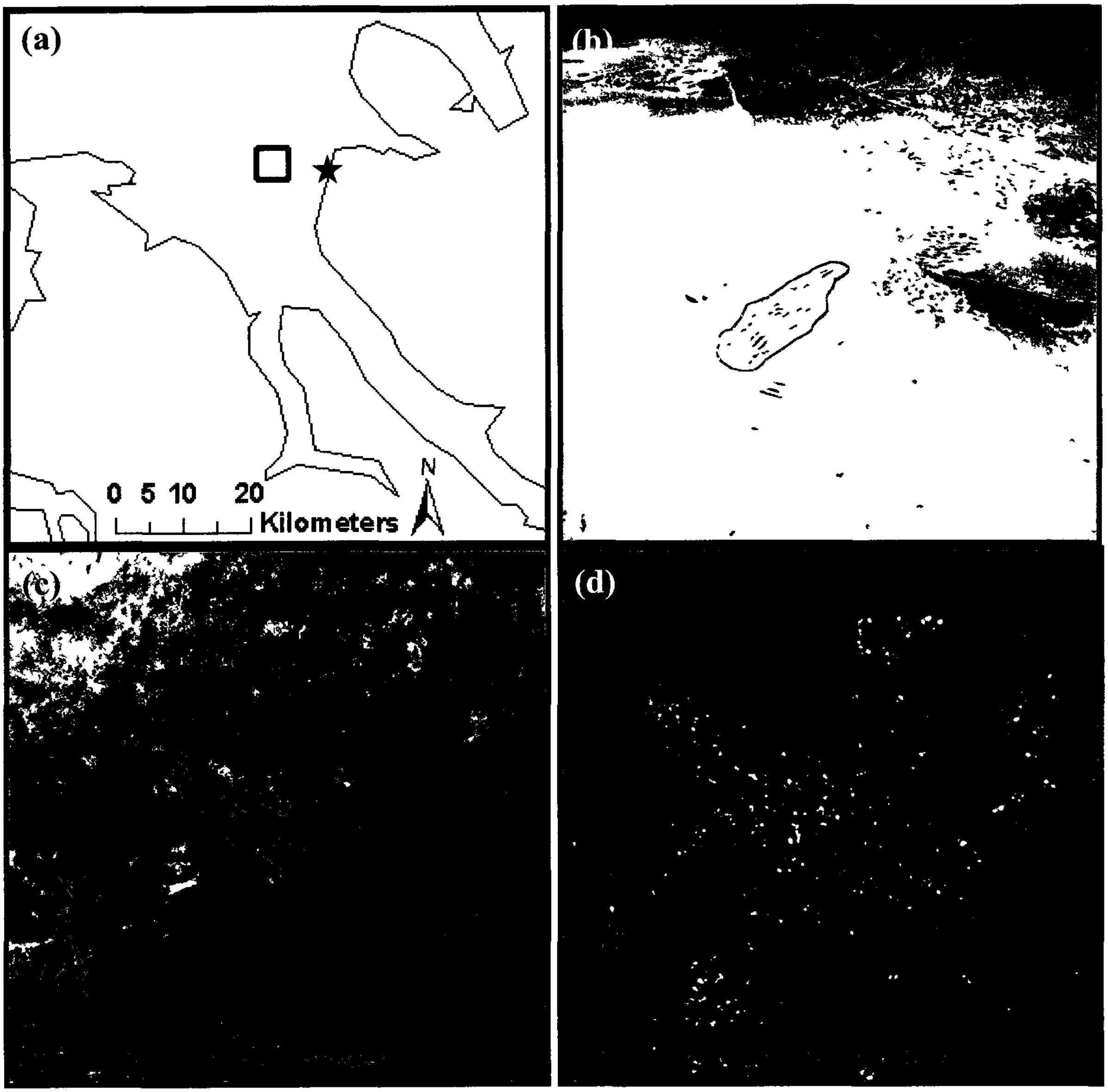

Figure 3.13: Images showing ice extents over 50 years in Yelverton Bay. a) Air photo mosaic, June – August, 1959. See Table 3.2 for image georectification details. (b) ASTER mosaic, July 2009. See Table 3.1 for image acquisition details.

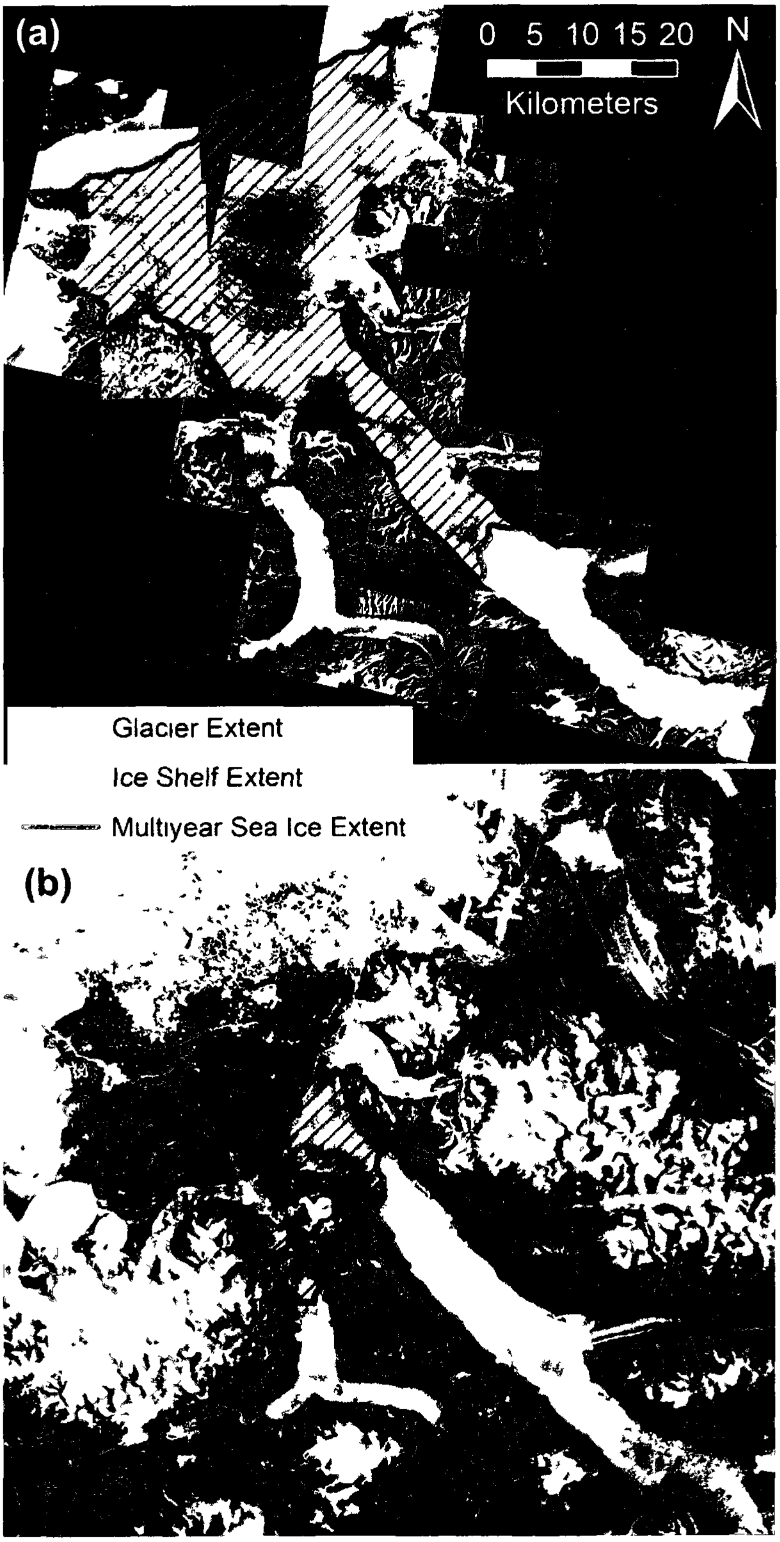

Figure 3.14: RADARSAT image (Standard Beam, March 18, 2005 19:58z) of Yelverton Bay with overlain MLSI extents for 1959, 1993, 2000, 2004, and 2005. These extents are specific to the acquisition date of the image used to determine them; see legend.

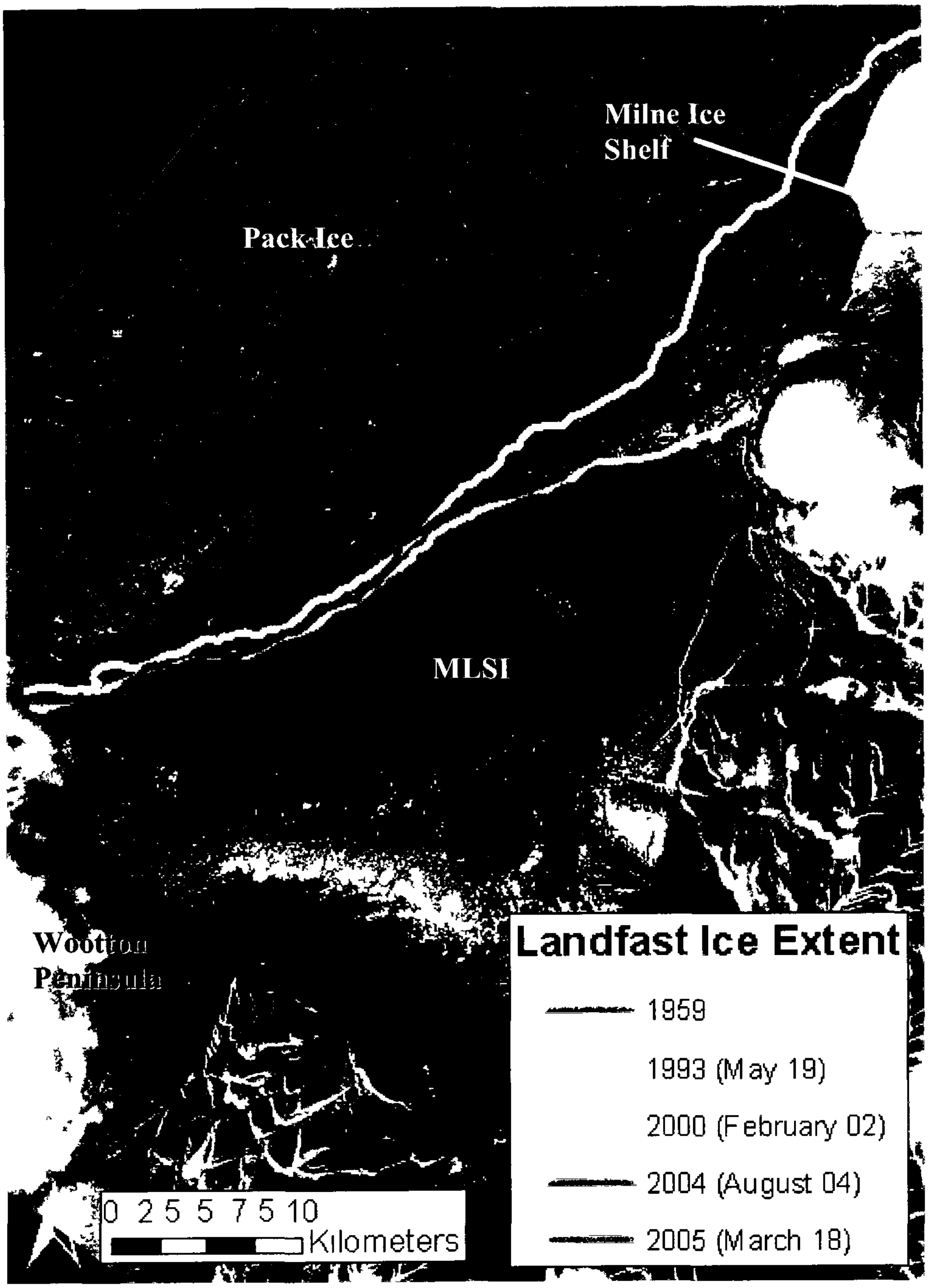

Figure 3.15: RADARSAT Scansar Wide images showing the August 2005 MLSI breakup in Yelverton Bay. (a) August 5, 2005 20:15z; old and reentrant MLSI intact. (b) August 8, 2005 20:28z; younger MLSI begins to break away. (c) August 18, 2005 20:36z; old MLSI has broken at the mouth of the inlet and moved into outer Yelverton Bay. (d) September 24, 2005 20:58z; MLSI fragments have refrozen into the FYI matrix of Yelverton Bay.

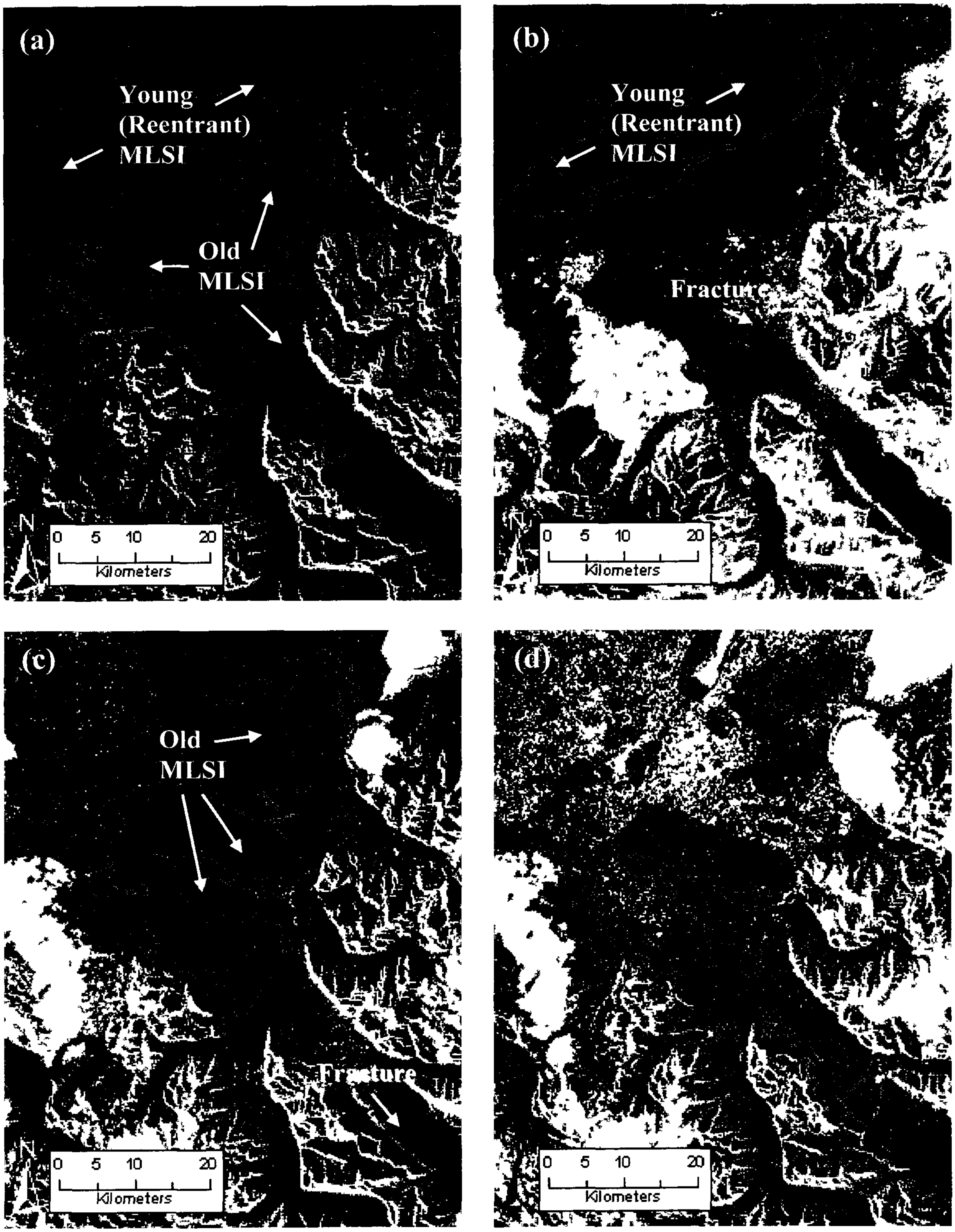

Figure 3.16: Fine-beam RADARSAT-1 (a) and MODIS TERRA (b-d) imagery showing removal of MLSI remnants from Yelverton Bay. a) February 14, 2008 21:33z and 21:34z. b) July 31, 2008 18:50z. c) August 6, 2008 18:10z. d) August 16, 2008 22:05.

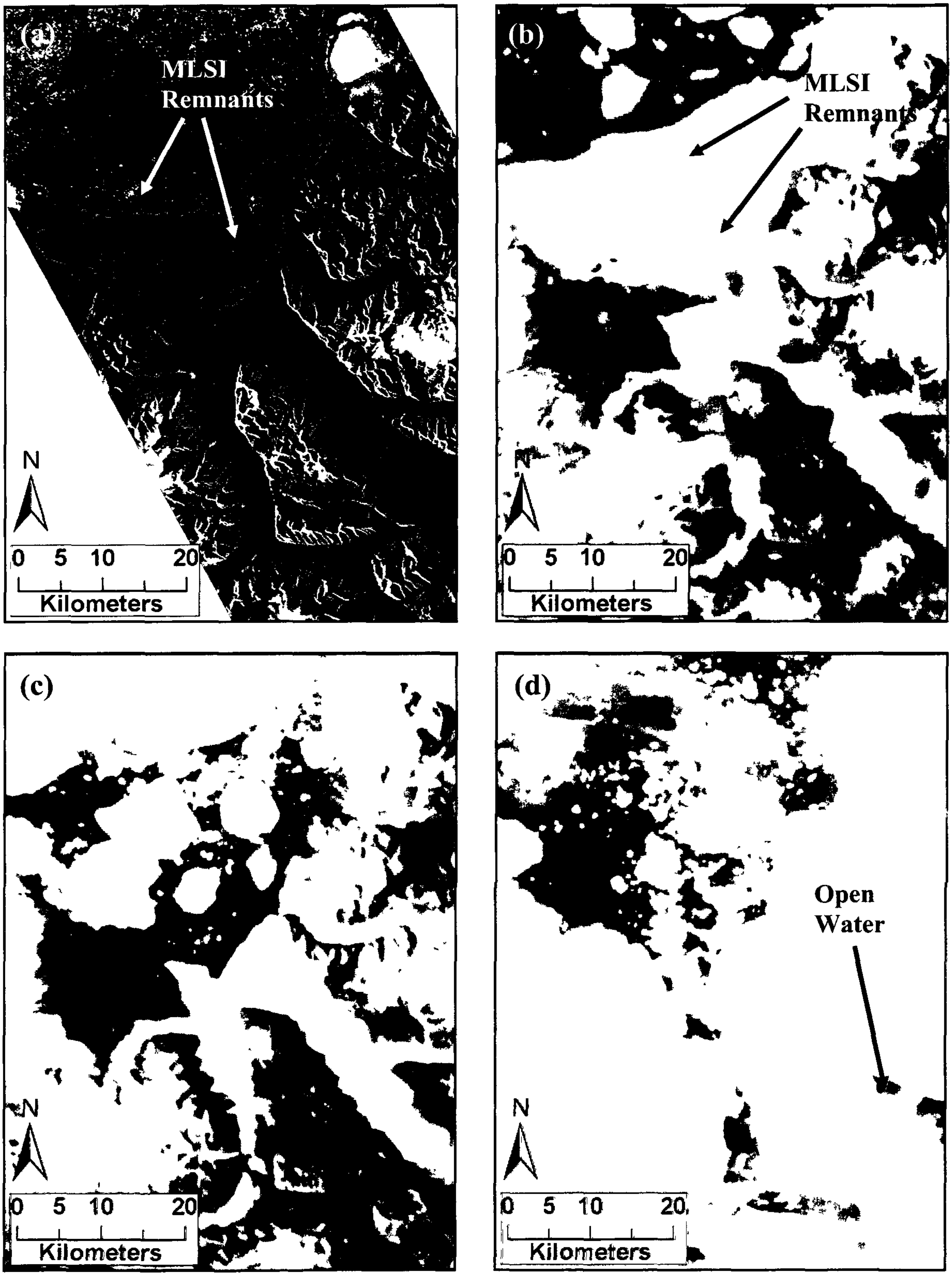

Figure 3.17: MODIS TERRA image (August 22, 2010, 22:05z) showing floating sea ice in Yelverton Bay and Yelverton Inlet. MLSI measured during June 2009 field season has been removed and replaced by open water.

Figure 3.18: Changes to Wootton Peninsula Ice Shelf between 1959 and 2009. a) Air photo (13 August 1959) showing extent of ice shelf in Yelverton Bay. b) RADARSAT Standard Beam image (16 July 2005, 19:58z) with overlain 1959 and 2005 ice shelf extents. c) ASTER image (16 July 2009, 20:41z) showing area loss of Wootton Peninsula Ice Shelf.

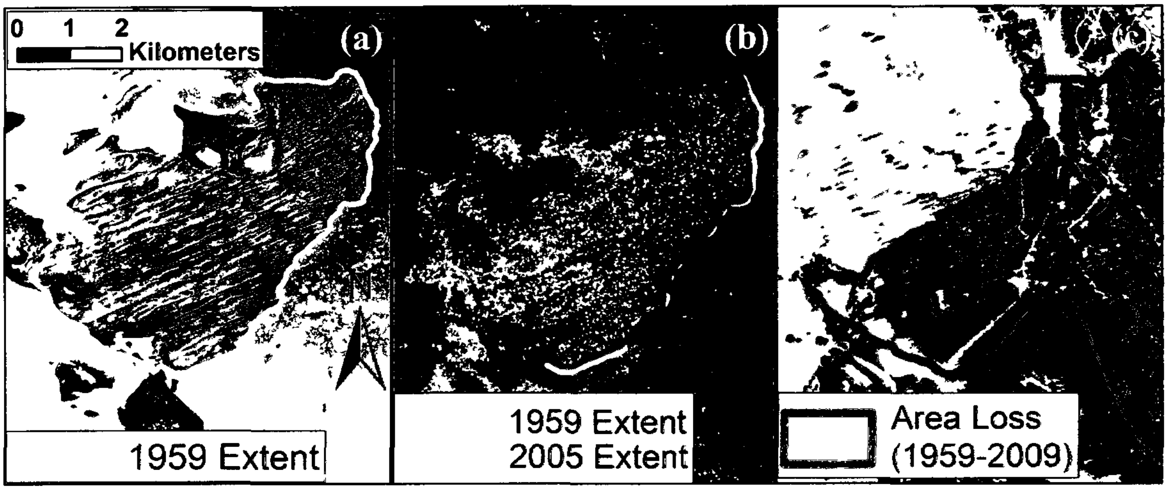

Figure 3.19: Ice type changes in Kulutingwak Fjord. (a) 1959 Air photo. (b) 15 March 2009 RADARSAT-2 (Widebeam, 20:26z) of Fjord, with 2009 ASTER showing surrounding land cover and glaciers. (c) March 3, 2010 13:50z RADARSAT-2 of Fjord areas, with land masked.

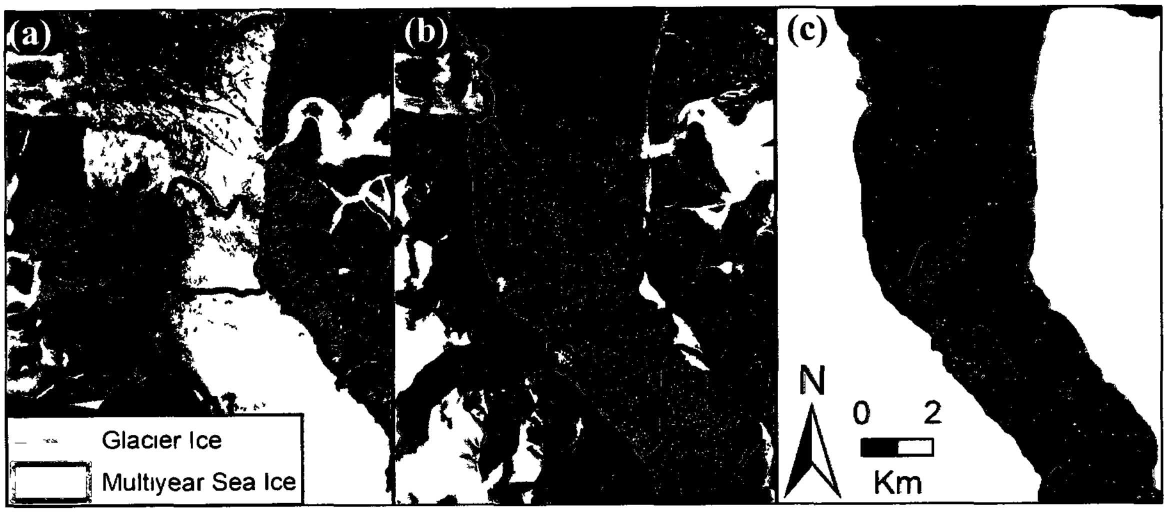

4. Conclusions

The Northern Canadian Arctic Archipelago (CAA) has historically featured large areas of thick, stable multiyear landfast sea ice (MLSI). The growth of this MLSI occurs in narrow channels between islands and in embayments along the island coastlines. These are areas where the ice can grow in situ via surface snow accumulation and basal accretion over time, stabilized by its anchoring against land, and protected from winds and currents. Such stable growth has historically occurred in Sverdrup Channel, Nansen Sound, and Yelverton Bay, facilitated also by the forcing of thick pack ice against the northwestern margin of the CAA by the Beaufort Gyre. The survival of these MLSI features for decades characterized them as 'semi-permanent' features in the Arctic sea ice regime (Agnew et al., 2001; Jeffers et al., 2001). A timeline of the formation and breakup of these MLSI features has been established from 1950 to present, over which time these previously stable features have disappeared entirely, replaced by a thinner, weaker sea ice cover.

The Nansen and Sverdrup MLSI Plugs, monitored over time using a sea ice chart database and satellite imagery, experienced simultaneous breakups in 1962, 1998, 2005, 2007, and 2008. The almost yearly breakup or fracture of one or both of the plugs since 1998 indicates that the ice in these channels is no longer able to form a strong enough cover to withstand the various factors encouraging breakup, including strong winds and the movement of surrounding pack ice. This increasing vulnerability is attributed to several changes in regional climate. Warmer winter temperatures in the region (Copland et al., 2007; Lesins et al., 2010; Serreze et al., 2007) limit the ability of the sea ice to grow in situ and stabilize, and warmer summer temperatures (Gardner and Sharp, 2007; Kaufman et al., 2009) encourage greater melting of the surrounding sea ice buffer and weaken the MLSI (Alt and Lindsay, 2005; Jeffers et al., 2001). Additionally, strong winds in the fall associated with the Alt Type III synoptic condition fracture the pre-weakened plug ice and force it out of the protected channels (Alt, 1987; Gardner and Sharp, 2007; Jeffers and McCourt, 2001).

The Yelverton Bay MLSI survived in situ for at least 55 to 60 years until 2005, forming an incipient ice shelf that covered the region between Petersen Ice Shelf to the east and the

Wootton Peninsula Ice Shelf to the west. This MLSI was detected in aerial photographs and satellite imagery from 1950 through to August 2005, when the dramatic breakup of 690 km^2 of MLSI left only a small portion of it intact in Yelverton Inlet. This event occurred in tandem with the simultaneous breakup of both Nansen and Sverdrup Ice Plugs and the loss of the Ayles Ice Shelf; all of these events were caused in part by extremely warm temperatures in 2005, and very low sea ice concentrations around the semi-permanent MLSI and ice shelf ice (Alt et al., 2006; Copland et al., 2007; Serreze et al., 2007).

This highlights the relationship between the MLSI in the northern CAA and the presence of sea ice around it. The 2005 MLSI loss in Yelverton Bay was preceded by the loss of a border of younger MLSI to the north of it, leaving open water at the old MLSI front for several days. Similarly, the Nansen and Sverdrup Ice Plug breakups were consistently preceded by a weakened or absent surrounding sea ice pack. The removal of sea ice from the MLSI edges increases the likelihood of breakup by exposing it to wave action and the relative heat of ocean water, and by no longer acting as a buffer against the removal of MLSI via wind and ocean currents.

The same relationship has been identified with the MLSI acting as the buffer against the movement of other forms of ice in the Arctic. The 2005 breakup of the Yelverton MLSI occurred in tandem with losses to the Petersen and Wootton Peninsula Ice Shelves, which had previously been held in place by persistent MLSI coverage across Yelverton Bay. The presence of MLSI plugs in Nansen Sound and Sverdrup Channel has historically limited the ability of Arctic Ocean sea ice to move into the CAA, and since their removal, increased import of ice into the CAA has been observed (Alt et al., 2006; Howell et al., 2008).

The 2009 field season provided an opportunity to examine sea ice conditions on northern Ellesmere Island in situ. GPR was found to be an effective means of measuring the thickness of MLSI and FYI in Yelverton Bay. Ice core depth measurements were used to calibrate GPR-derived thicknesses using a radar velocity of 0.15 m ns^{-1}, with average GPR-derived ice thickness in the MLSI remnant of 2.58 m. The GPR was also useful for identifying layering within the MLSI, with an internal reflector horizon in the returned traces occurring at the transition point between low salinity (0-1 psu) to higher salinity (4-5 psu) ice. GPR records, ice core measurements, and in situ observations of the MLSI served as ground-truthing for a RADARSAT image collected in 2009. The bright SAR signature of the MLSI relates to low salinities at the top of the ice, which allow the radar to penetrate into the ice, and internal bubble inclusions, which cause volume scattering. The classification of this bright MLSI distinguished it from other ice types in the imagery, including FYI and young MLSI, which appeared darker, and ice shelf ice, which appeared brighter. This allowed for the identification of the old MLSI in other satellite imagery over time.

The MLSI remnant observed in situ in 2009 broke away from the coast in August 2010, creating an MLSI-free Yelverton Bay and Inlet, unprecedented in recorded history. Along with the failure of the Nansen and Sverdrup MLSI plugs to reform within the last decade, this represents a significant change to the Arctic sea ice regime: the replacement of nearly 1000 km^2 of stable, old MLSI with weak first year ice and seasonal open water. The loss of the buffer against the removal of further old ice export and ice shelf breakup will have significant impacts on the presence and behavior of both landfast and floating ice in the CAA.

5. References

Arctic Climate Impact Assessment (ACIA). 2005. Impacts of a Warming Climate - Arctic Climate Impact Assessment. Cambridge University Press, Cambridge. 1024p.

Agnew, T., Lambe, A. and Long, D. 2008. Estimating sea ice area flux across the Canadian Arctic Archipelago using enhanced AMSR-E. *Journal of Geophysical Research* 113: C10011.doi:10.1029/2007JC004582.

Agnew, T.A., Alt, B., De Abreu, R. and Jeffers, S. 2001. The loss of decades old sea ice plugs in the Canadian Arctic Islands. Extended Abstracts: Polar Meteorology and Oceanography Conference, American Meteorological Society, San Diego, CA. May 14-18, 2001.

Alt, B., and Lindsay, D. 2005. Preliminary investigation of unique features of the Canadian Arctic Archipelago sea ice conditions: as they relate to short range forecast modeling with emphasis on differences from East Coast. Contract Report. Prepared by Balanced Environments Associates for Canadian Ice Service.

Alt, B., Wilson, K. and Carrieres, T. 2006. A case study of old-ice import and export through Peary and Sverdrup Channels in the Canadian Arctic Archipelago: 1998-2005. *Annals of Glaciology* 44: 329-338.

Alt, B.T. 1979. Investigation of summer synoptic climate controls on the mass balance of Meighen ice cap. *Atmosphere-Ocean* 3: 181–199.

Alt, B.T. 1987. Developing Synoptic Analogs for Extreme Mass Balance Conditions on Queen Elizabeth Island Ice Caps. *Journal of Applied Meteorology* 26: 1605–1623.

Alt, B.T., Jeffers, S., McCourt, S., and Chagnon, R. 2001. Spatial and temporal studies of maximum open water in the Queen Elizabeth Islands. In The State of the Arctic Cryosphere During the Extreme Warm Summer of 1998: Documenting Cryospheric Variability in the Canadian Arctic, Chapter II:5. Climate Change Action Fund summer 1998 Project Team, Final Report.

Annan, A.P. 2002. GPR – History, Trends, and Future Developments. *Subsurface Sensing Technologies and Applications* 3(4): 53 – 270.

Askne, J. and Dierking, W. 2008. Sea Ice Monitoring in the Arctic and Baltic Sea Using SAR. In Barale, V. and Gade, M. (eds.) Remote Sensing of the European Seas. Springer Science. 383-398.

Black, W.A. 1962. Sea-Ice Survey, Queen Elizabeth Islands Region, Summer 1962. Geographical Paper No. 39. Department of Mines and Technical Surveys, Ottawa.

Bradford, J. H., Dickins, D. F. and Liberty, L. 2008. Locating oil spills under sea ice using ground-penetrating radar. *The Leading Edge* 27: 1424–1435.

Bradford, J.H., Dickins, D.F., and Brandvik, P.J. 2010. Assessing the potential to detect oil spills in and under snow using airborne ground-penetrating radar. *Geophysics* 75(2): G1-G12.

Braun, C., Hardy, D.R., Bradley, R.S., and Sahanatien. V. 2004. Surface mass balance of the Ward Hunt Ice Rise and Ward Hunt Ice Shelf, Ellesmere Island, Nunavut, Canada, *Journal of Geophysical Research* 109: D22110. doi:10.1029/2004JD004560.

Campbell, K.J., and Orange, A.S. 1974. The electrical anisotropy of sea ice in the horizontal plane. *Journal of Geophysical Research Letters* 79(33): 5059-5063.

Canadian Ice Service (CIS). 2002. Sea ice climatic atlas: northern Canadian waters 1971–2000. Ottawa, Ontario, Environment Canada.

Canadian Ice Service (CIS). 2009. Weekly Regional Ice Charts: Online Archive. Available at http://ice-glaces.ec.gc.ca/

CCAF Summer 1998 Project Team. 2001. Brief Executive Summary. In The state of the Arctic cryosphere during the extreme warm summer of 1998: documenting cryospheric variability in the Canadian Arctic, CCAF Summer 1998 Project Team, CCAF Final Report.

Copland, L. and Sharp, M. 2001. Mapping thermal and hydrological conditions beneath a polythermal glacier with radio-echo sounding. *Journal of Glaciology* 47(157): 232–242.

Copland, L., Mueller, D. and Weir, L. 2007. Rapid loss of the Ayles Ice Shelf, Ellesmere Island, Canada. *Geophysical Research Letters* 34: L21501. doi:10.1029/2007GL031809.

Crary, A. P. 1960. Arctic ice islands and ice shelf studies, part II. *Arctic* 13(1): 32-50.

Dowdeswell and Jeffries. 2011. Arctic Ice Shelves: an Introduction. In Copland, L. and Mueller, D.R., (eds.). Arctic Ice Shelves and Ice Islands. Springer SBM, Dordrecht.

England, J., Lakeman, T.R., Lemmen, D.S., Bednarski, J.M., Stewart, T.G., and Evans, D.J.A. 2008. A millennial-scale record of Arctic Ocean sea ice variability and the demise of the Ellesmere Island ice shelves. *Geophysical Research Letters* 35: L19502. doi:10.1029/2008GL034470

Environment Canada. 1998. Eastern Arctic Regional Ice Analysis, Sept. 28, 1998, Canadian Ice Service.

Environment Canada 2009a. Historical climate data online: daily data. Available from http://www.climate.weatheroffice.gc.ca/climateData/canada_e.html

Environment Canada. 2009b. Weather Data: Canadian Climate Normals: Alert and Eureka. http://www.climate.weatheroffice.ec.gc.ca/climate_normals/index_e.html

Gades, A. M., Raymond, C.F., Conway, H., and Jacobel, R.W. 2000. Bed properties of Siple Dome and adjacent ice streams, West Antarctica, inferred from radio-echo sounding measurements. *Journal of Glaciology* 46(152): 88-94.

Gardner, A.S., and Sharp, M. 2007. Influence of the Arctic Circumpolar Vortex on the Mass Balance of Canadian High Arctic Glaciers. *Journal of Climate* 20: 4586–4598.

Goodman, R. H., Dean, A. M., and Fingas, M. F. 1985. The detection of oil under ice using electromagnetic radiation: Conference on port and ocean engineering under Arctic conditions, Danish Hydraulic Institute, Proceedings, 895–902.

Hattersley-Smith, G. 1957a. The Ellesmere ice shelf and the ice islands. *Canadian Geographer* 9: 65-70.

Hattersley-Smith, G. 1957b. The rolls of the Ellesmere Ice Shelf. *Arctic* 10: 32-44.

Hattersley-Smith, G. 1963. The Ward Hunt Ice Shelf: Recent changes at the ice front. *Journal of Glaciology* 4: 415-424.

Howell, S.E.L., Duguay, C.R., and Markus, T. 2009. Sea ice conditions and melt season duration variability within the Canadian Arctic Archipelago: 1979–2008. *Geophysical Research Letters*, 36, L10502. doi:10.1029/2009GL037681.

Howell, S. E. L., Tivy, A., Yackel, J.J., and McCourt, S. 2008. Multi-Year Sea Ice Conditions in the Western Canadian Arctic Archipelago Region of the Northwest Passage: 1968-2006. *Atmosphere-Ocean* 46(2): 229-242.

Intergovernmental Panel on Climate Change (IPCC). 2007. Climate Change 2007: The Physical Science Basis: Summary for Policy Makers: Contributions of Working Group I to the Fourth Assessment Report of the IPCC. 5-12.

Jeffers, S. 2001. Ice Conditions in the Queen Elizabeth Islands in 1998 (1962, 1981): A Detailed Analysis. In Chapter II:3 of The state of the Arctic cryosphere during the extreme warm summer of 1998: documenting cryospheric variability in the Canadian Arctic, CCAF summer 1998 Project Team, CCAF Final Report.

Jeffers, S. and McCourt, S. 2001. Winds and the Nansen Sd. and Sverdrup Ch. Sea Ice Plugs. In Chapter I:19 of The state of the Arctic cryosphere during the extreme warm summer of 1998: documenting cryospheric variability in the Canadian Arctic, CCAF Summer 1998 Project Team, CCAF Final Report.

Jeffers, S., Agnew, T.A., Alt, B.T., De Abreu, R., McCourt, S. 2001. Investigating the anomalous sea ice conditions in the Canadian High Arctic (Queen Elizabeth Islands) during the summer of 1998. *Annals of Glaciology* 33: 507-512.

Jeffries, M.O. 1986. Ice Island Calvings and Ice Shelf Changes, Milne Ice Shelf and Ayles Ice Shelf, Ellesmere Island, N.W.T. *Arctic* 39(1): 15-19.

Jeffries, M.O. 1987. The Growth, Structure and Disintegration of Arctic Ice Shelves. *Polar Record* 23(147): 631-649.

Jeffries, M.O. 1992. Arctic Ice Shelves and Ice Islands: Origin, Growth and Disintegration, Physical Characteristics, Structure-Stratigraphic Variability, and Dynamics. *Reviews of Geophysics* 30 (3): 245-267.

Jeffries, M.O. 2002. Glaciers of North America-Glaciers of Canada. Glaciers of the Arctic Islands. Ellesmere Island Ice Shelves and Ice Islands. Satellite Image Atlas of Glaciers of the World. U.S. Geological Survey Professional Paper 1386-J-1.

Jeffries, M.O. 2011. The Ellesmere Ice Shelves, Nunavut, Canada. In Copland, L. and Mueller, D.R. (eds.) Arctic Ice Shelves and Ice Islands. Springer SBM, Dordrecht.

Jeffries, M.O., Reynolds, G., and Miller, J. 1992. First Landsat multi-spectral scanner images of the Canadian Arctic north of 80 N. *Polar Record*, 28: 1–6.

Jeffries, M.O., and Sackinger, W.M. 1990a. Airborne SAR characteristics of arctic ice shelves and multiyear landfast sea ice, and the detection of massive ice calvings and ice islands. Geoscience and Remote Sensing Symposium, IGARSS'89. 12th Canadian Symposium on Remote Sensing.

Jeffries, M.O., and Sackinger, W.M. 1990b. Ice island detection and characterization with airborne synthetic aperture radar. *Journal of Geophysical Research* 95(C4): 5371-5377.

Johnston, M.E. and Timco, G.W. 2008. Understanding and Identifying Old Ice in Summer. Canadian Hydraulics Centre, NRC.

Kaufman, D.S., Schneider, D.P., McKay, N.P., Ammann, C.M., Bradley, R.S., Briffa, K.R., Miller, G.H., Otto-Bliesner, B.L., Overpeck, J.T., Vinther, B.M., and Arctic Lakes 2K Project Members: Abbott, M. Axford, Y., Bird, B., Birks, H.J.B., Bjune, A.E., Briner, J., Cook, T., Chipman, M., Francus, P., Gajewski, K., Geirsdóttir, Á., Hu, F.S., Kutchko, B., Lamoureux, S., Loso, M., MacDonald, G., Peros, M., Porinchu, D., Schiff, C. Seppä, H., Thomas, E. 2009. Recent Warming Reverses Long-Term Arctic Cooling. *Science* 325: 1236-1239.

Koenig, L.S., Greenaway, K. R., Dunbar, M., and Hattersley- Smith, G. 1952: Arctic ice islands. *Arctic* 5: 67–103.

Koerner, R.M. 1977. Ice thickness measurements and their implications with respect to past and present ice volumes in the Canadian High Arctic ice caps. *Canadian Journal of Earth Sciences* 14: 2697-2705.

Koerner, R.M. 1979. Accumulation, ablation and oxygen isotope variations on the Queen Elizabeth Islands ice caps, Canada. *Journal of Glaciology* 22: 25-41.

Kovacs, A. and Morey, R. 1978. Radar anisotropy of sea ice due to preferred azimuthal orientation of the horizontal c-axis of ice crystals. *Journal of Geophysical Research* 83(C12): 6037–6049.

Krüger Search Expeditions. 1934. *Polar Record* 1:121-129.

Kwok, R., Cunningham, G., Nghiem, S. 2003. A study of the onset of melt over the Arctic Ocean in RADARSAT synthetic aperture radar. *Journal of Geophysical Research* 108: 3363-3376.

Kwok, R. 2006. Exchange of sea ice between the Arctic Ocean and the Canadian Arctic Archipelago. *Geophysical Research Letters* 33: L16501. doi:10.1029/2006GL027094.

Kwok, R., 2007. Near zero replenishment of the Arctic multiyear sea ice cover at the end of 2005 summer. *Geophysical Research Letters* 34: L05501. doi:10.1029/2006GL028737.

Kwok, R., and Rothrock, D.A. 2009. Decline in Arctic sea ice thickness from submarine and ICESat records: 1958–2008. *Geophysical Research Letters* 36: L15501. doi:10.1029/2009GL039035.

Lesins, G., Duck, T.J., Drummond, J.R. 2010. Climate Trends at Eureka in the Canadian High Arctic. *Atmosphere-Ocean* 48(2): 59-80.

Lindsay, D.G. 1975. Sea ice Atlas of Arctic Canada, 1961-1968. Energy, Mines and Resources Canada, Ottawa.

Lindsay, D.G. 1977. Sea-ice Atlas of Arctic Canada, 1969-1974. Energy, Mines and Resources Canada, Ottawa.

Lindsay, D.G. 1981. Sea-ice Atlas of Arctic Canada, 1975-1978. Energy, Mines and Resources Canada, Ottawa.

Mahoney, A., Eicken, H. Gaylord, A.G., and Shapiro, L. 2007. Alaska landfast sea ice: Links with bathymetry and atmospheric circulation. *Journal of Geophysical Research-Oceans* 112(C2). doi:10.1029/2006JC003559.

Maslanik, J. A., Fowler, C., Stroeve, J., Drobot, S., Zwally, J., Yi, D. and Emery, W. 2007. A younger, thinner Arctic ice cover: Increased potential for rapid, extensive sea-ice loss. *Geophysical Research Letters* 34: L24501. doi:10.1029/2007GL032043.

Melling, H. 2002. Sea ice of the northern Canadian Arctic Archipelago. *Journal of Geophysical Research* 107(C11): 3181. doi:10.1029/2001JC001102.

Mueller, D. 2011. Changes in Canadian Arctic ice shelf extent 1960-2008. In Copland, L. and Mueller, D.R. (eds.) Arctic Ice Shelves and Ice Islands. Springer SBM, Dordrecht.

Mueller, D. R., Vincent, W.F., and Jeffries, M.O. 2003. Break-up of the largest Arctic ice shelf and associated loss of an epishelf lake. *Geophysical Research Letters* 30(20): 2031. doi:10.1029/2003GL017931.

Mueller, D.R., Copland, L., Hamilton, A., and Stern, D. 2008. Examining Arctic Ice Shelves Prior to the 2008 Breakup. *EOS, Transactions of the American Geophysical Union* 89(49): 502-503.

Mueller, D.R., Vincent, W.F. and Jeffries, M.O. 2006. Environmental gradients, fragmented habitats and microbiota of a northern ice shelf cryo-ecosystem, Ellesmere Island, Canada. *Arctic, Antarctic and Alpine Research* 38: 593-607.

Narod, B.B., Clarke, G.K.C., Prager, B.T. 1988. Airborne UHF sounding of glaciers and ice shelves, northern Ellesmere Island, Arctic Canada. *Canadian Journal of Earth Sciences* 25: 95-105.

National Snow and Ice Data Center (NSIDC). 2007. Press Release: Models Underestimate Loss of Arctic Sea Ice. NSIDC Press Room: April 30th, 2007. Available from http://nsidc.org/news/press/20070430_StroeveGRL.html

National Snow and Ice Data Center (NSIDC). 2009. Arctic sea ice extent remains low; 2009 sees third-lowest mark. Press Release, October 06, 2009. Available from http://nsidc.org/news/press/20091005_minimumpr.html

Nghiem, S.V., Chao, Y., Neumann, G., Li, P., Perovich, D.K., Street, T., Clemente-Colón, P. 2006. Depletion of perennial sea ice in the East Arctic Ocean. *Geophysical Research Letters* 33: L17501. doi:10.1029/2006GL027198.

Nghiem, S.V. Rigor, I.G., Perovich, D.K., Clemente-Colón, P., Weatherly, J.W. and Neumann, G. 2007. Rapid reduction of Arctic perennial sea ice. *Geophysical Research Letters* 34: L19504. doi:10.1029/2007GL031138.

Nyland, D. 2004. Profiles of floating ice in arctic regions using GPR. *The Leading Edge* 23: 665–668.

Overland, J.E., and Wang, M. 2010. Large-scale atmospheric circulation changes are associated with the recent loss of Arctic sea ice. *Tellus* 62a: 1-9.

Peary, R. E. 1907. Nearest the Pole. London, Hutchinson and Company.

Perovich, D., Kwok, R., Meier, W., Nghiem, S., and Richter-Menge, J. 2010. Sea Ice Cover. In "State of the Climate in 2009." *Bulletin of the American Meteorological Society* 91(6): S113-S114.

Polunin, N. 1955. Attempted dendrochronological dating of ice island T-3. *Science* 122(3181): 1184-86.

Pringle, D., Dubuis, G., and Eicken, H. 2009. Impedance measurements of the complex dielectric permittivity of sea ice at 50 MHz: pore microstructure and potential for salinity monitoring. *Journal of Glaciology* 55(189): 81-94.

Reeh, N., Thomsen, H.H., Higgins, A.K., Weidick, A. 2001. Sea ice and the stability of north and northeast Greenland floating glaciers. *Annals of Glaciology* 33: 474-480.

Rignot, E. and Kanagaratnam, P. 2006. Changes in the velocity structure of the Greenland Ice Sheet. *Science* 311: 986-990.

Rigor, I. G., and Wallace, J.M. 2004. Variations in the age of Arctic sea-ice and summer sea-ice extent. *Geophysical Research Letters* 31: L09401. doi:10.1029/2004GL019492.

Rothrock, D.A., Yu, Y., Maykut, G.A. 1999. Thinning of the Arctic Sea-Ice Cover. *Geophysical Research Letters* 26(23): 3469-3472.

Schwarzacher, W. 1959. Pack ice studies in the Arctic Ocean. *Journal of Geophysical Research* 64(12): 2357-2367.

Serreze, M. C., and Barry, R.G. 2005. The Arctic Climate System. Cambridge, England: Cambridge University Press.

Serreze, M. C., Holland, M.M., and Stroeve, J. 2007. Perspectives on the Arctic's shrinking sea-ice cover. *Science* 315(5818): 1533-1536.

Serson, H.V. 1972. Investigation of a plug of multi-year ice in the mouth of Nansen Sound. Technical Note 72-6. Defence Research Establishment, Ottawa.

Serson, H.V. 1974. Sverdrup Channel. Technical Note 74-10. Defence Research Establishment, Ottawa.

Shokr, M. and Sinha, N.K. 1995. Physical, electrical and structural properties of Arctic sea ice observed during SIMMS'92 experiment. Research report No. 95-005, Environment Canada, Atmospheric Environment Service, 148.

Stefansson, V. 1938. The Problem of Meighen Island. New York, The Explorers Club.

Stroeve, J., Holland, M. M., Meier, W., Scambos, T. and Serreze, M. 2007. Arctic sea ice decline: Faster than forecast. *Geophysical Research Letters* 34: L09501. doi:10.1029/2007GL029703.

Sverdrup, O. 1904. New Land. Longmans, London: Green Publishing.

VanWychen, W. and Copland, L. 2011. Ice island drift mechanisms in the Canadian High Arctic. In Copland, L. and Mueller, D.R. (eds.) Arctic Ice Shelves and Ice Islands. Springer SBM, Dordrecht.

Vincent, W.F., Gibson, J.A.E. and Jeffries, M.O. 2001. Ice shelf collapse, climate change and habitat loss in the Canadian High Arctic. *Polar Record* 37: 133-142.

Wadhams, P. 2000. Ice in the Ocean. Gordon and Breach Science Publishers, Amsterdam.

Wadhams, P. and Davis, N.R. 2000. Further evidence of ice thinning in the Arctic Ocean. *Geophysical Research Letters* 27(24): 3973-3975.

Wilson, K. J., Falkingham, J., Melling, H., De Abreu, R. 2004. Shipping in the Canadian Arctic: other possible climate change scenarios. In Conference Proceedings from IEEE International Geoscience and Remote Sensing Symposium, September 20-24, 2004, Anchorage, Alaska, USA: 1-4.

Woodward, J. and Burke, M.J. 2007. Applications of ground-penetrating radar to glacial and frozen materials. *Journal of Environmental & Engineering Geophysics* 12(1): 69-85.